Chapter 6

ULTRASOUND: ANALYSIS AND EXPERIMENTAL METHODS IN BIOLOGICAL RESEARCH*

William J. Fry and Floyd Dunn

I. Introduction

This chapter has a multifold purpose. First, it is designed to acquaint investigators interested in bringing various forms of energy to bear upon or interact with biological systems with at least some of the possible ways, established and potential, in which ultrasound[1] can be used to help elucidate structure and function in such systems. Specific studies employing both low "level" and high "level"[2] ultrasound are described to illustrate

* The authors gratefully acknowledge the support of the following organizations for the portion of the work, described in this chapter, accomplished at this laboratory over the past 10 years: Office of Naval Research, Physiology and Acoustics Branches; Institute of Neurological Diseases and Blindness of the National Institutes of Health; Aero-Medical Laboratory of the Wright-Patterson Air Force Base; The National Science Foundation; and The University of Illinois.

[1] This term is used here to designate frequencies of sound above 20 kc.

[2] These terms will be defined later.

this, and the basic physical mechanisms are discussed in each case. Second, it contains material on instrumentation and measurements which is thought to be sufficient to enable investigators entering the field to determine the types of instruments and their specifications which are needed for the studies contemplated. The quantitative relations and discussion included in the chapter will aid investigators in judging the applicability of ultrasound in a particular study and will also be useful in analyzing data resulting from experimental observations made on systems in which ultrasonic fields are employed.

Different forms of energy interact with biological systems in various ways and a single form can affect a specific system by different mechanisms. The mechanism of primary importance in any given case depends upon the physical and chemical state of the system and upon the physical parameters which characterize the form of energy. The study of the manner in which interactions occur results in methods of accumulating information on the organization and mechanisms of operation of such systems and, in some instances, in ways of modifying their structure and functions.

At low acoustic intensities, absorption and/or reflection may constitute the important interactions of interest. Here, an analogy may be drawn between the propagation of ultrasound and that of visible light in biological material. One form of the light microscope depends for its operation upon the selective absorption or the reflection of the incident light in various portions of the specimen under examination. As will be seen later in this article, ultrasound can be utilized in a similar fashion to detect the presence of microstructure which would be revealed as the result of different ultrasonic absorption coefficients or reflectivities.

At high acoustic energy levels, selective permanent disruption of structure and function or temporary interruption of function may be the primary effect of interest. Here, an analogy may be drawn between the use of high level ultrasound and the use of x-rays or other ionizing radiation and high-energy particles to produce permanent disruption of structure. It has become apparent, as the result of investigations which have been carried out over the past decade, that high-level ultrasound is extremely useful in producing selective changes in tissue structures (W. J. Fry, 1956, 1958).

Many investigations have been reported in the literature in which the disruption of cells, bacteria, viruses, etc., in suspension has been the objective. The destructive forces are the result of cavitation[3] in the suspending liquid caused by tension forces produced in the sound field. This extensive work will not be discussed in detail here since the application of

[3] This term applies to the phenomena associated with the growth and collapse of bubbles or vapor-filled cavities in the liquid. A discussion of cavitation appears later in this chapter.

ultrasound in this fashion has been reviewed a number of times (Grabar, 1953). However, a few comments on this work appears desirable at this point in order to place it in proper perspective. The work reported on the disruption of biological materials by cavitation has usually employed the procedure of first subjecting the materials to cavitation in the ultrasonic field and then examining the fragmented products. Much of this work has been accomplished in widely fluctuating ultrasonic fields under unknown or uncontrolled acoustical conditions. This situation has been a consequence of the unavailability of ultrasonic generators of precisely controllable field characteristics. However, results of considerable biological interest have been obtained from this work. It is now clear that precision instrumentation, for the production and control of high intensity ultrasound, is essential for the realization of important quantitative results (W. J. Fry, 1958; F. J. Fry, 1958). Consequently in this article, major emphasis will be placed (1) on outlining and discussing the requirements for precision instrumentation including calibration equipment, and (2) on the results which have appeared as a result of the use of precision methods in this field.

This chapter will not be concerned with clinical applications of low intensity (1–2 w/cm^2) ultrasound used as a diathermy procedure. This important medical application has been reviewed extensively elsewhere (Grabar, 1953; Lehmann and Krusen, 1958) and does not fit into the theme of this chapter—the use of ultrasound to elucidate and modify structure and function in biological systems.

In order to utilize ultrasonic fields for quantitative investigations of biological systems, a familiarity with certain aspects of ultrasonic phenomena in liquids is essential. These include velocity of propagation, attenuation of acoustic disturbances, reflection, refraction and energy conversion at interfaces, and nonlinear properties of the fields. This chapter does not treat these topics in a thorough fashion but furnishes an introduction and presents useful quantitative relations in a form for easy reference and calculation.

At the present time, precision instrumentation for the generation, control, and measurement of high-intensity ultrasonic fields is not commercially available. Therefore, it is essential that investigators considering the use of such ultrasound be able to specify the requirements of instruments when contacting organizations for their design and fabrication. One should be familiar with the important design factors of an instrument and should also be acquainted with appropriate designs. Since an important objective of this chapter is the presentation of sufficient information to enable the investigator inexperienced in ultrasonic work to specify his requirements for a specific biological study, various examples of designs capable of quantitative reproducible results are described.

Quantitative investigations of biological systems by ultrasound require

the use of mathematical expressions which relate the various acoustic field variables and the quantities characterizing the states or the changes induced in the system. Therefore, it is essential that a number of such relations be understood in order that they be properly employed to design appropriate experiments and to interpret the observed data. Such relations are also required to formulate the specifications for instruments. Accordingly, a number of quantitative relations are given in this chapter. The detailed derivations of most of these are not included since extensive background material upon which to base the derivations would also have to be incorporated. However, the formulas included here are discussed in sufficient detail so that they can be used to compute quantities of interest. References are given in the text for those readers who desire a thorough knowledge of the derivations in order to apply the ultrasonic methods to their particular fields of interest.

Section II includes a discussion of reflection and refraction, absorption, cavitation, the production of ultrasound by piezoelectric transducers, the design of focusing systems, calibration probes, general characteristics required of electronic equipment for generators and for calibration, and principles of ultrasonic microscopy. Section III deals with applications to the study of some specific biological systems as examples. Specific instrumentation required for these particular examples will be discussed there.

II. Characteristics of Ultrasonic Fields and Their Production and Measurement

This section is concerned primarily with the propagation of sound in liquid or liquid-like media since the liquid state is extremely important for biological systems. This importance arises from the fact that the physical properties of biological materials are very nearly those of liquids; i.e., the density and acoustic velocity are nearly those of dilute salt solutions (see Table II) and the absorption coefficient is similar to that of viscous oils (notable exceptions are bone and lung). Included are systems composed of suspensions of structural elements in liquids, for example, cells in salt solutions. Some examples illustrating particular points will be drawn from ultrasonic studies involving gases. Formulas derived for one-dimensional acoustic propagation in solids will also be discussed in order to clarify aspects of instrumentation design.

When biological systems are subjected to ultrasonic fields it is desirable, from the viewpoint of interpreting and reproducing results, to employ field configurations which are as simple geometrically as possible. This can be accomplished by utilizing plane waves[4] if the system, or the portion of

[4] This term applies to field configurations in which the wave fronts are plane surfaces.

it to be irradiated, can be subjected to the radiation without concentrating the field by focusing. Plane wave fields can be of the traveling wave type where no reflection of the waves into the region of interest occurs, or they can be of the standing wave type in which all or a portion of the wave energy is reflected from appropriately oriented plane surfaces. A traveling wave field is useful when *all sites* in the portion of the system to be irradiated can be subjected to the entire range of variation of all the physical parameters which undergo change during the acoustic disturbance. A standing wave field is useful when it is desirable to subject the specimen, or a portion of it, to changes in some of the field variables but not to all. This latter situation arises, for example, when it is necessary to separate, from the viewpoint of elucidation of mechanism, effects caused by particular field variables.

However, if the system, or a portion of it, is to be irradiated in depth and the intervening material cannot be subjected to the acoustic field at the level required at the desired site, it is then necessary to focus the ultrasonic energy to obtain higher values for the acoustic field parameters at some distance from the ultrasonic source (irradiator).

Portions of this section are concerned with the characteristics of plane and focused ultrasonic fields and their production and measurement. The range of acoustic field parameters important for examining and modifying biological systems is very extensive and includes both linear or first-order variations and nonlinear or higher order variations. These latter become especially important as the sound level, e.g., intensity, increases.

1. Plane Waves (Linear or First-Order Analysis)

The propagation of an acoustic disturbance or the presence of an acoustic field in an elastic medium is characterized by changes in a number of the physical variables which describe the state of the system or medium. Changes occur, for example, in the pressure, temperature, and density. For a sinusoidal plane traveling wave (traveling in the positive direction of the x axis) with no absorption of the acoustic energy occurring in the medium (i.e., no attenuation of the waves as they travel along the x axis), the changes in each of these (and other) physical parameters can be expressed as follows for the "linear range:"

$$q = Q \cos \omega(t - x/v) \tag{1a}$$

or in complex form

$$q = Qe^{-j\omega(t-x/v)} \tag{1b}$$

where q designates any one of the variables which undergoes change during the presence of the disturbance in the medium and Q designates the ampli-

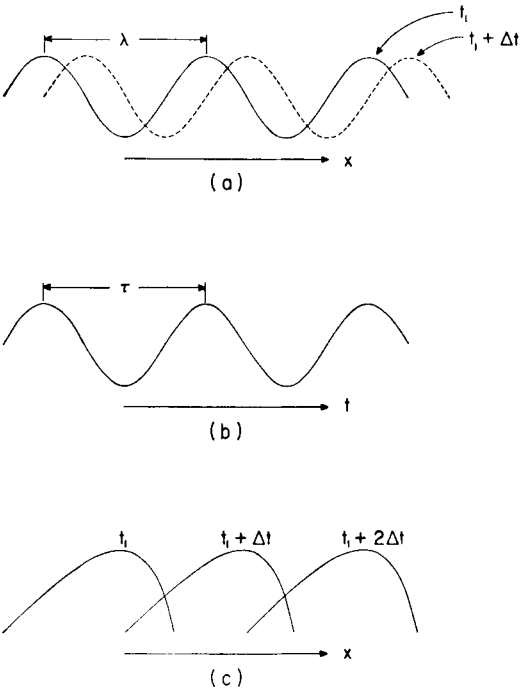

FIG. 1. (a) Instantaneous spatial distribution of a sinusoidally varying acoustic field variable shown at two instants of time. (b) Temporal distribution of variable at a specific point in field. (c) Nonrepetitive wave shown at several instants of time.

tude of the cyclic changes in the variable. The quantity v designates the free field sound velocity[5] for the medium, t and x designate the time and space variables, respectively, and ω is the angular frequency ($\omega = 2\pi f$). The wave described by relations (1) is traveling in the positive x direction since if the time is increased by an amount Δt the wave form is shifted a distance $\Delta x = v\Delta t$ in the positive direction so that

$$\omega\left(t + \Delta - \frac{x + v\Delta t}{v}\right) = \omega(t - x/v)$$

i.e., the argument of the cosine or exponential function is unchanged; see Fig. 1. It is clear that this wave travels without change in form. Relations (1) can be derived from the differential equation which describes small amplitude acoustical disturbances in a nonviscous fluid. The hydrodynamical equations, which describe the flow in a nonviscous fluid, are linearized by assuming, that the velocity of flow of the fluid (the acoustic

[5] Free field sound velocity is the speed with which a plane wave disturbance propagates in a medium of infinite extent.

velocity amplitude discussed below) is small compared to the velocity of sound in the medium, and that the adiabatic compressibility (discussed later in this paragraph) of the medium does not vary greatly with the pressure over the range of pressure variations present in the acoustic field. The adiabatic compressibility enters into the analysis since acoustic propagation is characterized by adiabatic changes in the state of the medium, that is, heat transfer does not occur to any great extent during the changes in pressure. It follows from such a derivation (Kinsler and Frey, 1950) that the free field velocity can be expressed as

$$v = \sqrt{\frac{1}{\rho_0 K_{\text{ad}}}} \tag{2}$$

where ρ_0 designates the undisturbed density of the medium (density of the medium in the absence of an acoustic disturbance) and K_{ad} designates the adiabatic compressibility. That is, for the linearized case with negligible absorption, the velocity of acoustic wave transmission is independent of the frequency and amplitude and is determined solely by the density and the adiabatic compressibility. Hence, waves of arbitrary shape travel without change of form. The adiabatic compressibility can be expressed as

$$K_{\text{ad}} = K_T \left(\frac{c_v}{c_p}\right) \tag{3}$$

where K_T is the isothermal compressibility of the fluid

$$K_T = -\frac{1}{V}\left(\frac{\Delta V}{\Delta P}\right)_T$$

i.e., the change in volume per unit volume caused by a change in pressure at constant temperature, and c_v and c_p are the heat capacities per gram at constant volume and pressure, respectively. The sound velocity can thus be expressed as

$$v = \sqrt{\frac{c_p/c_v}{\rho_0 K_T}} \tag{2a}$$

As the result of the presence of the acoustic wave, the molecules of a liquid and the particles of other materials imbedded in the liquid undergo periodic excursions from their undisturbed positions. The term "particle displacement" is used to designate this excursion from the undisturbed position. The amplitudes of the resulting "particle velocity" and "particle acceleration," which are the first and second time derivatives of the displacement, depend upon the amplitude of this excursion and the frequency of the acoustic waves. The "wavelength" λ, which is defined by the relation

$$v = f\lambda \tag{4}$$

is the distance separation between planes of equal phase of the waves, e.g., the distance from crest to crest. The frequency is equal to the reciprocal of the period τ of the wave (see Fig. 1). The physical mechanism of the interactions of ultrasound and biological systems may involve any of a number of physical parameters which undergo changes in the field. It is, therefore, desirable to summarize the relations between the more important parameters. For a plane traveling wave the variations in the pressure, condensation, particle velocity, particle acceleration, and the time-dependent temperature, all satisfy relation (1) where q designates any one of the parameters and Q designates its amplitude. The relations between the amplitudes of these parameters are listed in Table I. The quantity β appearing in the table designates the coefficient of thermal expansion, i.e., the fractional change in volume with the temperature at constant pressure

$$\beta = \frac{1}{V}\left(\frac{\Delta V}{\Delta T}\right)_p$$

The condensation is defined in terms of the variation in the density of the medium, i.e., $s = (\Delta\rho/\rho_0)$ where $\Delta\rho$ designates the change in density and ρ_0 the undisturbed density. The product, $\rho_0 v$, which appears in a number of these relations, is defined entirely in terms of constants characteristic of the medium itself and is called the "characteristic acoustic impedance" of the medium. Characteristic impedance ratios are of importance in determining the reflection properties at interfaces between media as discussed later (Section II, 2). Table II lists values for the various characteristic constants appearing in Table I for a number of materials of importance in biological investigations employing ultrasound. Blank spaces in the table indicate that the authors have not been able to locate appropriate data.

The intensity of the sound wave is defined as the time average of the rate of propagation of energy through unit area normal to the direction of propagation (unit area perpendicular to the x axis for waves designated by relation (1)). The intensity I, is expressible as

$$I = \tfrac{1}{2}\rho_0 v U^2 = \tfrac{1}{2}(P^2/\rho_0 v) \tag{5}$$

As indicated above, the linearizing of the hydrodynamical equations depends upon two assumptions which can now be expressed as the two symbolic relations

$$U/v \ll 1 \tag{6a}$$

$$\frac{\Delta K_{ad}}{K_{ad}} = \frac{(K_{ad})_{P_0+P} - (K_{ad})_{P_0-P}}{(K_{ad})_{P_0}} \tag{6b}$$

where P_0 designates the undisturbed pressure and K_{ad} the adiabatic compressibility which can be calculated from relation (3). The designation

TABLE I

RELATIONS BETWEEN AMPLITUDES OF THE VARIOUS PHYSICAL PARAMETERS[a]

Parameter	Parameter symbol q	Amplitude symbol Q	P (d/cm²)	s	D (cm)	V (cm/sec)	A (cm/sec²)	T (°C)
Pressure	p	P		$\begin{matrix}+\\-\end{matrix}\rho_0 v^2$	$\begin{matrix}+\\-\end{matrix}j\omega\rho_0 v$	$\begin{matrix}+\\-\end{matrix}\rho_0 v$	$\begin{matrix}+\rho_0 v\\-j\omega\end{matrix}$	$\begin{matrix}+\dfrac{\beta}{}\\+\left(K_T-\dfrac{1}{\rho_0 v^2}\right)\end{matrix}$
Condensation	s	S	$\begin{matrix}+\dfrac{1}{}\\-\rho_0 v^2\end{matrix}$		$\begin{matrix}+j\omega\\+v\end{matrix}$	$\begin{matrix}+1\\+v\end{matrix}$	$\begin{matrix}+\dfrac{1}{}\\+j\omega v\end{matrix}$	$\begin{matrix}+\dfrac{\beta}{}\\-\rho_0 v^2\left(K_T-\dfrac{1}{\rho_0 v^2}\right)\end{matrix}$
Particle displacement	ξ	D	$\begin{matrix}+\dfrac{1}{}\\-j\omega\rho_0 v\end{matrix}$	$\begin{matrix}+v\\+j\omega\end{matrix}$		$\begin{matrix}+1\\+j\omega\end{matrix}$	$\begin{matrix}-1\\-\omega^2\end{matrix}$	$\begin{matrix}+\dfrac{\beta}{}\\-j\omega\rho_0 v\left(K_T-\dfrac{1}{\rho_0 v^2}\right)\end{matrix}$
Particle velocity	$\dot{\xi}$	U	$\begin{matrix}+\dfrac{1}{}\\-\rho_0 v\end{matrix}$	$\begin{matrix}+\\+v\end{matrix}$	$\begin{matrix}+\\+j\omega\end{matrix}$		$\begin{matrix}+1\\+j\omega\end{matrix}$	$\begin{matrix}+\dfrac{\beta}{}\\-\rho_0 v\left(K_T-\dfrac{1}{\rho_0 v^2}\right)\end{matrix}$
Particle acceleration	$\ddot{\xi}$	A	$\begin{matrix}+j\omega\\-\rho_0 v\end{matrix}$	$\begin{matrix}+\\+j\omega v\end{matrix}$	$\begin{matrix}-\\-\omega^2\end{matrix}$	$\begin{matrix}+\\+j\omega\end{matrix}$		$\begin{matrix}+\dfrac{j\omega\beta}{}\\-\rho_0 v\left(K_T-\dfrac{1}{\rho_0 v^2}\right)\end{matrix}$
Temperature	ΔT	T	$\begin{matrix}+1\\+\beta\left(K_T-\dfrac{1}{\rho_0 v^2}\right)\end{matrix}$	$\begin{matrix}+\rho_0 v^2\\-\beta\end{matrix}\left(K_T-\dfrac{1}{\rho_0 v^2}\right)$	$\begin{matrix}+j\omega\rho_0 v\\-\beta\end{matrix}\left(K_T-\dfrac{1}{\rho_0 v^2}\right)$	$\begin{matrix}+\rho_0 v\\-\beta\end{matrix}\left(K_T-\dfrac{1}{\rho_0 v^2}\right)$	$\begin{matrix}+\rho_0 v\\-j\omega\beta\end{matrix}\left(K_T-\dfrac{1}{\rho_0 v^2}\right)$	

[a] Multiply expressions in table by column heading to obtain relations equal to the amplitude quantities tabulated in the Amplitude Symbol column. Note: $j = \sqrt{-1}$. The relations given apply to plane waves traveling in either direction. The upper sign applies to waves traveling in the positive direction and the lower sign applies to waves traveling in the negative direction. (See expression 1.) The amplitude of the change in any one physical parameter is simply equal to the amplitude of the change in any other parameter times the absolute value of the appropriate quantity in the table. One self-consistent set of units is included in the table.

TABLE II

PHYSICAL CONSTANTS OF VARIOUS MATERIALS

Material	T (°C)	P (atm)	ρ_0 (gm/cm³)	v (cm/sec)	$\rho_0 v$ (gm/cm² sec)	c_p/c_v	K_T (cm/d²)	β (1/°C)	α (cm⁻¹)
Multiply Figures in Table by	1	1	1	10^5	10^5	1	10^{-12}	10^{-5}	1
Degassed, distilled water. α proportional to f^{2a}	0	1	0.999841	1.4027	1.4025	1.000583	50.86	−5.89	
	10	1	0.999701	1.4476	1.4472	1.001085	47.79	+9.45	
	20	1	0.998207	1.4827	1.4800	1.00656	45.86	+21.19	25×10^{-5}
	30	1	0.995651	1.5094	1.5028	1.01526	44.76	30.75	
	40	1	0.992220	1.5292	1.5173	1.02575	44.20	38.93	
	0	136	0.9941	1.4245	1.4161	1.00012	49.58	2.01	
	10	136	0.9946	1.4700	1.4621	1.00356	46.69	15.09	
	20	136	0.9961	1.5057	1.4998	1.01041	44.74	25.10	
	30	136	0.9986	1.5329	1.5308	1.01827	43.40	34.05	
	40	136	1.0019	1.5531	1.5560	1.02672	42.48	40.92	
0.9% Normal saline[b]	0	1	1.00668	1.4134	1.4228			1.98	
	10	1	1.00631	1.4582	1.4674			8.46	
	20	1	1.00460	1.4932	1.5001			23.89	
	30	1	1.00189	1.5198	1.5268			29.94	
	40	1	0.99837	1.5394	1.5369			40.07	
Castor oil. At 30°C, α proportional to $f^{5/3a}$	0	1	0.972	1.580	1.536				0.26
	10	1	0.960	1.536	1.474				0.16
	20	1	0.952	1.494	1.422				0.096
	30	1	0.946	1.452	1.374				0.057
	40	1	0.941	1.411	1.328				0.037

Phenylated silicone oil, Dow-Corning No. 710, α proportional to f^2 to approximately 20 mc[a]	0	1	1.124	1.446	1.625				
	10	1	1.112	1.409	1.567				0.135
	20	1	1.102	1.378	1.518				0.070
	30	1	1.095	1.349	1.477				0.040
	40	1	1.089	1.321	1.438				0.024
Aluminum, rolled			2.70	6.42	17.3				
Steel, stainless, 347			7.91	5.79	45.8				
Lucite[a]			1.18	2.68	3.16				0.2
Polystyrene			1.056	2.35	2.48				0.05
Ceramic materials	approximate ranges		2.5	4.6	12				
			3.4	6.8	18				
Average Values for Mammalian Tissue									
Central nervous system[a, c-e]	37	1	1.03	1.51	1.56				0.11
Young mouse 24 hours after birth	2	1							0.02
	10	1							0.06
	28	1							0.11
Muscle (skeletal)[a, c, e]	37	1	1.07	1.57	1.68				0.13
Fat[a, c]	37	1	0.97	1.44	1.40				0.05
Human skull bone	37	1	1.7	3.36	6.0				
Frequency (mc) 0.6	↑	1							0.4
0.8		1							0.9
1.2		1							1.7
1.6	f	1							3.2
1.8		1							4.2
2.25		1							5.3
3.5	↓	1							7.8

[a] Values of α for 1 mc.

[b] Measurements of W. D. Wilson, U.S. Naval Ordinance Laboratory.

[c] α proportional to frequency.

[d] Average value for adult animal. In the cat, α for white matter is five-ninths that of gray matter. The young mouse cord is virtually unmyelinated and displays a value of α, at 37°C, greater than the average value for the adult animal.

[e] Varies with direction of sound propagation relative to fiber orientation.

[f] Temperature unknown, believed to be in the range 15–25°C.

TABLE III

NUMERICAL EXAMPLES OF PHYSICAL PARAMETERS FOR WATER AND AIR

Material	f (mc)	T (°C)	P_0 (atm)	I (w/cm^2)	P (atm)	S	D (cm)	U (cm/sec)	A (cm/sec^2)	T (°C)	U/v
Multiply figures in table by...	1	1	1	1	1	10^{-5}	10^{-6}	1	10^{6}	10^{-4}	10^{-5}
Water, degassed distilled	1	30	1	0.01	0.171	0.762	0.183	1.15	7.22	3.82	0.762
				1	1.71	7.62	1.83	11.5	72.2	38.2	7.62
				100	17.1	76.2	18.3	115	722	382	76.2
Multiply figures in table by...	1	1	1	1	10^{-3}	10^{2}	10^{-5}	10	10^{8}	1	10^{-3}
Air	1	30	1	0.01	2.81	2.01	1.12	7.01	4.40	0.243	2.01
				1	28.1	20.1	11.2	70.1	44.0	2.43	20.1
				100	281	201	112	701	440	24.3	201

$\ll 1$ implies a quantity of a few hundredths or less. It should be noted that nonlinear or second-order effects may be of importance for values of U/v much smaller than 0.01 but the linearized equations still constitute a good first approximation for calculating the values of the physical parameters listed in Table I. A discussion of second-order effects important at high sound intensities appears later in this section.

It is desirable to consider numerical examples in order to develop some feeling for the magnitudes of the changes exhibited by the various physical parameters. Accordingly, some values are listed in Table III. Reference can be made to Table II for values of the physical constants of the materials considered. It is convenient to express the intensity in watts per square centimeter and the acoustic pressure amplitude in atmospheres. However, for calculations using the expressions of Table I, the intensity should be expressed in dynes per centimeter per second and the pressure amplitude in dynes per square centimeter if the other parameters are expressed in the indicated units.

2. Reflection and Refraction

It is necessary to be familiar with certain quantitative relations describing the reflection and transmission of acoustic waves at boundaries in order to understand the transmission characteristics of ultrasound through tissue and to design ultrasonic instrumentation for the study of biological systems. Accordingly a number of simple cases are discussed in sufficient de-

tail to permit their use in evaluating the results of experiments involving interfaces and prescribing design requirements for instrumentation.

The amplitudes of the waves reflected and/or refracted at an interface between media are determined by the acoustic velocities and densities of the respective media and the angle at which the incident wave strikes the interface.

The acoustic disturbances described by either relation of (1) represent unattenuated traveling plane waves. In this type of wave the magnitude of the change in each physical parameter is the same at all positions in the field. However, if reflection of acoustic energy takes place, then the simple traveling wave field no longer describes the acoustic conditions. Consider first the case of partial reflection at normal incidence. The pressure variation in the medium can be represented analytically as

$$p = P_+ e^{j\omega(t-x/v)} + P_- e^{j\omega(t+x/v)} \tag{7}$$

where P_+ is the amplitude of a pressure wave traveling in the positive direction of x and P_- is the amplitude of a pressure wave traveling in the negative direction of x (Kinsler and Frey, 1950). The term "standing waves" is applied here and the quantity "standing wave ratio" S is introduced. This is defined as the ratio of the maximum to minimum values of the pressure amplitudes in the field. Symbolically

$$S = \left| \frac{P_{\max}}{P_{\min}} \right| \tag{8}$$

where the absolute value notation indicates that only the magnitude of the ratio is to be considered. The standing wave ratio can be determined from experiment by observing, for example, the maximum and minimum values of some variable proportional to the acoustic pressure amplitude. The standing wave ratio can be expressed in terms of the ratio of P_- to P_+ as

$$S = \left| \frac{P_{\max}}{P_{\min}} \right| = \frac{|P_+| + |P_-|}{|P_+| - |P_-|} \tag{9a}$$

$$S = \frac{1 + \left| \frac{P_-}{P_+} \right|}{1 - \left| \frac{P_-}{P_+} \right|} \tag{9b}$$

Obviously if the sound is completely reflected, $P_- = P_+$ and the standing wave ratio is infinite. In practice there are always some losses so that the standing wave ratio is always finite. It is clear from the definition that $S \geqslant 1$ ($S = 1$ for the traveling wave case).

The configurations listed in Table IV are for media within which no acoustic absorption occurs and for which the wavefronts are parallel to all interfaces.

CASE 1. Reflection and transmission at a single interface between two media. The reflection coefficient C_r, the transmission coefficient C_t, and the standing wave ratio in medium 1 are functions only of the ratio of the characteristic acoustic impedances of the two media, $r_{2/1} = (\rho_2 v_2/\rho_1 v_1)$.

CASE 2. A slab of a third medium of thickness L interposed between two media. The reflection coefficient C_r and the transmission coefficient C_t are functions of the ratios of the characteristic impedances and of the quantity $\omega L/v_3$ (equal to $2\pi L/\lambda_3$) which is determined by the ratio of the thickness L and the wavelength in medium 3. If the characteristic impedance of medium 3 is intermediate between those of media 1 and 2, then the transmission coefficient can be maximized by choosing the thickness L to satisfy the relation

$$\frac{L}{\lambda} = \frac{2n - 1}{4} \qquad n = 1,2,3\ldots \tag{10}$$

The transmission coefficient then becomes

$$C_t = \left| \frac{2r_{2/1}}{r_{3/1} + r_{2/3}} \right| \tag{11}$$

That is, the best choice of thickness that can be made for any interposed material (if its characteristic acoustic impedance is anywhere between the values of the other media) is one-quarter wave or odd multiples thereof. In addition, if one is free to choose the interposed material so that its characteristic acoustic impedance is optimum for transmitting the acoustic energy, then the reflected wave in medium 1 can be completely eliminated by choosing the intermediate material so that

$$(\rho_3 v_3)^2 = (\rho_1 v_1)(\rho_2 v_2) \tag{12}$$

If the characteristic acoustic impedance of medium 3 is not between those of the other two media, then the optimum choice of thickness for the slab to obtain the maximum value of the transmission coefficient is an integral multiple of a half-wavelength, i.e.,

$$L/\lambda = n(\tfrac{1}{2}) \qquad n = 1,2,3\ldots$$

the transmission coefficient then becomes the same as that for case 1. If media 1 and 2 have nearly equal characteristic acoustic impedances and if the thickness of the interposed slab satisfies the relation

$$r_{3/1}\left(\frac{\omega L}{v_3}\right) \leqslant \frac{1}{10} \tag{13}$$

then the transmission coefficient does not differ from that of case 1 by more than 1 %. If the characteristic acoustic impedance of medium 3 is less than that of media 1 and 2, then $r_{2/3}$ should be used in place of $r_{3/1}$ in (13).

CASE 3. A plane wave is incident at any angle θ_1 on the plane interface between two media. The angle of refraction θ_2 is the function of the angle of incidence and the ratio of the velocity of sound in the two media. The pressure transmission and reflection coefficients also involve the ratio of characteristic impedances. If $\sin \theta_1 > (v_1/v_2)$, then the incident wave is totally reflected and there is no propagation of a refracted wave in medium 2. It should also be observed from the form of the reflection coefficient that there is no reflected wave if the ratio of velocities satisfies either of the relations

$$\frac{\rho_2}{\rho_1} > \frac{v_1}{v_2} > 1 \qquad \text{or} \qquad \frac{\rho_2}{\rho_1} < \frac{v_1}{v_2} < 1 \tag{14}$$

and if the angle of incidence satisfies the relation

$$\sin \theta_1 = \frac{r_{2/1}^2 - 1}{r_{2/1}^2 - (v_2/v_1)^2} \tag{15}$$

The formulas given in this section are important, for example, in calculating at least approximately, the amplitude of the waves reflected at tissue interfaces, the accuracy of geometric placement or localization of a beam focus deep in tissue, the acoustic velocity values from standing wave data, the magnitude of the effect of the reflected acoustic energy on driving transducers, etc. The formulas are also useful in the design of ultrasonic instruments where considerations of energy transfer from the transducer to the material of interest arise. More complicated configurations of materials and interfaces may arise in practice and examples of such cases will be discussed in the section on focused fields. The formulas of the table which apply to normal incidence can also be used to calculate transmission and reflection properties for plane wave propagation in systems involving liquids and solids. The effects on the field of absorption within a medium will be considered in the section dealing with the physical mechanisms of absorption.

It is desirable to illustrate the formulas of Table IV and to develop some appreciation of the acoustical reflection and refraction characteristics of various combinations of media. Accordingly, some results are listed in Table V.

3. Piezoelectric Transduction

Ultrasound above approximately 100 kc is most conveniently and practically produced by using piezoelectric materials as elements to convert

TABLE IV

PRESSURE AMPLITUDE OF REFLECTED AND TRANSMITTED WAVES FOR VARIOUS COMBINATIONS OF MEDIA[a]

CASE 1: Wave in medium 1 at normal incidence on boundary between medium 1 and medium 2. No energy returned to interface in medium 2. No absorption within media.

Configuration

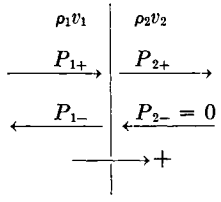

Definition

$$r_{2/1} = \frac{\rho_2 v_2}{\rho_1 v_1}$$

Formulas

$$C_r = \left|\frac{P_{1-}}{P_{1+}}\right| = \left|\frac{1 - r_{2/1}}{1 + r_{2/1}}\right|$$

$$C_t = \left|\frac{P_{2+}}{P_{1+}}\right| = \left|\frac{2r_{2/1}}{1 + r_{2/1}}\right|$$

$$S_1 = \begin{cases} r_{2/1} & \text{when } r_{2/1} \geqslant 1 \\ 1/r_{2/1} & \text{when } r_{2/1} \leqslant 1 \end{cases}$$

CASE 2: Wave in medium 1 at normal incidence. Slab of medium 3 interposed between medium 1 and medium 2. No energy returned to interface in medium 2. No absorption within media.

Configuration

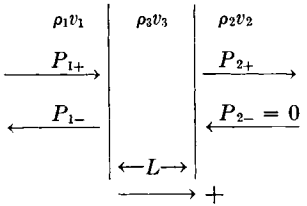

Definitions

$$r_{2/1} = \frac{\rho_2 v_2}{\rho_1 v_1}$$

$$r_{3/1} = \frac{\rho_3 v_3}{\rho_1 v_1}$$

$$r_{2/3} = \frac{\rho_2 v_2}{\rho_3 v_3}$$

Formulas

$$C_r = \left|\frac{P_{1-}}{P_{1+}}\right| = \left[1 - \frac{4r_{2/1}}{(r_{2/1} + 1)^2 \cos^2 \frac{\omega L}{v_3} + (r_{3/1} + r_{2/3})^2 \sin^2 \frac{\omega L}{v_3}}\right]^{1/2}$$

$$C_t = \left|\frac{P_{2+}}{P_{1+}}\right| = \left[\frac{4r_{2/1}^2}{(r_{2/1} + 1)^2 \cos^2 \frac{\omega L}{v_3} + (r_{3/1} + r_{2/3})^2 \sin^2 \frac{\omega L}{v_3}}\right]^{1/2}$$

CASE 3: Wave in medium 1 incident at angle θ_1 with respect to normal on boundary between medium 1 and medium 2. No energy returned to interface in medium 2. No absorption within media.

Configuration

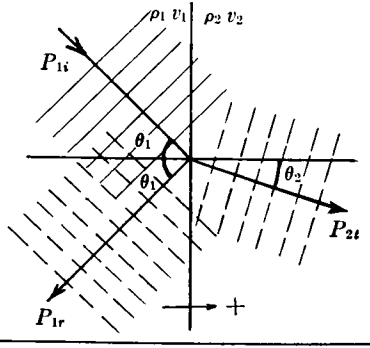

Definition

$$r_{2/1} = \frac{\rho_2 v_2}{\rho_1 v_1}$$

Formulas

$$C_r = \left|\frac{P_{1r}}{P_{1i}}\right| = \left|\frac{\dfrac{\cos\theta_2}{\cos\theta_1} - r_{2/1}}{\dfrac{\cos\theta_2}{\cos\theta_1} + r_{2/1}}\right|$$

$$C_t = \left|\frac{P_{2t}}{P_{1i}}\right| = \left|\frac{2r_{2/1}\cos\theta_1}{\cos\theta_2 + r_{2/1}}\right|$$

$$\frac{\sin\theta_1}{\sin\theta_2} = \frac{v_1}{v_2}$$

[a] *Note:* Only the ratios of the magnitudes of the pressure amplitudes are listed, i.e., the phase factors are not included.

TABLE V

NUMERICAL EXAMPLES OF ACOUSTICAL REFLECTION AND REFRACTION CHARACTERISTICS AT 30°C

System	Angle of incidence	$r_{2/1}$	Transmission coefficient	Reflection coefficient
Water–air	Normal	0.000271	0.00054	0.99946
Water–castor oil		0.9136	0.9548	0.0452
Water–air	10°	0.000271	0.00054	0.99946
Water–castor oil		0.9136	0.9473	0.0457
Water–air	45°	0.000271	0.00039	0.99961
Water–castor oil		0.9136	0.7847	0.0630
Water–castor oil	60°	0.9136	0.6229	0.0954

electrical energy to mechanical or acoustical energy (Hueter and Bolt, 1955). These elements can also be used to transform in the inverse direction, i.e., acoustical energy to electrical energy. Such elements are cut, with proper orientation, from crystals which possess the piezoelectric property to a sufficiently marked degree or from suitably prepared ceramic materials (Mason, 1950). The problem of choosing the proper orientation is not discussed here; rather, information concerning particular elements suitable for ultrasonic transducers is presented. This is illustrated by the diagrams of Fig. 2. Three different types of piezoelectric elements are illustrated. In the first type, Fig. 2a, a pressure applied to the large faces of a plate (of any peripheral shape) produces a change in dimensions of the type shown and an electric field $\mathcal{E}$ in the direction indicated by the arrow. If the large faces are covered with electrodes, a voltage will be developed between the two faces. Conversely, if a voltage is applied across the two faces, then dimensional changes of the type indicated will occur. For most of the materials presently available for use as such plate elements, it is not possible simultaneously to apply the pressure to the lateral and plate surfaces and still have a voltage difference develop between the two faces. Quartz and various ceramic materials are most conveniently employed for such elements for the ultrasonic frequency range above 100 kc. Since operation at resonance is essential for high power output and since the thickness of the plate determines the resonant frequencies, this results in a practical configuration, i.e., the electric driving voltage is applied across the smallest dimension and sound is radiated from the large face(s). The piezoelectric element illustrated in Fig. 2b produces an electric field when pressure is applied simultaneously to all faces. This type of element is useful in ultrasonic probes, small compared to a wavelength, where the

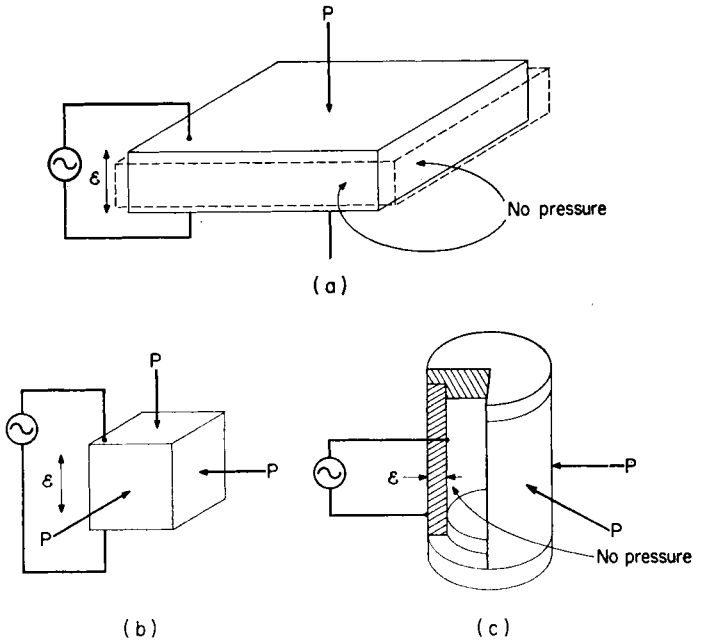

FIG. 2. Piezoelectric transducer elements: (a) plate element; (b) hydrostatic probe element; (c) cylindrical probe element.

sound pressure about the element is essentially constant. Materials such as lithium sulfate and tourmaline are useful in this type of application. A hollow cylindrical ceramic element is illustrated in Fig. 2c. The ceramic materials are advantageous since they can be produced in a variety of shapes and the preparation can be accomplished so that a variety of configurational relations between applied pressure and produced electric field (and conversely) can be realized. For the particular element shown, a pressure applied to the outer cylindrical surface only will generate an electric field between the inner and outer surfaces and vice versa.

The type of element illustrated in Fig. 2a is of primary concern here for the generation of ultrasound and some discussion of the element illustrated in Fig. 2b is given for probe applications.

a. TRANSMITTERS

The suitability of a material for use in transducers for producing ultrasound is dependent upon a number of factors, the relative importance of which is determined by the application. These factors include the magnitude of the piezoelectric coefficients, stability, dielectric properties, electrical breakdown strength, and tensile strength of the material. Quartz (the X-cut orientation is the one used for the plate mode) has high sta-

bility, high electric and tensile strength, but it requires relatively high electric field strengths to obtain high power outputs. On the other hand, barium titanate ceramic possesses a much higher dielectric constant, requiring much lower electric field strength for an equal power output from the same size radiating area. It has the disadvantages of lesser stability than quartz and too low an impedance at high frequencies. Consequently, at the present time, if accurate reproducibility of irradiation conditions is essential to a study (for example, the induction of selective changes in tissue structures), then quartz is the material of choice for transducers. However, if accurate reproducibility is not important, the ceramic materials may be used. It is necessary to estimate the acoustic output from transducer elements as a function of driving voltage in order to assess the feasibility of proposed ultrasonic studies. The design and size of transducers required to obtain desired values of the ultrasonic field parameters or configurations of acoustic fields are also dependent on the power output characteristics. It is also necessary to estimate the electrical impedance of the transducer so that it can be driven by an appropriate electronic power amplifier and coupling circuit. Accordingly, the values of the appropriate constants of a number of transducer materials, together with simplified formulas and graphs for estimating quantities of importance, are included in Table VI.

It should be noted that the relation between the voltage applied to an element (which is equal to the product of the electric field strength and the distance between the electroded faces) and the pressure or particle velocity produced at its boundary in contact with a medium is linear; that is, the pressure or particle velocity amplitude is proportional to the first power of the applied voltage. The pressure or particle velocity produced in the medium in contact with the element is also a function of the acoustic properties of that medium and the configuration, dimensions, and acoustic properties of other media to which it in turn is coupled. That is, these media constitute the load on the element and they determine the magnitude of the pressure which must be exerted by the element on the bounding medium under a given electrical driving situation.

Consider the configuration of Fig. 3 in which a piezoelectric element is electrically excited to vibrate in a plate thickness mode to radiate acoustic energy into a medium of characteristic impedance ρv which is in contact with the element over one of the large faces. It is assumed that the medium in contact with the opposite face has an extremely low impedance so that virtually no radiation occurs from this face, i.e., ρv for this medium may be considered equal to zero in comparison with that of the other medium. It is possible to achieve this situation for all practical purposes if the medium on the right is a liquid and the element is supported near its periphery

and is air-backed. It is also assumed, for purposes of simplifying the relations given here, that comparatively no losses occur in the holder and that the element is essentially unrestrained as far as its vibration is concerned except by the medium into which it radiates. Under these conditions the "average" intensity I produced at the face of the crystal operating at the lowest resonant frequency is given by

$$I = \frac{4}{(10)^4} e^2 \left(\frac{E}{L_c}\right)^2 \frac{1}{\rho v} \tag{16}$$

where E designates the applied voltage and e is a constant determined by the type and orientation of the material from which the piezoelectric element is made (Hueter and Bolt, 1955). If, from the formula, one wishes to obtain the intensity in watts per square centimeter, the value of e should be expressed as coulombs per square meter as listed in Table VI. The units of ρv should be kilograms per square meter per second which can be obtained by multiplying the value of ρv in grams per square centimeter per second by 10. The unit of L_c should be the meter. The value of the intensity given by (16) is constant over the area of the vibrating element at the surface of the element. Due to Fresnel and Fraunhoffer diffraction of the waves in the regions "near to" and "far from" the sound source, the distribution of the acoustic field variables (intensity, pressure, particle ve-

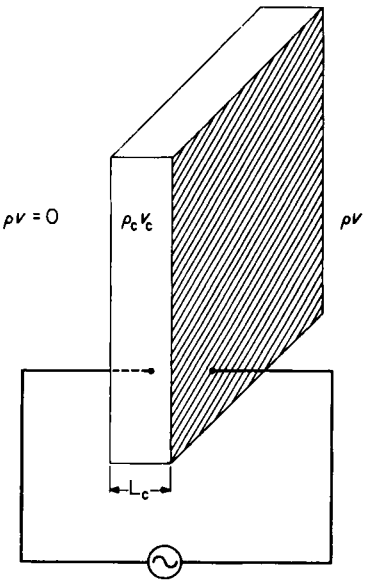

FIG. 3. Schematic arrangement showing piezoelectric element excited to vibrate in a plate thickness mode to radiate acoustic energy into medium of characteristic impedance ρv.

locity, etc.) is not constant over a plane parallel to the vibrating surface. (This is discussed more fully in Section III.) Consequently, the transverse intensity distribution may exhibit one or more maxima and minima; one such form is shown in Fig. 4, as an example. The average intensity I_{av} in the plane is determined by integrating the intensity distribution to obtain the total acoustical power and then dividing by the area of the distribution. The peak value of the intensity I_p is related to I_{av} and the integration procedure by

$$\sigma = \frac{2\pi \int_0^{r_0} I_r(r) r \, dr}{I_p A_{r_0}} = \frac{I_{av}}{I_p} \tag{17}$$

The intensity given by (16) can be related to I_p by the relation

$$I_p = \frac{\eta I A}{\sigma A_{r_0}} \tag{18}$$

where A_{r_0} is the area of the distribution, A is the area of the vibrating element, and η is an efficiency factor. Refer to Section III for illustrations of the use of (18) in the evaluation of I_p from a knowledge of intensity distribution (beam pattern) and representative values for the efficiency factor. The lowest resonant frequency of the element is determined by the relation

$$f_r = \frac{v_c}{2L_c} \tag{19}$$

where L_c designates the thickness of the element and v_c is the plate velocity (the speed of sound across the thickness of the element). Table VI lists

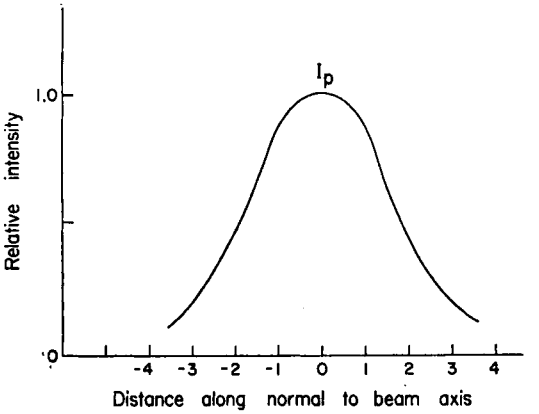

FIG. 4. Relative acoustic intensity distribution in a plane parallel to the vibrating surface.

TABLE VI

PHYSICAL CONSTANTS OF PIEZOELECTRIC MATERIALS

Material	ρ_c (gm/cm³)	v_c (cm/sec)	$\rho_c v_c$ (gm/cm² sec)	e (coul/m²)	d (m/v)	$\epsilon_0 K$ (farad/m)	r (Ω-m)	T_b (d/cm²)
Multiply Figures in Table by	1	10^5	10^5	1	10^{-12}	10^{-12}	10^9	10^8
Quartz, X-cut	2.65	5.72	15.16	0.176	2.04	40.6	>1000	7.6
95 wt % $BaTiO_3$ 5 wt % $CaTiO_3$, plate	5.5	5.68	31.24	16.65	150	10,800	>100	10
PZT-4	7.5	4.0	30.0	17.15	256	10,600	>100	10
Lithium sulfate, Y-cut	2.06				13	91.5	>10	
Tourmaline, Z-cut	3.1				2.16	66.5	>100	

values of the constants e, v_c, and $\rho_c v_c$ for different materials used as elements for thickness mode operation. In order for (16) to apply, it is necessary that no acoustic energy be reflected back to the radiating face and that the diameter of the vibrating element be greater than about one wavelength. This implies that the input acoustic impedance P/U into the contacting medium approximates a pure resistance (equal to ρv in this case). Calculations for a few typical cases are listed in Table VII.

Values for the breaking stress of the various materials are listed in Table VI from which one may calculate the maximum intensity obtainable (plane wave) with this as a limiting factor. The relation between the breaking stress T_b and the particle velocity amplitude $U_{\max}$ at the surface of a resonating element is (Hueter, 1951)

$$U_{\max} = \frac{T_b}{\rho_c v_c} \tag{20}$$

where $U_{\max}$ is in centimeters per second if T_b is in dynes per square centimeter and $\rho_c v_c$ is in grams per square centimeter per second. Relation (20) can be used with (5) to determine the maximum value of the intensity

TABLE VII

ACOUSTIC INTENSITY PRODUCED IN WATER BY QUARTZ RADIATOR AT 30°C

f (mc)	L_c (cm)	E (v)	I (w/cm²)
1	0.286	1000	1
1	0.286	5000	25
10	0.0286	1000	100
10	0.0286	5000	2500

that can be produced in a medium when the tensile strength of the vibrating element is the limiting factor. The electric field required to obtain the maximum stress can be computed using relations (5) and (16). The limitation imposed by the breaking stress does not set an upper limit on the obtainable intensity. Focusing systems and other configurations enable the production of acoustic intensities far in excess of those limited by the mechanical strength of the piezoelectric material (see Section II, 4, *b*). The maximum intensity obtainable using X-cut quartz limited by mechanical failure is 2000 w/cm^2 in water and 0.5 w/cm^2 in air. The corresponding values for barium titanate are 800 w/cm^2 in water and 0.2 w/cm^2 in air. The ceramic materials are made piezoelectric by prepolarization. During each half-cycle of operation, the applied electric field is opposite to the original polarizing field and if sufficiently great may produce partial depolarization, which reduces the piezoelectric activity of the element. That is, under some conditions of operation, the applied electric field, rather than the breaking stress, may limit the maximum intensity obtainable with these materials (Hueter and Bolt, 1955).

The variation of the radiated intensity as one moves off resonant operation (at constant driving voltage across the element) is illustrated by the graph of Fig. 5. This figure can be used to compute the output intensity for the type of system just discussed for a range of values of the ratio $\rho_c v_c/\rho v$ of the characteristic impedances of the crystal and the medium, and for a wide range of values of the frequency. The quantity γ_c is given by the relation

$$\gamma_c = 180(f/f_r)$$

where f is the operating frequency, f_r is the first resonant frequency, and γ_c is expressed in degrees. It should be noted that *relative* intensity is plotted along the vertical axis of the graph. The figure thus illustrates the relative sharpness of resonant operation under different loading conditions, i.e., for media of different characteristic impedances. The intensity at any off resonant frequency is obtained by calculating the product of the result of (16) and the value of the relative intensity for the value of γ_c corresponding to the frequency of interest and for the value of the parameter $\rho_c v_c/\rho v$ for the materials under consideration. This assumes that the driving voltage across the element is constant. Since the input electrical impedance of the element changes with frequency, some adjustment of the generator may be necessary to maintain the constant voltage condition.

It is necessary to know, at least approximately, the electrical input impedance of the piezoelectric elements in order to be able to specify the characteristics of the electronic generators required to furnish the power. For elements loaded as just discussed, i.e., no load on one face and terminated in the characteristic impedance of the bounding medium on the

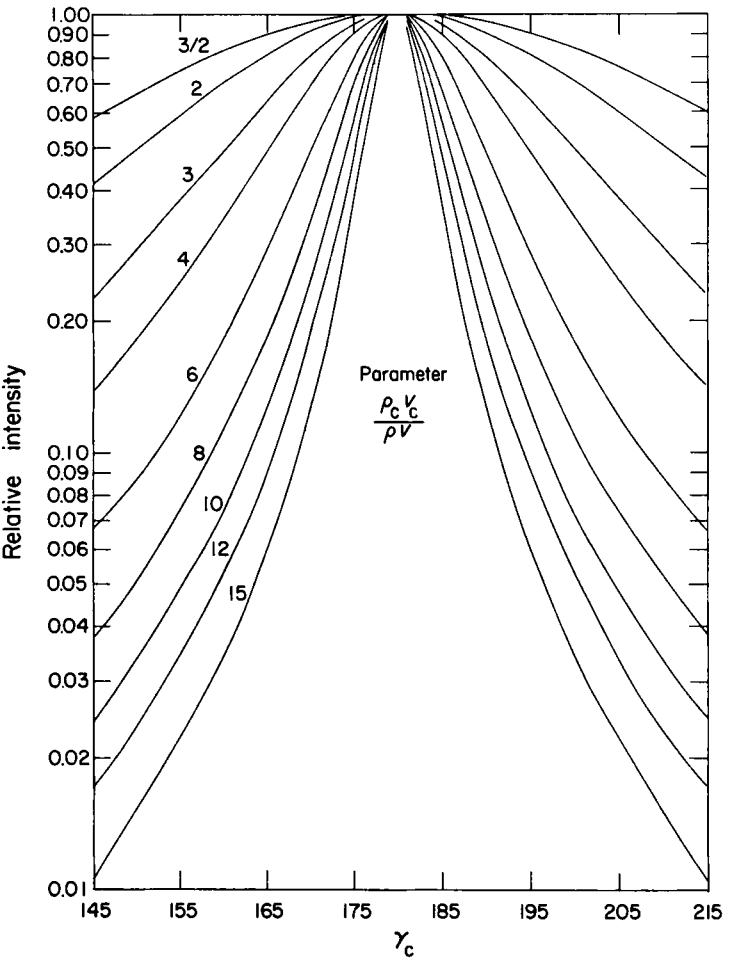

FIG. 5. Relative acoustic intensity radiated by piezoelectric element versus frequency, at constant driving voltage. The parameter from curve to curve is the ratio of the characteristic acoustic impedance of the piezoelectric element to that of the medium.

other large face, the electrical input impedance relation takes the following form at resonance (W. J. Fry *et al.*, 1948)

$$Z_e = \frac{1}{j\omega C_0 + (4e^2/\rho v)(A/L_c^2)} \tag{21}$$

where

$$C_0 = \frac{\epsilon_0 K A}{L_c} \tag{22}$$

The first term in the denominator of (21) arises as a result of the "static" capacitance of the element and can be calculated from (22) where K designates the dielectric constant relative to free space, ϵ_0 designates the dielectric permittivity of free space, and A is the radiating area of the element. The product $\epsilon_0 K$ is listed in Table VI for various piezoelectric materials. All other symbols have been defined previously. The term ρv designates the characteristic impedance of the bounding medium as in relation (16). Expression (21) can be represented as an equivalent electrical circuit of two branches as illustrated in Fig. 6. One branch of this parallel circuit represents the static capacitance of the piezoelectric element and the other branch represents the "motional" impedance, i.e., the part of the electrical input impedance which results from the fact that mechanical motion of the element and bounding medium modify the electric field between the electrodes. Since (21) applies to resonant operation, the electrical impedance of the motional branch is a pure "resistance" and is thus represented as a real number. For off-resonant operation, the motional branch would contain both a real and an imaginary part. Formula (21) is derived by neglecting all losses except radiation losses into the bounding medium and by assuming that the piezoelectric element holder does not appreciably affect the operation of the element (W. J. Fry *et al.*, 1948). These assumptions are reasonable for calculating approximate values of the electrical input impedance if the element is radiating into a liquid medium and if the opposite face is bounded by a gas or by a material of comparatively low characteristic impedance. It should be noted that if the electrical power to the element is supplied by a cable of capacitance C_c, then the quantity C_0 of (21) is replaced by $C_0 + C_c$ when calculating the electrical input impedance at the cable terminals.

b. Receivers

Piezoelectric elements are also used to measure ultrasonic field characteristics. Used in this way, the element responds by producing an electric field between two electrodes, placed on appropriate faces, when the element is subjected to the changing pressure of the sound field. Several different types of elements are useful. The plate type (Fig. 2a) is of the same form as that

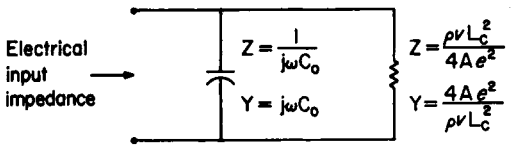

Fig. 6. Equivalent electrical circuit of piezoelectric plate element operating at resonance and radiating from one face only. See relation (21).

discussed above for the generation of sound. This type of element is useful when the energy to be detected is in the form of waves whose fronts or surfaces of constant phase are closely planar and when it is *not* desired to observe variations in the field which occur over an area small compared to the area of the detector. Such plate detectors interfere drastically with the field. The other types of piezoelectric detectors are illustrated in Figs. 2b and 2c. The desired design is one in which the maximum dimension of the detector is small compared to one wavelength of the sound in the medium. This goal is easily attained at frequencies below 100 kc but it cannot be achieved at a few hundred kilocycles per second and higher. Two major difficulties arise. First, the input impedance becomes so high that it is difficult to realize a reasonable sensitivity. Second, construction of the device and the associated electrical connections raise major technique problems. Consequently in the neighborhood of 1 mc, the smallest probes of the piezoelectric type are not smaller than ½ to 1 wavelength in maximum dimension. In general, they are sensitive to direction of orientation in the field and with them precision measurements of sound levels are not possible in the megacycle per second frequency range. However, such probes are employed in this frequency range for the determination of field characteristics in which the relative time phase at different positions in the field is desired. Precision measurements of sound levels capable of resolving the fine structure of ultrasonic fields in the megacycle per second frequency range can be realized with the thermocouple probes discussed in Section III.

Consider first receivers for which the "maximum diameter" is small compared to a wavelength of sound in the medium. One such configuration is the rectangular solid element illustrated in Fig. 2b. The usual difficulty which arises at ultrasonic frequencies, even below 1 mc, is the realization of small size. Hence, it is most convenient to use a piezoelectric element which responds when it experiences a pressure over all faces simultaneously. Elements such as lithium sulfate and tourmaline possess this property and in this case it is not necessary to design a holder which decouples some of the faces from the medium in which the sound field exists.

When such an element is subjected to an acoustic pressure amplitude P, a voltage of amplitude E will appear across a load. The relation between the magnitudes of these quantities is

$$\left|\frac{E}{P}\right| = \frac{\omega A d}{10\sqrt{(1/R^2) + (\omega C)^2}} \tag{23}$$

where C is the shunt capacitance of the electrical load C_L, combined with that, C_0, of the crystal, i.e., $C = C_0 + C_L$; R is the shunt resistance R_e of the piezoelectric element combined with that, R_L, of the load; A is the

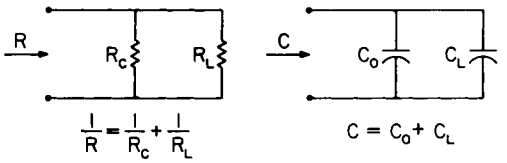

FIG. 7. Equivalent electrical circuits showing shunt capacity and shunt resistance of hydrostatic piezoelectric probe. See relation (23).

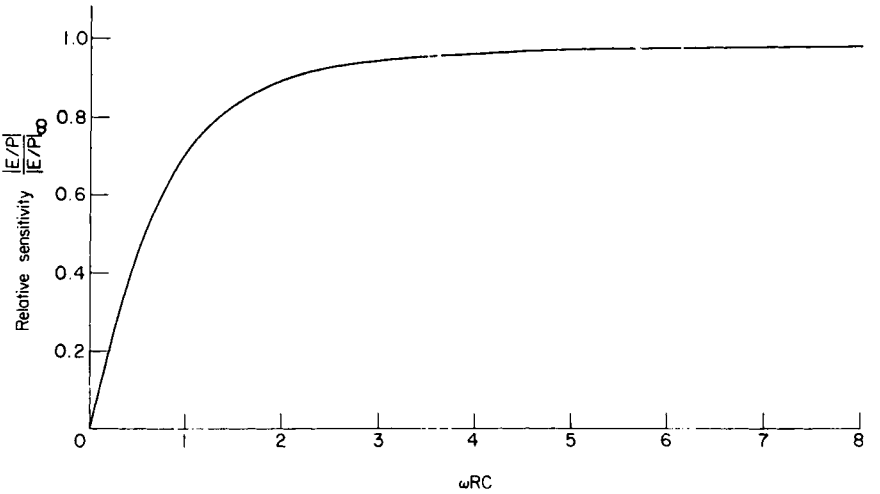

FIG. 8. Relative sensitivity of probe versus ωRC. See relation (23).

area of an electroded face; and d is the piezoelectric coupling parameter listed in Table VI. See Fig. 7 for the relations between these quantities. If R and $1/\omega C$ are expressed in ohms, d in meters per volt, A in square meters, and P in dynes per square centimeter, then E is in volts. From (23) it is clear that an increase in the shunt capacitance across the element results in a decrease in sensitivity. In addition it is apparent that, as the frequency decreases for any given element, the sensitivity begins to decrease when the magnitude of the capacitive reactance $1/\omega C$ becomes comparable to and larger than the shunt resistance R. This is illustrated in Fig. 8 where the voltage output per unit pressure is shown as a function of the nondimensional quantity ωRC. The sensitivity is independent of the frequency (as long as the maximum diameter of the element is much smaller than the wavelength) when $R \gg 1/\omega C$ and is given by

$$\left|\frac{E}{P}\right|_\infty = \frac{Ad}{10(C_0 + C_L)} \tag{24}$$

The sensitivity drops to one-half this value for a frequency $f_{1/2}$, which satisfies the relation

$$f_{1/2} = \frac{1}{2\pi\sqrt{3}} \frac{1}{R(C_0 + C_L)} \tag{25}$$

The frequency is in cycles per second if R is in ohms and $C_0 + C_L$ in farads. It is clear that the flat portion of the sensitivity curve can be extended to lower frequencies by increasing the capacitance of the load, but the sensitivity is correspondingly decreased over that flat portion of the frequency range. It is important therefore, if low-frequency operation at high sensitivity is required, to use for the piezoelectric element a material of high volume resistivity. Specific examples are shown in Table VIII. The upper end of the flat response range of sensitivity is limited by the resonant frequency f_r which can be estimated, for probes of such shape, by a computation employing expression (19) and values of v_c from Table VI.

Another probe configuration with maximum diameter small compared to the wavelength is illustrated in Fig. 2c. This is a tubular piezoelectric ceramic type designed so that an electric field oriented along the radii between the inner and outer electrodes appears in response to a pressure exerted over the entire outer surface of the cylinder including the end terminations. The fluid in the interior of the cylindrical tube is decoupled from the external medium by the end caps. In order for such a probe to be nondirectional in the sound field, it is necessary that it be of small linear dimensions compared to a wavelength. Such probes have been constructed with dimensions as small as $\frac{1}{16}$ in. in length and $\frac{1}{16}$ in. in outside diameter (Ackerman and Holak, 1954). With these dimensions the probes are nondirectional at frequencies up to about 100 kc (λ = 1.5 cm in saline) and are useful qualitatively up to nearly 1 mc. They cannot be used to determine sound levels quantitatively above about 100 kc, but are useful in obtaining some idea of acoustic field configurations at frequencies up to the 1 mc range (λ = 1.5 mm). A probe of the size just indicated with a

TABLE VIII

NUMERICAL EXAMPLES OF NONRESONANT PIEZOELECTRIC PROBES

Material	d (m/v)	A (m^2)	C (farad)	R (ohms)	E/p (v/d/ cm^2)	E/p (v/ atm)	$f_{1/2}$ (cps)	f_r (kc)
Multiply figures in table by	10^{-12}	10^{-6}	10^{-14}	10^{12}	10^{-5}	1	1	1
Lithium sulfate (Y-cut)	13	4	18.3	5	2.84	28.8	0.1	1380
Tourmaline (X-cut)	2.16	4	13.3	50	0.65	6.6	0.014	1800

wall thickness of 0.012 in. has an "open circuit" pressure sensitivity of the order of 10^{-7} v/d/cm^2.

A very important consideration in the design of piezoelectric probes of the types just described is the decoupling of the piezoelectric element from the supporting structure which may also be excited to vibrate by virtue of its presence in the sound field. If sufficient sound energy is conducted to the element by the supporting structure, then the probe can exhibit a voltage across its output terminals which corresponds more nearly to the sound level along the supporting structure rather than that at the piezoelectric element.

Consider now receivers which operate at resonance. The piezoelectric element, in many such cases in which the operating frequency is of the order of one megacycle per second or above, takes the form illustrated in Fig. 2a. That is, the thickness of the element is chosen to result in resonant operation at the frequency of the acoustic field. In this case the "diameter" of the large plate face may be many wavelengths across and in fact in some applications the same element may act as transmitter and receiver. For example in studies of macroscopic tissue structure visualization, the element is of such a diameter as to produce a directed pulsed beam which, after partial reflection at tissue interfaces and structural discontinuities, is received by the same element.

The relation between element thickness and resonant frequency is given by relation (19) when the vibrating element is backed by a low acoustic impedance, air for example. The sensitivity can be increased by employing an inductance in parallel with the element and associated cable of such value as to result in a parallel resonance at the mechanical resonant frequency of the element. If C is the total capacitance of the element and cable, i.e.,

$$C = C_0 + C_L \tag{26}$$

then the condition for parallel resonance is

$$\omega_r L = \frac{1}{\omega_r(C_0 + C_L)} \tag{27}$$

where L is the magnitude of the inductance of the tuning coil or element. At resonance if the electrical Q of this coil is equal to or greater than 10, then the impedance of this parallel circuit is equal to $Q\omega_r L$ and is resistive. Then if the shunt resistance of the piezoelectric element and associated losses are designated by R_c and the resistance of the load is R_L (the in-

put impedance into an amplifier), the sensitivity of the receiver is

$$\frac{E}{P} = \frac{4}{100} \frac{\left(\frac{eA/L_c}{\rho v}\right)}{\frac{1}{R_L} + \frac{1}{R_c} + \frac{1}{Q\omega_r L} + \frac{4(eA/L_c)^2}{10A\rho v}} \tag{28}$$

where P is the pressure amplitude of the acoustic field without the receiver and E is the voltage produced across the load. The quantity e is the appropriate piezoelectric coupling parameter for the element as given in Table VI and ρv is the characteristic acoustic impedance of the medium in which the receiver is placed. If A is expressed in square meters, L_c in meters, ρv in grams per square centimeter per second, R_L and R_c in ohms, L in henries, e in coulombs per square meter, and P in dynes per square centimeter, then E is in volts. The form of the denominator of (28) permits the representation in terms of electrical circuit elements as illustrated in Fig. 9, i.e., a parallel arrangement of the four elements, the reciprocal of the input impedance being equal to the denominator expression.

If the quantity $1/R_L$ is much smaller than the combination of other terms in the denominator of (28) and $C_L = 0$, then it is possible to rewrite (28) as

$$\frac{E}{P} = \frac{4}{100} \frac{e/\rho v}{(1/r) + \omega_r[(\epsilon_0 K/Q) + (40e^2/\pi v_c \rho v)]} \tag{29}$$

where the same units as used for (28) apply and v_c is in units of centimeters per second. Values for the quantities e, $\epsilon_0 K$, r, and v_c are tabulated in Table VI. Several numerical examples illustrating the magnitudes of the quantities involved for various types of piezoelectric elements are given in Table IX.

4. Ultrasonic Field Configurations

a. Unfocused Fields

When ultrasound is employed in studies of biological systems, it is desirable to arrange the experimental conditions so that all positions within

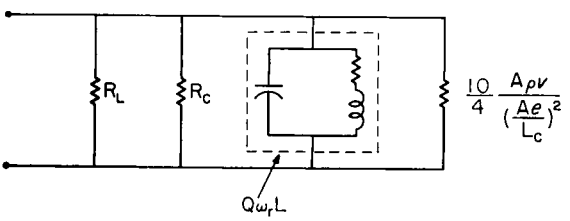

FIG. 9. Equivalent electrical circuit of resonant, plate-type piezoelectric receiver and associated circuitry. See relation (28).

TABLE IX

NUMERICAL EXAMPLES OF RESONANT PIEZOELECTRIC PROBES

Material	Q	A (m^2)	f_r (mc)	C_L (farads)	ρv (gm/ cm^2 sec)	E/P (v/d/ cm^2)	E/P (v/ atm)	$R_L \gg$ (ohms)
Multiply Figures in Table by	1	10^{-4}	1	1	10^5	10^{-4}	10^{-10}	10^3
Quartz (X-cut)	100	1	1	0	1.5	16	16	1000
Barium titanate (plate)	100	1	1	0	1.5	0.15	0.15	0.1

a particular volume of the system (tissue, cell suspension, solution of macromolecules) receive identical irradiation. Also, in order to facilitate interpretation of the experimental results in terms of a particular mechanism, etc., it is desirable to use as simple a field configuration as possible, for example, one in which the pressure amplitude does not vary with the time during the exposure period at a fixed site. Appropriately designed unfocused fields can be used provided that the intervening material can be subjected to radiation at the level required at the target sites or volumes. Uniformity of field parameters at high sound levels, over volumes of the medium several wavelengths in diameter, is not attained without careful design of the irradiator. It is possible to attain any desired degree of uniformity in a volume of fixed size by going further and further away from the source. However, since the intensity decreases as the inverse square of the distance, it is not possible to utilize this method if high sound levels are required, since the irradiators may not be capable of producing the needed acoustic power. Much of the interesting work requires sound levels approaching the limits which can be produced by nonfocusing irradiators (Section II, 3, *a*). Increasing the size of the source does not solve the problem since the distance at which one can realize a desired degree of field uniformity increases as the source size increases. In addition, if the simultaneous irradiation of a relatively large volume of material is desired and a large diameter (relative to wavelength) source is used, the so-called "near field" extends so far from the source that the apparatus becomes cumbersome from the viewpoint of size. That is, in order to avoid the processing (degassing or other treatment) of large volumes of liquid in preparation for each operation at high sound levels, the sound tank must possess, for example, an hermetically sealed degassed liquid-filled chamber sufficiently large to contain the near field.

The important factors for determining the detailed acoustic field distribution produced by a nonfocusing irradiator are: (1) size of the irradi-

ator relative to the wavelength of the sound in the transmitting medium; (2) shape of the irradiator; (3) vibration amplitude distribution over the surface of the irradiator; and (4) acoustic absorption coefficient of the medium at the frequency of the acoustic field. It is convenient to discuss acoustic fields produced by nonfocusing irradiators by first considering the field near the irradiator (the Fresnel region)[6] and then considering the far field (the Fraunhofer region).

The dependence of the field configuration on the factors listed above is illustrated by discussing fields produced by plane circular vibrating surfaces. The formulas given can be used to estimate the effects of varying various dimensional parameters. At present, the design of an acoustic field must depend to a certain extent on experimental measurement since it is extremely difficult to give a complete and precise theoretical account encompassing all the factors which influence the detailed structure of the field. The relatively simple expressions given here, together with the diagrams, illustrate and permit computation of the principal features. When a high degree of uniformity (of the order of 1%) over a relatively large volume (a few wavelengths or more in diameter) is desired, recourse to alternate computation and measurement appears to be the most practical approach to irradiator design.

(1) Near Field. The near field distribution exhibits a number of maxima and minima along the axis of the irradiator (Hueter and Bolt, 1955; Kinsler and Frey, 1950). The positions and amplitudes of these extrema depend greatly upon the velocity amplitude distribution over the source and upon the ratio of source diameter to wavelength. Characteristics of the near field for the case of a uniform particle velocity amplitude distribution over the irradiator surface are discussed with the aid of a number of relatively simple quantitative relations and graphs. The effects of modifying the uniform distribution function by superimposing upon it space dependent functions are then illustrated graphically.

The graphs of Fig. 10 show, for the plane circular vibrating element, the calculated axial field distributions of the near field for three different values of the ratio of the radius R to the wavelength λ. The velocity amplitude distribution is uniform over the element. The field distribution (relative pressure amplitude) is shown as a function of the ratio of the distance along the axis of the element to the radius of the element. The vibrating surface of the element is at $x/R = 0$. At distances beyond the furthest maximum, the pressure amplitude decreases monotonically and inversely as the distance from the vibrating surface. The extent of the near field and the number of maxima and minima along the axis are determined by the quantity

[6] This terminology will be made more precise later in this subsection.

R/λ. The distance to the maximum furthest from the vibrating surface (called the zeroth-order maximum) is given by

$$\left(\frac{x_0}{R}\right)_{\max} = \frac{R}{\lambda} - \frac{1}{4(R/\lambda)} \tag{30}$$

If $R/\lambda \gg 1$,

$$\left(\frac{x_0}{R}\right)_{\max} \simeq \frac{R}{\lambda} \tag{31}$$

The quantity $(x_0/R)_{\max}$ is the distance (measured in terms of radii of the vibrating element) from the face of the irradiator at which the transition from near to far field occurs. The number of maxima N in the near field can be obtained from the relation

$$\frac{R}{\lambda} + \frac{1}{2} > N \tag{32}$$

that is, N is the nearest integer less than the numerical value of the left-hand term of this relation. It should be noted that, when $R/\lambda \gg 1$, the extent (in terms of radii of the element) and number of maxima in the near field region are both nearly equal to the number of wavelengths of sound contained in the radius of the vibrating element exposed to the medium. The distance between adjacent extrema decreases as one moves from the transition region toward the element. This spacing distance between adjacent maxima and minima may be expressed as

$$\left(\frac{x_m}{R}\right)_{\max} - \left(\frac{x_m}{R}\right)_{\min} \simeq \left(\frac{R}{\lambda}\right)\left[\frac{1}{2(m+1)(2m+1)}\right] + \frac{1}{4(R/\lambda)} \tag{33}$$

The integer m designates the order of the extrema starting with zero as most distant from the element both for the set of maxima and the set of minima. The distance from the sound source to the extrema is

$$\left(\frac{x_m}{R}\right)_{\max} = \left(\frac{1}{2m+1}\right)\frac{R}{\lambda} - \left(\frac{2m+1}{4}\right)\frac{1}{R/\lambda} \tag{34a}$$

$$\left(\frac{x_m}{R}\right)_{\min} = \left(\frac{1}{2m+1}\right)\frac{R}{\lambda} - \left(\frac{m+1}{2}\right)\frac{1}{R/\lambda} \tag{34b}$$

If $R/\lambda > 1$, the situation of interest here, the integer m satisfies the relation $1 \leqslant m \leqslant R/\lambda$. The spacing distance between the most distant maximum, $(x_0/R)_{\max}$, and minimum, $(x_0/R)_{\min}$, is

$$\left(\frac{x_0}{R}\right)_{\max} - \left(\frac{x_0}{R}\right)_{\min} = \frac{1}{2}\left(\frac{R}{\lambda}\right) + \frac{1}{4(R/\lambda)} \tag{35}$$

If $R/\lambda \gg 1$, this distance expression becomes

$$\frac{1}{2}\left(\frac{R}{\lambda}\right) \tag{36}$$

The distance between the maximum and minimum nearest the element is, if $R/\lambda \gg 1$, given approximately by

$$\frac{1}{2(R/\lambda)} \tag{37}$$

It is clear from (31), (32), (36), and (37) that for any element, as the operating frequency increases, i.e., the wavelength in the medium decreases, the zero-order maximum recedes further from the element, the number of extrema increase, the distance between the zero-order maximum and minimum increases, all of which changes are proportional to the first power of the frequency. Further, the distance between the maximum and minimum nearest the element decreases in such a way as to be directly proportional to the first power of the wavelength. That is, even though the distance from the source to the transition region increases and the number of extrema in the near field increases proportionally, the spacing between extrema nearest the element and furthest from it change—spreading occurring between the more distant ones and compression occurring between the proximal ones. These features are illustrated by the three graphs of Fig. 10 computed for R/λ equal to $1\frac{1}{6}$, $5\frac{5}{6}$, and $11\frac{2}{3}$. It should be noted that the amplitude of the swing from maximum to minimum decreases starting from the furthest maximum and moving in the direction of the element. Table X contains several numerical examples which serve to illustrate the order of magnitude of the quantities involved.

The field distribution normal to the axis of the beam also exhibits a fairly complex structure in the near field. The number of extrema in the transverse field pattern changes with position along the axis of the beam. Such pattern shifts occur in increments of distance along the axis corresponding to positions of adjacent extrema. Calculated transverse distribution patterns are not presented here, but examples of experimentally determined patterns are given in Section III, 2.

When nonuniform vibration amplitude distributions exist over the radiating face of the element, some shifting of the positions of the various extrema in the near field and drastic modifications of the amplitude of the swing from maximum to minimum of these extrema occur (W. J. Fry and Brunschwig, 1958). The position of the zero-order maximum and the number of extrema are still given approximately by expressions (30) and (32). The relatively simple picture of Fig. 10 is modified so that, in place of the monotonic decrease in amplitude of swing, as the vibrating element is

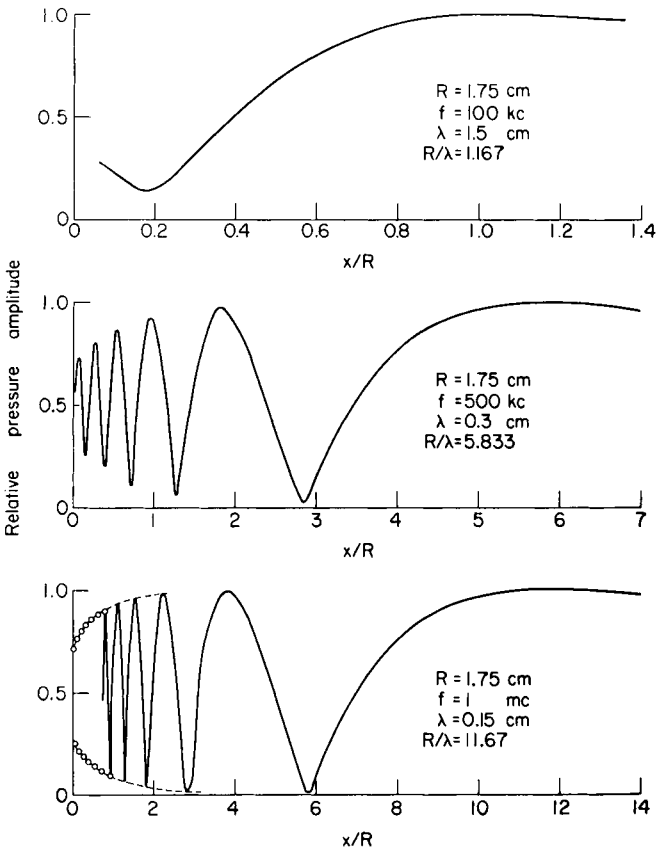

FIG. 10. Axial pressure amplitude distribution in the near field produced by a uniformly vibrating plane circular element (after Brunschwig).

approached from the position of the zero-order maximum, the axial field distribution exhibits swing amplitudes which are completely different in magnitude for some extrema. An interesting feature of the case of nonuniform amplitude distribution is that the ratios of the maxima to the minima in the axial distribution are not nearly so large as in the case of the uniform distribution. Thus by appropriate choice of amplitude distribution, it is possible to "flatten out" the axial distribution over a considerable distance. This is illustrated in Fig. 11 where the particular vibration amplitude distribution required to realize the indicated axial distribution is generated by exciting the center portion of the element at twice the driving level (twice the voltage) of that applied to the outer ring. Periodic components in the amplitude distribution over the vibrating element do not produce corresponding periodicities in the axial field generated by the element.

TABLE X

NUMERICAL EXAMPLES OF NEAR FIELD CHARACTERISTICS IN WATER AT 30°C

f (mc)	R (cm)	R/λ —	Number of maxima along axis —	Distance to furthest maximum (cm)	Spacing between furthest maximum and minimum (cm)	Spacing between maximum and minimum nearest element (cm)
0.1	1.75	1.167	1	1.67	1.39	1.39
0.5	1.75	5.833	6	10.13	3.01	0.168
1.0	1.75	11.67	12	20.48	10.45	0.086

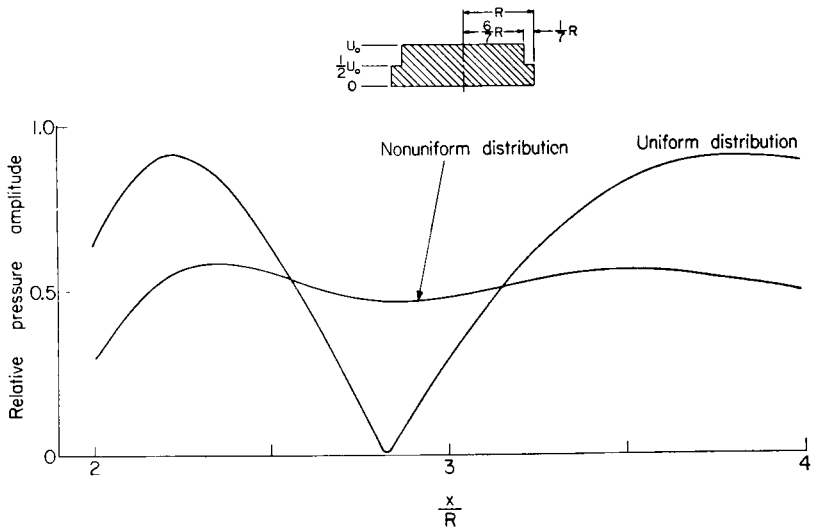

FIG. 11. Axial pressure amplitude distribution in the near field produced by a nonuniformly vibrating plane circular element (after Brunschwig).

If the medium has an acoustic absorption coefficient sufficiently large at the frequency of the field such that an appreciable fraction of the acoustic energy is absorbed in traversing the distance from the element to the position in the near field under attention, then the swing of the extrema at that position is modified compared with that characteristic of the field produced in a nonabsorbing medium having the same value of the sound velocity. This effect increases in importance as the frequency increases since the absorption per unit path length increases with the frequency. This is illustrated in Section III, 1, *b* which is concerned with ultrasonic microscopy.

(*2*) *Far Field.* The far field, or Fraunhofer region, may be considered to begin at the position of the zero order maximum of the near field [see

relation (30)]. Beyond this position the acoustic pressure amplitude varies inversely with the distance from the source and the intensity varies as the inverse square of the distance.

The structure of the far field for a circular source, having a uniform velocity amplitude distribution, can be described in terms of the pressure amplitude as follows (Hueter and Bolt, 1955; Kinsler and Frey, 1950; Morse, 1948)

$$|p| = \left(\frac{P}{x}\right) \left| \frac{2J_1\left(\frac{2\pi R}{\lambda} \sin \phi\right)}{\frac{2\pi R}{\lambda} \sin \phi} \right| \tag{38}$$

The first factor of this expression describes the (already mentioned) decrease in the pressure amplitude which occurs with increasing distance from the source. The second factor, in which J_1 designates the Bessel function of the first kind of order one (McLachlan, 1955) and ϕ is the azimuthal angle measured from the axis of the radiating element, describes the angular width of the beam and the number and magnitude of the "side lobes." This is called the "directivity function" and is exhibited graphically in Fig. 12. For a radiator of specified radius operating at a fixed frequency, there exists a minimum angular width of the main beam which cannot be reduced regardless of the vibration amplitude distribution over the radiating surface. The effect of the radius of the source (measured in wavelengths) upon the width of the main beam and the number of side lobes is illustrated

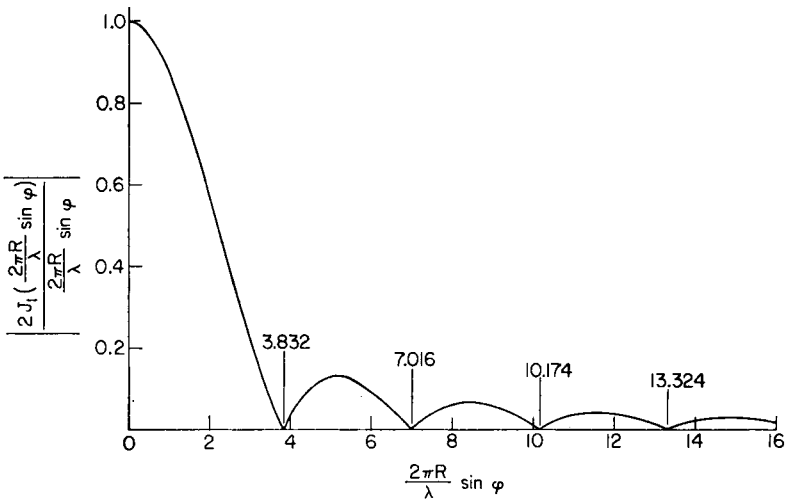

FIG. 12. Directivity function for a circular source with a uniform velocity amplitude distribution. See relation (38).

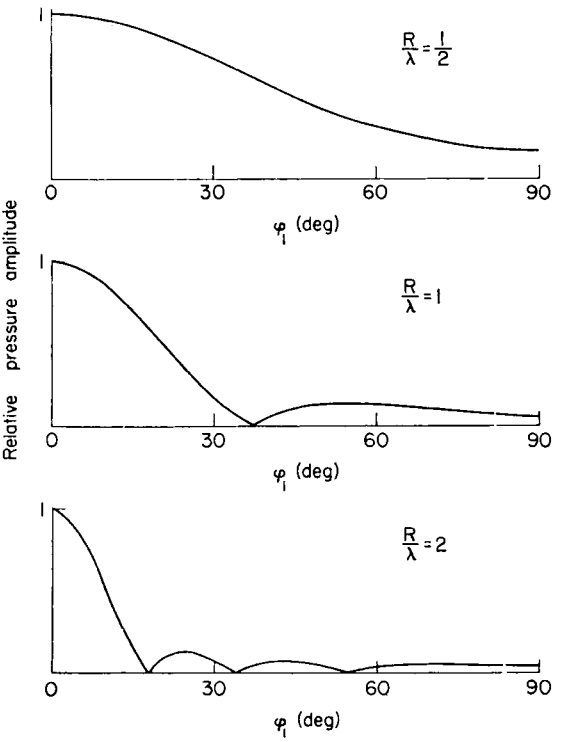

FIG. 13. Beam patterns for circular sources with uniform velocity amplitude distributions.

in Fig. 13. Three "beam patterns" are shown for a circular source, which is mounted flush in a rigid surrounding wall, and which has a uniform velocity amplitude distribution over the vibrating surface. The abscissa is the azimuthal angle measured from the axis of the vibrating element. It is apparent that the beam narrows as the ratio R/λ varies from $\frac{1}{2}$ to 2. The minimum width of the main beam, as measured between the zeros on either side, is given by

$$\sin \phi_1 = 0.61 \frac{\lambda}{R} \tag{39}$$

where ϕ_1 is the half-width, in angular measure, of the beam.

If the vibration amplitude is nonuniformly distributed (so-called "shading" of the vibration amplitude) over the irradiator face, the beam characteristics can be greatly altered (Davids *et al.*, 1952). That is, the amplitudes of one or more side lobes can be increased or decreased; however, the width of the main beam increases. Broadening of the main beam does not in general constitute a disadvantage in present applications of ultrasound

to the study of biological systems. A focusing irradiator can be employed if a narrow beam is required. In fact, in designing systems to be used to attain uniformity of irradiation over large volumes, it is desirable to minimize changes in the magnitudes of the acoustic radiation parameters as one moves off the axis of the beam. Such nonuniform distributions of vibration amplitude are approximated by constructing the irradiator from an array of elements driven at levels appropriate to generate the desired field pattern. Arrays are possible with plate mode elements; however, since the thickness of the element controls the resonant frequency, it is necessary to drive the elements with different relative magnitudes of applied voltage.

b. Focused Fields

The induction of changes by ultrasound in the depths of a biological structure or system without the concomitant induction of changes in intervening tissue requires the use of focusing irradiators (Section III, 2). Similarly, the examination of tissue structure requires focusing systems in order to confine the ultrasonic radiation to the direction of propagation (Section III, 1, *c*). Focusing can be accomplished by employing either lenses or reflectors. Non-planar-shaped transducer elements have received attention but precision instrumentation employing this type of element has not been developed. Shaped ceramic elements are utilized to focus the radiated acoustic energy for engineering applications in which accurate control of the field parameters is not essential (Hueter and Bolt, 1955). This section is primarily concerned with lens and reflector systems.

It is possible to employ lenses and reflectors in various configurations to realize a focusing system. For example, a single piezoelectric element may be combined with a lens (Fig. 14a) or an array of elements may be used in conjunction with a single lens (Fig. 14b). Multiple focused beam systems, consisting of four units of the type illustrated in Fig. 14a and operated with the four focal regions in spatial coincidence, have proved to be very useful (Fig. 14c) (W. J. Fry, 1958). Reflector irradiators employing two reflecting surfaces have also received attention (Fig. 14d) (Hueter and Bolt, 1955; W. J. Fry, 1958).

Applications of these various types of focusing transducers to investigations of biological systems are presented in Section III. The material of this section is concerned with the acoustical characteristics of these systems which are important for such investigations, *viz.*, the gain in the intensity over that produced by the unfocused field, the focal length, and the "dimensions" of the focal region.

(*1*) *Lens Focusing Systems.* For certain applications, the lens type of focusing system, illustrated in Fig. 14 by (a), (b), and (c), enjoys some distinct advantages over the reflector system. (1) The radiating area of

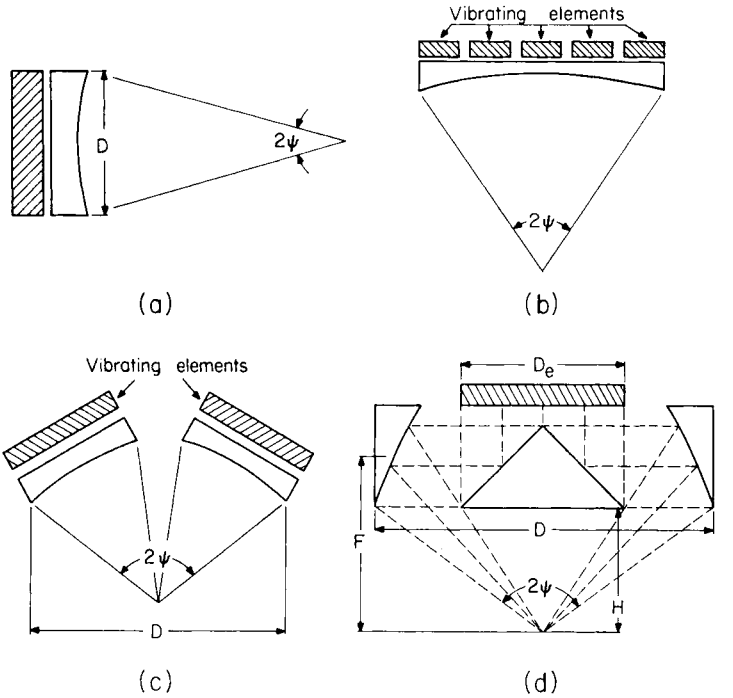

FIG. 14. Schematic diagrams of acoustic focusing systems.

piezoelectric elements available for the generation of acoustic energy is much larger for a given diameter of the transducer face. (2) By appropriate design (discussed in this section), more power can be obtained from the lens type, per unit area, than from the pure reflector type, for equal electric driving levels. (3) It has been possible to design more compact lens systems than reflector systems to obtain focal regions and focal lengths of given size. That is, the angle of convergence is somewhat smaller for the lens systems which means that the port of entry of the sound into the biological system to be irradiated can be smaller for equal depths of the focal region. Disadvantages are: (1) the acoustic output from lens systems varies more with the operating temperature than that for reflector systems. This can be alleviated by incorporating into the systems suitable means for compensation and/or heat exchange methods (Brunschwig and W. J. Fry, 1959). (2) The acoustic absorption coefficient of the plastic lens materials currently in use is relatively high at the working frequencies. This means that continuous operation at high power produces heat which can alter the physical characteristics of the lens and, in some cases, cause structural failure. These difficulties can be partially overcome by utilizing lens materials having much lower absorption coefficients, e.g., metals.

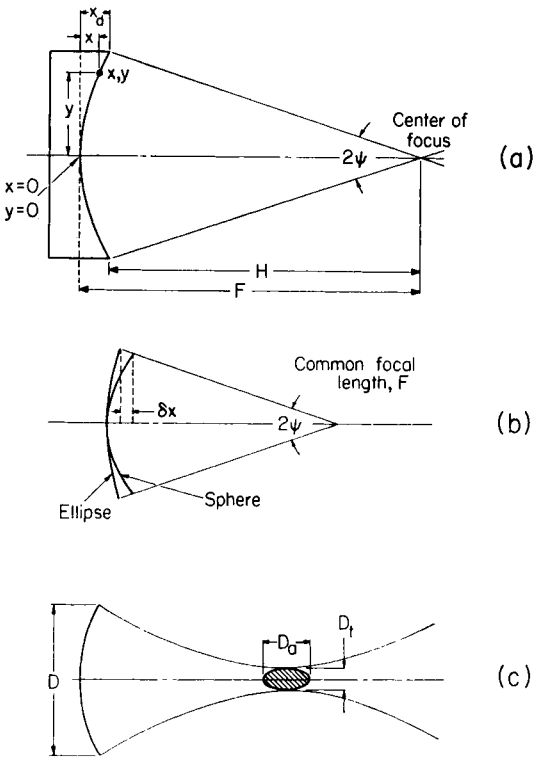

FIG. 15. Geometric illustration of quantities defined for lens focusing systems.

The quantitative description of the characteristics of the lens systems of interest here is expressed in terms of the quantities defined in Fig. 15. Since solids are commonly used in the fabrication of lenses for precision transducers and since the velocity of sound in most solids is greater than that in water or physiological media, the lens shape is plano-concave. The index of refraction n of the lens material relative to the medium of interest is greater than unity so that plane waves incident normal to the plane surface of the lens are refracted toward the principal axis when emerging at the concave surface and thus, for a properly shaped lens, are brought to a focus. Referring to Fig. 15a, the focal length F of the lens is defined as the distance from the point of the curved surface on the axis to the midpoint of the region of convergence, i.e., the "center" of the focal region. The working distance H is the distance from the plane containing the peripheral boundary of the curved surface of the lens to the center of the focal region. In many cases, this distance is the maximum working depth for the irradiation of biological systems since these systems are, in general, too large to be brought into the region bounded by the peripheral plane and the

concave surface. The aperture angle 2ψ (hereinafter referred to as simply the aperture) of the lens is the angle of the right cone with apex at the center of the focal region and altitude equal to the working distance. The coordinates (x,y) locate the position of any point on the surface with respect to the origin at 0.

A spherical lens of small aperture can be used to focus sound. The limitation on the size of the aperture, above which such a lens no longer focuses the radiation into a common region, is given by expression (46a) of this section. If R designates the radius of curvature of the concave surface and n designates the index of refraction of the lens material relative to the medium, then the focal length F is

$$F \simeq \frac{R}{1 - (1/n)} \tag{40}$$

where it has been assumed that the depth x_d of the lens is small compared to $R(x_d < 0.1\ R)$ and that the angles of incidence and refraction are small enough so that the sine function can be approximated by the tangent function. The working distance is given by

$$H \simeq F\left(1 - \frac{F \tan^2 \psi}{2R}\right) \tag{41}$$

The elliptic lens design is not limited to small apertures. Its generating curve can be written as

$$y^2 = 2Fx\left(1 - \frac{1}{n}\right) - x^2\left(1 - \frac{1}{n^2}\right) \tag{42}$$

where the symbols have the same meaning as for the spherical lens. The focal length can be expressed in terms of the angle ψ (see Fig. 15) and the depth x_d of the lens as

$$F = \frac{x_d}{n}\left(\frac{n \sec \psi - 1}{\sec \psi}\right) \tag{43}$$

and the working distance is given by

$$H = F\left(\frac{n - 1}{n \sec \psi - 1}\right) \tag{44}$$

The working distance is positive if the focal region falls outside the volume bounded by the concave surface and the plane of the periphery and is negative if the focus falls inside this volume. It should be noted that the working distance is very nearly equal to the focal length if

$$\sec \psi \simeq 1 \tag{45}$$

The restriction limiting plano-spherical lens designs to small apertures

can be made quantitative by employing the criterion that acoustic rays should not arrive out of phase at the focus by more than 90°. This criterion is satisfied by requiring that δx (see Fig. 15b) be not greater than one quarter of a wavelength in the medium. However, if $\psi > 45°$, this criterion is too stringent and a similar one, using the difference in the y coordinates of the intercepts of a line passing through the center of the focal region and intersecting the generating curves may be employed. The two curves of Fig. 15b represent the generating curves for spherical and elliptical lenses of equal focal lengths. Here δx is the difference in the x coordinates of the intercepts with the generating curves of a line through the center of the focal region and having a slope determined by the angle ψ. The criterion is expressed approximately as

$$\delta x = F\left(\frac{F}{R}\right)\frac{\tan^4\psi}{8n^2}\frac{1}{1-(1/n)+\tan^2\psi} \tag{46a}$$

where

$$\delta x \leqslant \lambda/4 \tag{46b}$$

λ is the wavelength of the sound in the medium and F is the common focal length for the two lenses.

The use of formulas (40), (41), (43), (44), and (46) can be illustrated by a specific example. Assume a focal length of 5 cm is desired in water and the lens material is Lucite which has an index of refraction of 2.2 relative to water. If the aperture angle 2ψ is chosen as 30°, then from (40) the radius of the spherical lens is 2.7 cm and from (41) the working distance is 4.7 cm. For the case of an elliptical lens of slightly larger diameter than that of the spherical lens, corresponding to the configuration of Fig. 15b, the depth is 0.3 cm [from (43)] and the working distance is 4.7 cm [from (44)]. From (46a), the quantity δx is 0.002 cm and if this is to be less than one-quarter wave length then the maximum operating frequency is 18 Mc/sec.

The design of lens focusing systems requires calculations of the size or "dimensions" of the focal region which depend upon the wavelength of sound in the medium and the lens parameters. The size and shape of the focal region impose a lower limit on the *minimum* volume of material which can be irradiated as well as determine the geometric shape which can be affected without simultaneous alteration of bounding structures. (See Section III, 2 for examples involving the central nervous system.) It is convenient to describe the size of the focal region in terms of transverse and axial diameters (see Fig. 15c). The transverse diameter D_t is the distance across the focal region, perpendicular to the direction of propagation, at which the square of the acoustic pressure amplitude is reduced to one-

half the peak value. The transverse diameter may be expressed as

$$D_t \simeq k_t(F/D)\lambda \tag{47}$$

where D is the diameter of the lens as indicated in Fig. 15c, F is the focal length, and λ is the wavelength in the medium. The units used for F and D should be the same and the unit of D_t is then the same as that of λ. The quantity k_t is dimensionless and is somewhat dependent upon the half-aperture angle ψ. For values of $\psi \leqslant 50°$, an average value of k_t which permits calculation of D_t to within about 20%, is 1.0. Similarly, the axial diameter D_a of the focal region, the distance between points along the direction of propagation at which the square of the pressure amplitude is reduced to one-half the peak value, is given by

$$D_a \simeq k_a D_t \tag{48}$$

where the unit of D_a is the same as that used for D_t. The quantity k_a is dependent upon the half-aperture angle ψ as shown in Fig. 16. It is seen from expression (48) and Fig. 16 that the ratio of axial diameter to transverse diameter decreases as the aperture angle increases. Further, since k_a is always greater than unity, the ellipsoid-like focal region will always have its major diameter along the axis of the lens system. Expressions (47) and (48) can also be used to estimate the transverse and axial diameters of multibeam irradiators of the type illustrated in Fig. 14c.

It should be noted that the volume of biological material (tissue or suspension) included within the region defined by the transverse and axial diameters does not in general correspond to the volume modified or affected by the focused sound (Dunn, 1956; Fry, 1956). For example, the effect of interest may be produced by the region wherein at all points the square of the pressure amplitude is not less than 90% of the peak value. In this

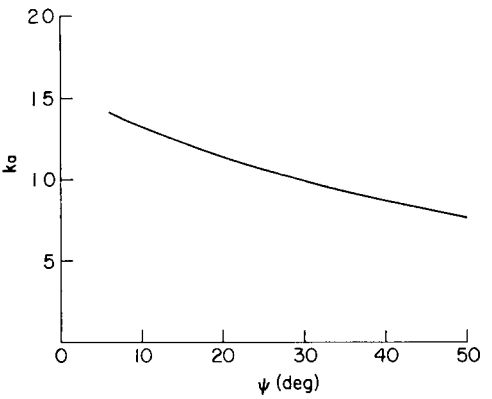

FIG. 16. The parameter ka versus the half-aperture angle ψ.

case, the volume in which the change is induced is much smaller than that determined by the diameter calculated from expressions (47) and (48). The diameters defined above are chosen only for convenience in describing the size of the focal region and do not imply that effects induced by the sound are confined to or completely fill the region so described.

The "gain" of the lens is defined as the ratio of the square of the pressure amplitude at the center of the focal region (peak amplitude P_p) to that at the surface of the lens in contact with the medium (amplitude P) when the lens is driven uniformly. This gain factor G_l can be expressed approximately in terms of the lens diameter and the transverse diameter of the focal region as

$$G_l = (P_p/P)^2 \simeq 0.8(D/D_t)^2 \tag{49}$$

When the relations between the acoustic parameters at the focus are identical with those of a plane wave field, which is the case for lenses with small aperture angle ($2\psi \leqslant 30°$), the gain G_l can be expressed in terms of the ratio of the peak intensity I_p at the focus and the intensity at the lens-medium interface, i.e.,

$$G_l = I_p/I \simeq 0.8(D/D_t)^2 \tag{50}$$

In practical systems, acoustic energy is supplied to the lens by a piezoelectric element, as illustrated in Fig. 17c, and the gain G_s of the composite focusing system (piezoelectric element, spacing material, and lens), is defined as the ratio of the square of the acoustic pressure amplitude at the center of the focal region to that developed in the medium when the piezoelectric element radiates into it directly, the driving voltage being held constant. G_s can be expressed as the product of G_l and a factor G_c, dependent upon the dimensions and acoustic characteristics of the media of the composite system, as

$$G_s = G_c G_l \tag{51}$$

The quantity G_c can be evaluated approximately by first considering the gain or increase in acoustic intensity which is realized by employing the composite system illustrated in Fig. 17a as compared with that obtained from the same piezoelectric element radiating directly into the medium (Fig. 17b) and operated at the same driving voltage. The operating frequency is the same in each case, i.e., the resonant frequency of the element as given by relation (19). The gain obtained by this scheme arises as a result of modification of the electrical input impedance at the terminals of the piezoelectric element which allows the element to draw more current, and more power for the same driving voltage, from the electronic generator. The characteristic acoustic impedances of the transmission plate and spac-

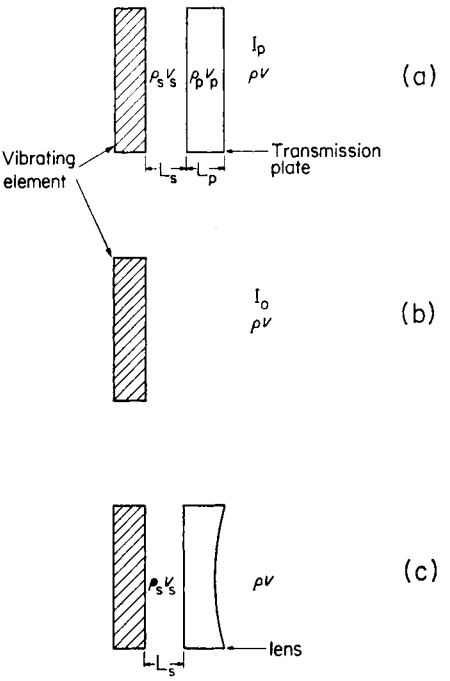

FIG. 17. Schematic diagram illustrating composite systems.

ing material are respectively, $\rho_p v_p$ and $\rho_s v_s$ and the corresponding thicknesses of these two media are, respectively, L_p and L_s. For all values of the ratio $\rho_p v_p/\rho v > 1$ and for any fixed thickness of transmission plate, it is possible to realize values of the gain G_p greater than unity by choosing L_s equal to an odd multiple of a quarter-wavelength. It is possible by appropriate choice of the acoustic parameters to realize rather high gains, e.g., 10 to 100. For this case, the gain is given by (W. J. Fry and Dunn, 1961)

$$\bar{G}_p = \frac{I_p}{I_0} = \left(\frac{\rho v}{\rho_s v_s}\right)^2 \left[\frac{1 + \tan^2 \dfrac{\omega L_p}{v_p}}{1 + \dfrac{1}{(\rho_p v_p/\rho v)^2} \tan^2 \dfrac{\omega L_p}{v_p}}\right] \tag{52}$$

where $L_s = (\lambda_s/4)(2m - 1)$ and $m = 1,2,3, \ldots$. The symbol I_0 designates the intensity produced when the element radiates directly into the medium and I_p designates the intensity produced in the same medium by the composite system. Large values of $\bar{G}_p$ are obtained by choosing materials such that the ratios $\rho v/\rho_s v_s$ and $\rho_p v_p/\rho v$ are large. The optimum thickness of the transmission plate, for high gain, is one-quarter wavelength. The graph of

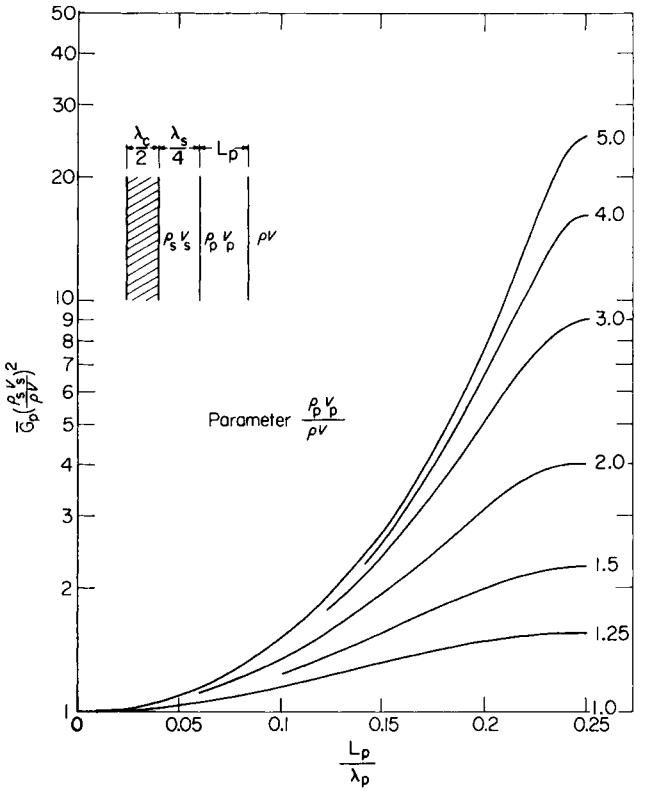

FIG. 18. Gain of composite system for λ/4-length of spacing material versus thickness of transmission plate. Symmetrical about $L_p/\lambda_p = 0.25$ and repeats every $L_p/\lambda_p = 0.5$.

Fig. 18 shows the bracketed factor of (52) plotted as a function of L_p/λ_p (the thickness of the plate divided by the wavelength of sound in the plate). The parameter from curve to curve is $\rho_p v_p/\rho v$.

The gain G_p is equal to or less than unity if $\rho_p v_p/\rho v > 1$ and if the thickness of the spacing material is zero or any multiple of a half-wavelength for all thicknesses of the transmission plate. For this case, the gain is given by (W. J. Fry and Dunn, 1961)

$$G_p = \frac{I_p}{I_0} = \left[\frac{1 + \tan^2 \frac{\omega L_p}{v_p}}{1 + (\rho_p v_p/\rho v)^2 \tan^2 \frac{\omega L_p}{v_p}} \right] \tag{53}$$

where $L_s = (\lambda_s m/2)$; $m = 0,1,2,\ldots$. Figure 19 shows G_p plotted as a function of L_p/λ_p .

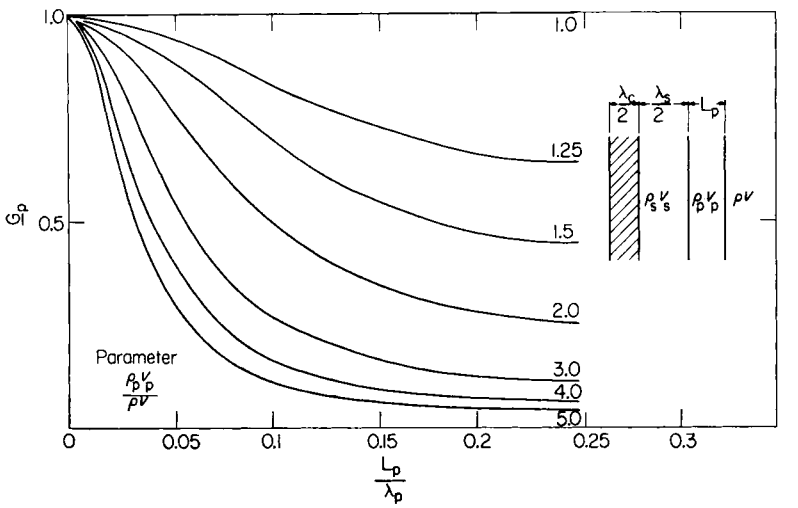

FIG. 19. Gain of composite system for λ/2-length of spacing material versus thickness of transmission plate. Symmetrical about $L_p/\lambda_p = 0.25$ and repeats every $L_p/\lambda_p = 0.5$.

Thus a lens system to be used for obtaining maximum intensity in the focal region, for a given electric driving voltage, is designed with a thickness of the spacing medium of one-quarter wavelength or odd multiples thereof, e.g., $L_s = (\lambda_s/4)$ in Fig. 17c. It should be noted that it is desirable to keep this layer thin in order to reduce the effect of changes in temperature of the system which result in changes in the sound velocities and dimensions sufficiently large to affect the output power. The thinner the materials, the smaller will be the effects produced by temperature changes.

As a first approximation in estimating the gain of a lens system, it is possible to consider the lens as subdivided into a series of concentric rings with each ring behaving as a plate of thickness equal to the average thickness of the ring. The calculation is made assuming that the transverse diameter of the focal region is the same for the individual rings radiating separately as for the group radiating simultaneously. That is, the beam is not narrowed by the group of rings operating together. This corresponds to assuming incoherence between contributions from the individual rings (optical case) and yields a value for the gain which is less than the minimum that can be realized with coherent radiation supplying energy to the rings (the usual case in ultrasonic practice). However, at the present stage of the art of designing lens systems, one seldom realizes the maximum theoretical gain. Consequently, in designing a new system, it is convenient to calculate the sound level at the focus on the above basis as a lower estimate. It is assumed that the angle formed by the tangent to the generat-

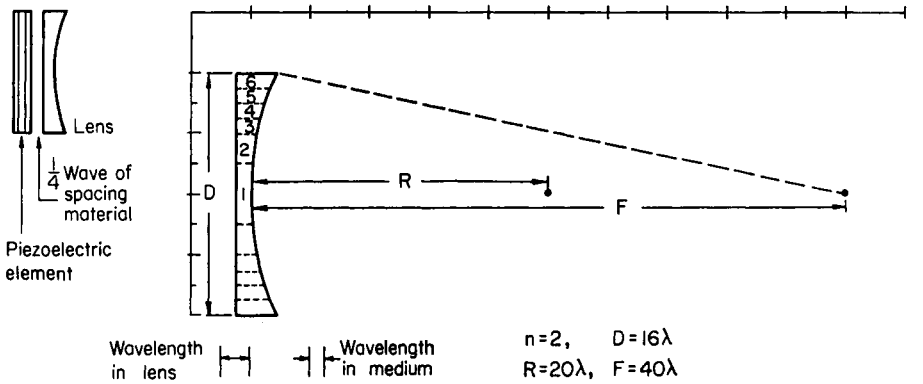

$$D_f = \left(\frac{40\lambda}{16\lambda}\right)\lambda, \quad \text{from (47)}$$

$$G_f = 0.8\left[\frac{16\lambda}{\left(\frac{40}{16}\right)\lambda}\right]^2 = 33, \quad \text{from (50)}$$

$$G_s = G_c G_f = 73, \quad \text{from (51)}$$

Ring	Average path lengths in rings: to right	to left	Average "ring thickness"	Ring area	Gain per ring	Area x Gain
1	0.50	0.50	0.50	1.00π	1.0	1.0π
2	0.61	0.61	0.61	3.00π	1.4	4.2π
3	0.77	0.77	0.77	2.25π	3.8	8.6π
4	0.90	0.90	0.90	2.75π	1.3	3.6π
5	1.04	1.08	1.06	3.25π	1.1	3.6π
6	1.24	1.32	1.28	3.75π	3.7	13.9π
			Total	16π		34.9π

$$G_c = \frac{34.9\pi}{16\pi} = 2.2$$

FIG. 20. Illustration of approximation method of computing gain of lens system.

ing curve and lens axis does not differ greatly from 90°. The gain G_c can be estimated by summing the products, gains times areas, of the individual rings and dividing by the total area of the lens. This method is illustrated in Fig. 20 which shows a plano-concave spherical lens fashioned of such material as to have an index of refraction and ratio of acoustic impedances equal to 2.0 with respect to the medium. The radius of curvature of the spherical surface is chosen equal to 20 wavelengths and its diameter equal to 16 wavelengths in the medium. The thickness of the lens at the axis is

taken as one-half wavelength in the lens material. The aperture angle is thus approximately 24° and the focal distance is 40 wavelengths in the medium. The lens is divided into a series of concentric rings with the diameters indicated in the figure. The ring diameters are chosen so that the variation in thickness is not more than about 0.1 wavelength different from the average thickness. Since the sound is incident upon the spherical surface at different angles, moving from the axis to the periphery of the lens, the average distance that the waves travel through each ring of the lens and back, due to reflection at the curved surface, is not equal to twice the average ring thickness. This means that, as a first approximation in determining the gain for the ring, the thickness of each ring appears ro be somewhat greater than its average thickness. The value is determined by averaging the thickness of the ring with the length of the return path obtained by making the angle of reflection equal to the angle of incidence at the mid-diameter of the ring. This process is illustrated in the tabulation inserted in Fig. 20. The gain for each ring is obtained by using the computed average thickness as the abscissa in conjunction with the curve for $\rho_p v_p/\rho v = 2$ of Fig. 18. The ring gains thus obtained are multiplied by the ring areas and the products summed. Division of this sum by the sectional area of the lens yields G_c. It is apparent that this process constitutes a rough approximation and that it becomes worse as the lens aperture angle increases since the angle of incidence of the sound on the spherical surface increases with increasing aperture angle. The gain G_c thus obtained is 2.2 and since the gain of the lens is 33 as indicated in Fig. 20, the gain of the lens-piezoelectric element system is approximately 73. That is, the intensity at the center of the focal region is 73 times the intensity which would be produced in the medium by the piezoelectric element radiating directly into it. The system of Fig. 20 is applicable at any frequency. If 1.0 mc sound in water is desired ($\lambda = 1.5$ mm) then the diameter of the lens is 2.4 cm and the focal length is 6.0 cm.

(*2*) *Reflector Focusing Systems.* As already indicated, one of the major design difficulties of lens systems is the minimizing of the effects resulting from changes in operating temperature and from temperature gradients produced by conversion of some of the acoustic energy into heat in the device. When precision control of the acoustic parameters is required (see Section III, 2), the employment of such transducers requires expenditure of considerable effort in making check and calibration measurements and in controlling the temperature factor. The reflector system, illustrated in Fig. 14d, is less critically affected by temperature changes. This system has the advantage over the plastic lens system in that it can be operated at high power for much longer periods of time without failure. One disadvantage of the reflector system results from the fact that the ultrasonic

irradiation of the paraboloidal reflecting surface is supplied by a piezoelectric element whose area is small compared with the area of the paraboloid. This means that the maximum power output, which can be obtained for a given driving voltage across the element and for a given irradiator diameter D, is much smaller than that obtained using a lens focusing system of equal diameter (see example below). A second disadvantage is that it has not been possible to obtain axial diameters of the focal region as short as those obtainable with lens focusing systems of equal aperture diameter and focal length.

The dimensions of the focal region (defined as in the case of the lens) are given by formulas similar to (47) and (48). The focal length F is defined as the distance from the center of the focal region to a plane perpendicular to the axis and passing through the paraboloid reflecting surface at its middepth, as illustrated in Fig. 13d and D is the diameter of the "face" of the reflector. The transverse diameter can be estimated from expression (47). The axial diameter of the focal region is greater than that expressed by (48) and, from the data presently available, it appears that a value of k_a of the order of 75% greater than that for lens systems is applicable to the reflector system described here. The gain G_r of the reflector focusing system can be estimated from a knowledge of the piezoelectric element diameter D_e and the transverse diameter of the focal region by a relation similar to (49), i.e.,

$$G_r = (P_p/P)^2 = 0.8(D_e/D_t)^2 \tag{54}$$

The layout for the generating curve of the paraboloidal surface is illustrated in Fig. 21. The reflecting cone has an apex angle of 90° to reflect the incident sound outward in rays which lie in planes perpendicular to the transducer axis. The diameter of the base of the cone must equal the diameter of the face of the piezoelectric element exposed to the medium in order to intercept all radiation. The minimum length of the paraboloid is determined by first passing a line through the desired position F of the center of the focal region and the vertex of the base angle of the cone. The intersection of this line with the ray reflected at the apex of the cone determines the point P on the generating curve of the paraboloid. The extension of the apex-reflected ray a distance equal to PF determines the position of the directrix of the parabolic generating curve. Since all points of the parabola must be equidistant from the directrix and the point F, the remainder of the curve is immediately determined.

(*3*) *Other Focusing Systems.* Curved or "bowl"-shaped focusing systems can be fabricated from piezoelectric materials. Such units focus the sound directly (Hueter and Bolt, 1955). They can be made by casting a single block of ceramic material into the desired shape or by forming the desired

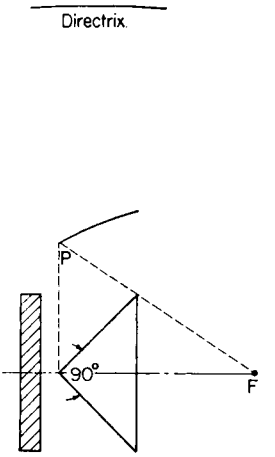

FIG. 21. Layout for generating curve of paraboloidal surface of reflector focusing system.

shape from a mosaic of numerous elements. This type of system will not be discussed here since the ceramic materials do not as yet possess the desired stability and low loss characteristics necessary for use in precision irradiation equipment at high power levels.

In order to obtain uniform acoustic field conditions simultaneously over a volume larger than can be realized with the types of focusing systems already discussed, and not subject intervening material to the same high sound levels, it is necessary to consider more complex lens systems. Such lens systems will not be considered here since the work is still in the formative stages and practical designs have not yet been produced. However, sufficient work has been accomplished (Brunschwig and W. J. Fry, 1959) to demonstrate that an appropriately modified plano-concave cylindrical lens offers great promise and that the design theory for such focusing systems will be considerably more complex than that for systems employing plano-concave spherical or plano-concave elliptical lenses.

It has not been possible, within the scope of this chapter, to treat the design of focusing systems in a comprehensive fashion. however, the material presented should serve to clarify the important features of such systems as well as to indicate what can be realized at the present time.

5. Absorption

The presence of an ultrasonic field in a medium is accompanied by the production of heat. The time rate of heat production, in a selected volume in which the field exists, is determined by the amplitude, frequency, and spatial distribution of the field parameters, and by certain structural char-

acteristics and geometric distribution of the various media within the volume. A variety of different mechanisms may play a role in the conversion of acoustic energy into heat and it is the purpose of this subsection to discuss briefly those which are important for liquids and liquid-like media. Before embarking on this objective, it is desirable to indicate how the conversion of acoustic energy into heat modifies the macroscopic propagation characteristics of ultrasonic waves.

The propagation of a plane traveling wave in an absorbing medium is described as

$$q = Qe^{-\alpha x}e^{j\omega(t-x/v)} \tag{55}$$

where α is the amplitude absorption coefficient per unit path length. The amplitude, $Qe^{-\alpha x}$, of the wave decreases exponentially as it progresses in the positive direction of x. The intensity I of a plane progressive wave moving in the positive direction, at any position x in the medium, can be expressed in terms of the intensity I_0 at $x = 0$ as

$$I = I_0e^{-\mu x} \tag{56}$$

where μ is the intensity absorption coefficient per unit path length, i.e., $\mu = 2\alpha$.

If a sound field is established in a bounded medium and the source of excitation is removed, the amplitudes of the field parameters at any point decay temporally. The form of the decay function is dependent upon the configuration and acoustic characteristics of the boundaries, the particular spatial and temporal form of the field distribution established by the sound source, and the acoustic absorbing properties of the medium. No analytical relations expressing fields in terms of temporal attenuation quantities will be given since the cases of interest in this chapter are more conveniently described in terms of functions involving spatial attenuation parameters. The particular mathematical description used in any specific case is determined by the boundary conditions (both spatial and temporal). See Mintzer and Tanenbaum (1960) for the treatment of a single problem by two different analytic methods.

a. Discussion of Absorption Mechanisms

Absorption occurs in a homogeneous liquid when the changes in density are not in time phase with the changes in pressure, i.e., when the instant of time at which the maximum density occurs does not coincide with the instant of time at which the maximum pressure occurs. This type of behavior is produced by a variety of mechanisms classified here under two general categories, viscosity or frictional lag and relaxation processes. The processes included in the first category result from the fact that liquids

exert some resistance to shearing forces. For a Newtonian liquid, the magnitude of the shearing force per unit area, F_A, acting on a surface between contiguous layers of a fluid medium is proportional to the velocity gradient normal to the surface. Symbolically,

$$F_A = \eta \left| \frac{dv_f}{dn} \right| \tag{57}$$

where η is the coefficient of shear viscosity. Thus far it has not been necessary to postulate that biological systems (soft tissues) behave as non-Newtonian liquids (the viscosity coefficient changes with the velocity gradient) in order to correlate the results obtained from *ultrasonic* propagation studies. The propagation of sound or vibration in tissue at relatively low frequencies requires that such systems be treated as viscoelastic media possessing both shear and volume elasticity (von Gierke *et al.*, 1952). At frequencies above 100 kc, the propagation can be adequately described, at present, by analyses which include only volume elasticity together with viscous and relaxational processes which result in absorption.

The term relaxation process is used here to include heat conduction (which is relatively unimportant for biological systems) and thermal and structural relaxation and combinations of these mechanisms (Markham *et al.*, 1951; Herzfeld and Litovitz, 1959). Heat conduction refers to the transfer of heat out of high-pressure regions and into low-pressure regions as the result of the cyclic temperature gradients which are produced in the medium by the sound field.

Thermal relaxation results when the temperature of a fluid is changed due to the propagation of a sound wave and the transfer of energy between the external degrees and the internal degrees of freedom of the constituent molecules requires a time interval comparable to the period of the wave. Consequently, some of the energy of the internal degrees of freedom is transferred to the external degrees of freedom at an instant of time corresponding to a reduced pressure when the temperature is less than the equilibrium value. The amplitude of the temperature variation is therefore less than it would have been if the transfer process were able to follow the cyclic temperature changes without appreciable lag. This process results in the conversion of acoustic energy into heat and consequently a plane traveling wave is attenuated as it propagates as described by relation (55).

Structural relaxation results when a time interval comparable to the period of the sound wave is required for redistribution of the mutual orientation or change in degree of association of the molecules of a liquid in response to the pressure changes produced by the field. Such configuration changes entail the transfer of energy. Consequently, acoustic energy is converted into heat when the rate constant of the process is not large

enough to follow, without appreciable lag, the variations in pressure produced by the sound field. If the equilibrium state of a chemical reaction is dependent to a sufficient degree upon the pressure of the reactants, then acoustic absorption in the medium takes place and a relaxation type of behavior ensues.

All the relaxation processes just discussed may occur simultaneously, the relative importance of each being determined by the structure and composition of the medium. One type of relaxation process may predominate over a certain frequency range while another type may constitute the important mechanism in a different portion of the acoustic spectrum. A quantitative knowledge of these relaxation effects can furnish useful information on structure, energy transfer processes, and molecular species in biological systems (see Section III).

Absorption of ultrasound can occur by other mechanisms in addition to those already considered. One such important process is relative motion between suspended structures and the imbedding medium in inhomogeneous media such as cells in suspension or tissue. The relative motion results from the fact that the densities of the suspended materials are not in general equal to that of the matrix. Consequently, friction-like forces exist between the matrix and the suspended material which result in the conversion of acoustic energy into heat. Relative motion can also occur even if the mass of the suspended structure is equal to that of the displaced liquid since the "densities" of the various parts of a suspended structure may not all be equal. In such instances rotations may occur which result in loss of acoustic energy.

Gas bubbles present in biological systems can be responsible for the extraction of energy from the field by thermal, acoustic radiation, and viscous processes (Devin, 1959). The process of thermal damping results from the fact that heat conduction takes place between the gas of the bubble and the surrounding liquid during the alternate compressions and expansions of the bubble produced by the cyclic pressure changes of the sound field. Acoustic radiation damping is the result of the energy expended by the pulsating bubble in the form of spherical sound waves. Viscous damping results from relative motion between the bubble and the imbedding medium and viscous stresses near the bubble surface (Gould and Nyborg, 1960). The magnitudes of these effects are maximum when the bubble resonant frequency coincides with the frequency of the acoustic field. Quantitative expressions, including the relation between bubble size and resonating frequency, which can be used for calculating the magnitudes of these effects for specific cases are given later in this subsection.

Liquids can be subdivided into various classes on the basis of their ultrasonic absorption characteristics (Pinkerton, 1949; Markham *et al.*, 1951; Herzfeld and Litovitz, 1959). The first group has an ultrasonic absorption

coefficient close (within 10 to 20%) to that calculated on the basis of shear viscosity losses. Monatomic liquids such as argon and mercury are in this group as well as some diatomic liquids such as oxygen and nitrogen. As far as is known at the present time, no biologically interesting material appears in this class.

The second group is characterized by a positive temperature coefficient of absorption (i.e., absorption increases as the temperature increases) and by values of the absorption coefficient from 3 to 400 times the value calculated on the basis of a shear viscosity mechanism alone. Polyatomic, unassociated liquids such as benzene, carbon tetrachloride, and carbon disulfide are in this group. The "excess" absorption of these liquids may be the result of a slow rate of exchange of energy between the external and internal degrees of freedom. To the writers' knowledge, the only biological materials for which ultrasonic absorption coefficients have been determined as a function of temperature are nerve tissue and blood proteins. The nerve tissue measurements were made on spinal cords of one day old mice at a frequency of 0.98 mc. The temperature coefficient of the intensity absorption coefficient is positive, increasing from 0.06 cm^{-1} at 2°C to 0.22 cm^{-1} at 28°C (Dunn, 1958). These values for spinal cord are comparable in magnitude with the values of the more highly absorbing liquids of this type, e.g., carbon disulfide. At present, it is unwarranted to assume that the absorption mechanisms operative in this case are predominately of the thermal relaxation type. Both thermal and structural relaxation mechanisms may be equally important.

The blood proteins exhibit a negative temperature coefficient of absorption (Carstensen *et al.*, 1953). This type of temperature dependence is characteristic of the third class of liquids—the associated, polyatomic liquids. The liquids of this type, which include water and alcohols exhibit values of absorption coefficient between one and three times that calculated from the shear viscosity. Values for hemoglobin solutions (horse, with sodium citrate solution added) are shown in Fig. 22 as a function of temperature and frequency. It appears that the acoustic absorption properties of blood are largely determined by the protein content.

From the meager amount of precise data available on ultrasonic absorption properties of biological materials and from the widely different values reported for presumably the same materials (Goldman and Hueter, 1956), it is apparent that determination of these properties is in an early stage of development.

b. Methods of Determining Absorption Coefficients

The gross or "average" ultrasonic absorption coefficients of bulk tissue and suspensions can be determined, under the conditions of continuous radiation, by measuring the relative sound level of a plane wave after

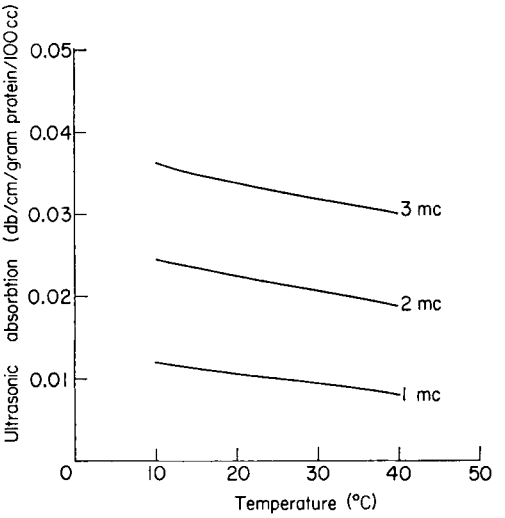

FIG. 22. Ultrasonic absorption versus temperature for hemoglobin solutions at three frequencies (after Carstensen *et al.*).

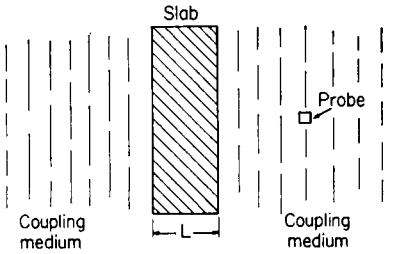

FIG. 23. Schematic arrangement for determining the acoustic absorption coefficient of a material using several specimens of different thicknesses.

transmission through slabs of various thicknesses of the material (see Fig. 23). The absorption coefficient obtained by this method includes losses resulting from all causes including scattering. Here, slabs of different thickness are irradiated with a constant sound level at normal incidence. The probe, depending upon the design, can respond proportionally to either a field variable (e.g., pressure amplitude or particle velocity amplitude) or the square of a field variable (e.g., intensity). For the case of a piezoelectric probe which responds to, for example, the sound pressure amplitude, the voltage produced at the probe terminals can be expressed as

$$E = Be^{-\alpha L} \tag{58}$$

where B is the proportionality constant, L is the slab thickness, and α is the pressure amplitude absorption coefficient per unit path length. For

the case of a probe whose response is proportional to the intensity, α of (58) is replaced by $\mu(=2\alpha)$, the intensity absorption coefficient per unit path length. In order to obtain α or μ from experimental measurements, the logarithm of the voltage E is plotted as a function of the slab thickness L. The slope of the resulting straight line yields α or μ, depending upon the type of probe used. That is, if m is the graphically determined slope, α or μ is equal to

$$-(m/\log_{10} e) \tag{59}$$

This method is appropriate under either of the two following circumstances. (1) The pressure amplitudes of the waves reflected at the two interfaces are small fractions of the incident pressure amplitudes, i.e., the characteristic acoustic impedances of the media are almost equal (within a few per cent). This condition implies that the reaction of reflected energy on the transducer is sufficiently small so that a constant driving voltage assures a constant sound level incident on the slab and that the acoustic level at the probe is not affected by sound which has traversed the slab more than once. (2) The reflection coefficient can be unrestricted if the thickness of the slab is sufficiently great so that after two transits through it the sound level is reduced to a small fraction (less than a few per cent) of the incident value. In this case, it is necessary to place the interface proximal to the transducer at the same distance from it for each measurement to assure a constant sound level at the interface for a constant driving voltage across the transducer. Analytically, the voltage exhibited by the probe is given by an expression of the form (58) where the proportionality constant now includes the effect of reflection. Therefore the logarithm of the probe voltage can be plotted as a function of the thickness L and the slope yields the pressure absorption coefficient per unit path length in accordance with relation (59).

The use of pulses of duration sufficiently short such that (for the dimensions of the apparatus and specimen) the direct transmitted pulse can be observed unaffected by reflected energy eliminates the limitation on the magnitudes of the reflection coefficients which can be determined without critical positioning of the slab in the field and without restricting the size of the receiver. It is possible, in order to realize greater sensitivity, to use resonant piezoelectric receivers of large size. In this case, quantitative determination of the absorption coefficient is exactly analogous to the continuous radiation method if a series of slabs of different thicknesses are available. Good use can be made of multiply reflected waves in the specimen if it is possible unambiguously to identify the number of transits, and in such a case two thicknesses of sample suffice for determination of both the absorption coefficient and the reflection coefficient at the coupling mate-

rial interface. If the reflection coefficient at the slab interface is C_r, then the pressure amplitudes of the temporal array of pulses arriving at the receiver after multiple reflection in the specimen of thickness L are proportional to $1, \beta, \beta^2, \ldots$, where

$$\beta = C_r^2 e^{-2\alpha L} \tag{60}$$

Here, the relative amplitude of the direct transmitted pulse is unity, that resulting from the first internally reflected pulse is β, etc. If the pulse number designating the direct transmitted pulse is represented by 0, that designating the first reflected pulse by 1, the second by 2, etc., then the logarithm of the relative amplitudes plotted as a function of the pulse number yields a straight line of slope m given by

$$m = \log_{10} \beta \tag{61}$$

If the probe response is proportional to the square of the pressure amplitude (e.g., intensity), then

$$m = 2 \log_{10} \beta \tag{62}$$

Specimens of two different thicknesses can be used to determine both the reflection and absorption coefficients from the following pair of relations:

$$\begin{aligned} \beta_1 &= C_r^2 e^{-2\alpha L_1} \\ \beta_2 &= C_r^2 e^{-2\alpha L_2} \end{aligned} \tag{63}$$

For the case where $C_r = 1$, the absorption coefficient can be determined from measurements made on a single thickness of specimen, i.e., $\beta = e^{-2\alpha L}$. Relations (60) through (63) are true only for the case where coupling media on both sides of the specimen have identical acoustic properties.

If neither of the circumstances previously listed as (1) and (2) are satisfied and if it is not possible to utilize short pulse wave trains as described in the preceding paragraph (e.g., because the acoustic wavelength is nearly as long or longer than the thickness of the specimen), then the arrangement illustrated in Fig. 24 can be used. Here, a focused beam of small aperture angle impinges on an interface of the specimen (with plane parallel faces) at oblique incidence. This arrangement eliminates the difficulties associated with the reaction of reflected energy at the transducer and avoids the difficulties arising from multiply reflected energy in the specimen. The incident beam should have a diameter at the specimen no greater than approximately one-fourth the thickness of the specimen. This is essential in order to avoid overlapping of the wave trains reflected in the specimen with the direct transmitted train. An appropriate beam can be produced for measurements of this type by focusing the radiation with a lens of aperture angle sufficiently small such that the axial length of the focal

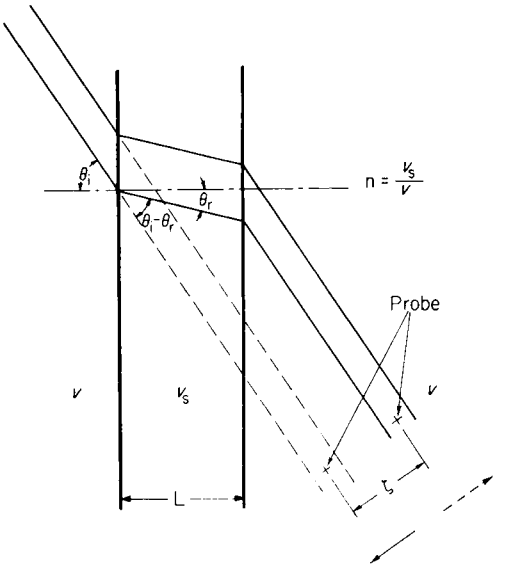

FIG. 24. Illustration of oblique incidence method of determining acoustic velocity and absorption.

region [refer to relation (44)] is as long or longer than the distance from the site at which the radiation enters the specimen to the site of the probe; i.e., the beam should neither diverge nor converge greatly in traversing the distance across the specimen. The position of the axis of the beam and the level of the ultrasonic radiation are first determined with the specimen removed from the field and then the lateral shift in the beam axis and the altered level of radiation are determined with the specimen inserted in the field. The lateral shift ζ of the beam axis determines the index of refraction n of the specimen relative to the imbedding medium and, hence, the velocity of sound in specimen according to the following relation,

$$n^2 = \sin^2 \theta_i + \left(\frac{\sin \theta_i \cos \theta_i}{\sin \theta_i - \zeta/L} \right)^2 \tag{64}$$

where θ_i is the angle of incidence and L is the thickness of the specimen. The quantity ζ is positive if the shift of the beam axis is in the direction of the dotted arrow and negative if the shift is in the direction of the solid arrow (see Fig. 24). In order to identify the direct transmitted beam, measurements are made starting with the probe away from the original position of the beam axis in the direction of the dotted arrow; the beam first observed is the direct one. It is apparent that the faces of the specimen slab, in the region of entry and exit of the direct beam, must be plane and parallel. The remainder of the specimen need not be so, although the varia-

tions in the immediate neighborhood should not be so great as to direct reflected acoustic energy into the direct beam.

Once the index of refraction is known, the absorption coefficient can be determined (for the case where the probe response is proportional to pressure amplitude, etc.) from the following relation,

$$\log_{10}\left(\frac{E_{\text{in}}}{E_{\text{out}}}\right) = -\frac{\alpha n L}{\sqrt{n^2 - \sin^2\theta_i}}\log_{10} e \tag{65}$$

where E_{in} is the voltage produced at the probe terminals with the specimen in the field and E_{out} is that voltage with the specimen out of the field. The left-hand side of relation (65) is plotted as a function of the thickness L for a series of specimens irradiated at a constant angle of incidence θ_i. The slope m of the resulting straight line yields the absorption coefficient α according to the following relation:

$$\alpha = -\frac{m\sqrt{n^2 - \sin^2\theta_i}}{n \log_{10} e} \tag{66}$$

If the probe response is proportional to intensity, then the slope of the straight line is proportional to the intensity absorption coefficient and α is replaced by μ in (65) and (66).

The portion of this chapter (Section II, 3, *b*) dealing with ultrasonic receivers did not include discussion of probes which respond to the acoustic intensity or the square of an acoustic field variable. Since the type of probe most important in this regard is a thermoelectric device which depends upon absorption of acoustic energy for its operation (W. J. Fry and R. B. Fry, 1954a, b; Dunn and W. J. Fry, 1957) a discussion of it is more appropriately treated in this subsection.

One convenient configuration of this type of probe is illustrated schematically in Fig. 25. A small thermocouple junction (0.0005 in. in diameter) is imbedded in a liquid sound absorbing medium which is separated from the ambient medium by two thin membranes supported by an appropriate structure. The acoustic absorbing liquid is chosen such that its density and the speed of sound in it closely match those of the ambient liquid in which the sound field is to be examined. For investigation of sound fields in water, dilute salt solutions and suspensions of biological materials. castor oil, and some silicone liquids possess suitable properties.

The thermocouple probe functions as follows (W. J. Fry and R. B. Fry, 1954a, b). The sound source is excited to produce a single acoustic pulse having a temporally rectangular envelope. The form of the thermoelectric emf produced in response to a one-second pulse shown in Fig. 26 results. A relatively rapid rise occurs just after initiation of the pulse followed by a slower "linear" rising phase for the remainder of the one-second interval.

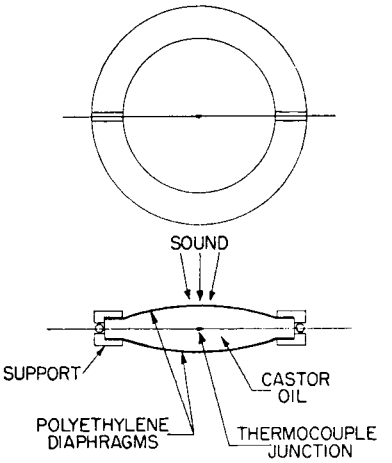

FIG. 25. Schematic diagram of thermocouple probe.

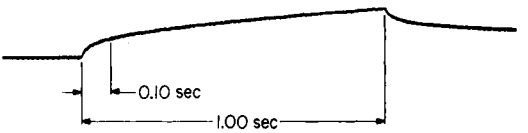

FIG. 26. Thermoelectric emf produced at the probe terminals in response to 1-sec pulse of ultrasound.

After cessation of the pulse, a rapid fall in temperature occurs followed by a slower return of the temperature to its value preceding the acoustic pulse. The initial, rapid increase in temperature results from the conversion of acoustic energy into heat by the viscous forces acting between the thermocouple wire and the imbedding medium (W. J. Fry and R. B. Fry, 1954a). This phase of the temperature events approaches equilibrium rapidly. The second phase of the temperature sequence, the "linear" part, is produced by absorption of sound in the body of the imbedding medium. The closeness of approach of this phase to linearity during irradiation is dependent upon the acoustic amplitude, the form of the variation of the acoustic absorption coefficient with temperature, the heat conductivity coefficients of the fluid and the wires, the duration of the acoustic disturbance, and the acoustic field of distribution. With a suitably designed probe, the second phase enables one to compute [see relation (67) below] the absolute sound intensity for the plane traveling wave case if the absorption coefficient of the imbedding medium is known. If the absolute sound intensity is known, the acoustic absorption coefficient can be determined. The relatively rapid decrease in temperature immediately following termination of the irradiation period results from the removal of the viscous force

mechanism which contributed a heat source confined to the immediate neighborhood of the thermocouple wire. The subsequent slow phase of the decline in temperature is a consequence of the cooling of the imbedding medium previously heated by absorption in the body of the medium. The temperature rise in the thermocouple junction resulting from absorption of sound in the body of the medium is independent of the direction of the wire relative to the direction of the acoustic particle velocity. However, the temperature rise resulting from the action of the viscous forces between wire and imbedding medium is a function of the angle between the direction of the acoustic particle velocity and the direction of the wire (W. J. Fry and R. B. Fry, 1954a). For absorbing materials such as castor oil, the temperature rise resulting from the viscous force action is comparable in magnitude to that resulting from absorption in the body of the medium for pulse durations of the order of one second.

It is convenient, for field configuration studies, to use 0.1-sec duration pulses because thermal recovery is quite rapid and therefore a great deal of experimental data may be obtained in a relatively short period of time. For plane wave fields, the absorption phase of the probe response can be used to determine either the intensity of the field or the absorption coefficient of the imbedding fluid since the slope of this phase is proportional to the square of the acoustic pressure amplitude. The relation basic to this type of operation of the probe is

$$I = \frac{\rho C}{\mu}\left(\frac{dT}{dt}\right)_0 \tag{67}$$

where $(dT/dt)_0$, the initial time rate of change of the temperature due to absorption in the body of the imbedding medium, being proportional to the slope of the slow phase of the thermocouple response, can be determined from a knowledge of the thermocouple sensitivity. In relation (67), the product ρC designates the heat capacity of the imbedding medium per unit volume, μ is the intensity absorption coefficient per unit path length, and I is the acoustic intensity. If ρC is expressed in units of joules per cubic centimeter per degree centigrade, μ in units of reciprocal centimeters, and dT/dt in units of degrees centigrade per second, then the intensity is in watts per square centimeter. The evaluation of the quantity $(dT/dt)_0$ from the experimentally determined temperature-time relation can be readily accomplished if certain criteria are satisfied (W. J. Fry and R. B. Fry, 1954a). An adequate discussion of these criteria cannot be presented in the space permitted here. However, let it suffice to indicate that for a copper-constantan thermocouple junction 0.0005 in. in diameter, imbedded in castor oil and irradiated with a pulse duration of one second by a 1 mc sound beam having a width at half-intensity of 4 mm and an intensity

level such that the total temperature rise is not greater than 1°C, the total error introduced by assuming that the time rate of rise of the slow phase of the thermocouple response is identical with $(dT/dt)_0$ in expression (67) is not more than 1%.

The methods described earlier in this subsection for the measurement of ultrasonic absorption coefficients require relatively large quantities of material. This is not a problem when the necessary amount of "homogeneous" material is available; however, it becomes one when the absorption coefficients of portions of intact biological systems are to be determined. The thermocouple probe method is very useful under these conditions since the junction can be placed at the site, in the specimen, at which the absorption coefficient is to be determined; i.e., the specimen acts as the thermocouple imbedding material. Then, irradiation with a pulse of known intensity produces a $(dT/dt)_0$ value which can be used with (67) to compute the absorption coefficient. In this fashion, absorption coefficients characteristic of only a few cubic millimeters of tissue can be determined. The work reported thus far in which this method has been employed has yielded useful results (W. J. Fry and R. B. Fry, 1953; W. J. Fry and Dunn, 1956; Dunn, 1958).

It is not necessary to utilize expression (63) in order to obtain the acoustic intensity (or the derived field variables) if a procedure is followed wherein the probe is calibrated in an ultrasonic field for which the acoustic field variables are known. This latter procedure is extensively employed since then it is not necessary to know values of the acoustic absorption coefficient and the other quantities appearing in (67). Such calibration of the probe in a field of known values of the acoustic variables permits the amplitude of the fast phase of the response to be related to the square of the particle velocity amplitude and the amplitude of the slow phase to be related to the square of the acoustic pressure amplitude. The proportionality constants determined in this way can then be used to compute the particle velocity and pressure amplitudes when the probe is placed in a pulsed field (at the same frequency and temperature) of unknown characteristics.

The thermocouple probe described here has a number of advantages over piezoelectric probes. It can be made extremely small in size, it is highly stable, it is insensitive to stray radio-frequency fields, it has a low electrical input impedance, and it can be used as a primary standard for accurately determining absolute sound levels at ultrasonic frequencies. The disadvantages are as follows: (*a*) in the 1 mc frequency range it is relatively insensitive, requiring intensities of the order of 1 w/cm^2 to obtain a suitable output; (*b*) it cannot be used to determine the temporal waveform of an acoustic disturbance.

c. Analytic Results

Analyses of the various absorption mechanisms have yielded results which can be used to correlate experimental data and deduce useful information. The available absorption data on materials of biological significance are very meager and consequently it is not possible to identify the specific mechanisms which underlie the ultrasonic absorption behavior of tissue components and other biological structures. It appears reasonable, however, to list here, with a few comments, quantitative expressions describing various absorption mechanisms.

(*1*) *Viscosity.* Shear viscosity alone gives rise to a dependence of the absorption coefficient per unit path length with the frequency as follows (Markham *et al.*, 1951),

$$\alpha = \left(\frac{3\rho\omega_v}{8\eta}\right)^{1/2} \left\{\frac{(\omega/\omega_v)^2}{(\omega/\omega_v)^2 + 1}\left[\langle 1 + (\omega/\omega_v)^2\rangle^{1/2} - 1\right]\right\}^{1/2} \tag{68}$$

where

$$\omega_v = 3v_0^2\rho/4\eta \tag{69}$$

The symbol v_0 is the acoustic velocity at low frequencies, η is the shear viscosity coefficient, ρ is the density of the medium, and ω is 2π times the frequency. At 38°C, the value of ω_v is 2.1×10^{12} sec^{-1} for water, 0.56×10^{10} sec^{-1} for castor oil, and 1.3×10^{8} sec^{-1} for macroscopic soft tissue ($\eta \simeq 150$ poises at 38°C). When $\omega \ll \omega_v$, the expression for α reduces to

$$\alpha = 2\eta\omega^2/3\rho v_0^3 \tag{70}$$

i.e., the absorption coefficient per unit path length is proportional to the square of the frequency. At frequencies where $\omega \gg \omega_v$,

$$\alpha = (3\rho\omega/8\eta)^{1/2} \tag{71}$$

and the absorption coefficient per unit path length is proportional to the square root of the frequency. At low frequencies where $\omega \ll \omega_v$, the acoustic velocity is independent of the frequency. However, as the value of ω approaches ω_v, the velocity increases and at high frequencies it is proportional to the square root of frequency. The type of dependence of the absorption coefficient on the frequency exhibited by (68) has not been observed for any material. The frequency range accessible for experimental work has not permitted ω_v to be attained for most materials of interest (see Section III, 1, *b*). The low-frequency behavior of the absorption coefficient for monatomic liquids does approximate the values calculated from (70). The absorption coefficient of cottonseed oil at 20°C also exhibits this behavior in the frequency range measured, i.e., from 4 to 100 mc (Mikhailov, 1958;

Dunn, 1960). For castor oil at 30°C, α varies as the 5/3 power of the frequency from 1 mc to the maximum frequency (116 mc) at which measurements have been made (Dunn, 1960). The absorption coefficient calculated for soft tissue from (70) does not agree with measured values in the frequency range 1–10 mc. All soft tissues studied thus far exhibit a nearly linear dependence of the absorption coefficient on frequency rather than a quadratic dependence. It has been shown (Schwan *et al.*, 1957) that measured values of protein absorption coefficients fall in the magnitude range to account for the major fraction of the tissue absorption.

(*2*) *Relaxation.* It appears that relaxation processes are involved in the absorption of ultrasound by protein (and therefore tissue) in the frequency range thus far investigated. However, the observed dependence of the absorption coefficient on the frequency cannot be explained by a mechanism involving a single relaxation frequency. Consequently, both continuous distributions and appropriately chosen discrete spectra of relaxation frequencies have been postulated to explain the observed dependence. Both structural and thermal relaxation mechanism must be involved since both negative and positive temperature coefficients of absorption have been identified (negative for blood proteins, positive for tissue of the central nervous system). Since this work is in the early stages, it seems appropriate to discuss the characteristics of absorption coefficient dependence on a single relaxation frequency which will permit its application to biological materials and to illustrate how distributions of relaxation frequencies can be constructed to fit specific data. For a single relaxation frequency f_r the absorption coefficient per unit path length is given by

$$\alpha = \alpha_r(v_r/v) \frac{2(\omega/\omega_r)^2}{1 + (\omega/\omega_r)^2} \tag{72}$$

where $\omega_r = 2\pi f_r$, α_r is the absorption coefficient, and v_r is the acoustic velocity at this frequency. The relaxation frequency is most readily identified from the data as the frequency at which the absorption coefficient per wavelength $\alpha\lambda$ is maximum. The acoustic velocity of biological materials (tissue, cell suspensions) does not change very much with frequency (Carstensen and Schwan, 1959b). The maximum change in velocity Δv over the entire frequency range for a single relaxation frequency is

$$\frac{\Delta v}{v} = \frac{\alpha_r \lambda_r}{\pi} \tag{73}$$

and for soft tissue this is of the order of 1 %. Therefore (68) can be simplified to

$$\alpha = \alpha_r \frac{2(\omega/\omega_r)^2}{1 + (\omega/\omega_r)^2} \tag{74}$$

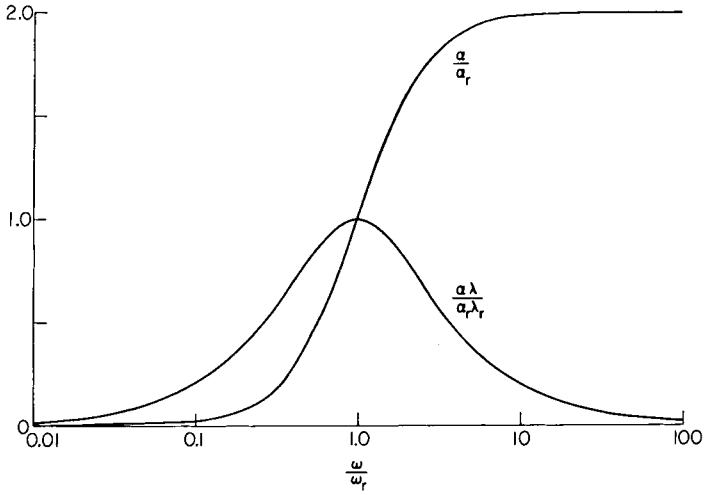

FIG. 27. Relative absorption per unit path length and relative absorption per wavelength versus relative frequency for a single relaxation process.

Figure 27 shows the relative absorption per unit path length and the relative absorption per wavelength as a function of relative frequency for a single relaxation process.

It is clear from (74) that, if $\omega \ll \omega_r$, α is a quadratic function of the frequency, the same type of frequency dependence exhibited by the shear viscosity mechanism. It is possible to distinguish between these two types of mechanisms on the basis of frequency dependence if the dependence is not quadratic even if a relaxation frequency is not specifically identified as a peak in the absorption per wavelength relation. This follows from the fact that a shear viscosity mechanism can only yield a quadratic dependence whereas a relaxation mechanism can yield practically any type of frequency dependence of absorption by appropriate choice of a spectrum of relaxation frequencies. This is illustrated in Fig. 28 where a choice of two relaxation frequencies (one centered at 1 mc and the second centered at such a high frequency that only the quadratic dependence is evident) is shown to yield a value of the absorption coefficient per wavelength which varies less than 20% over the frequency range from 0.66 to 6.6 mc. One is free to choose both the value of ω_r, which determines the position of the maximum absorption per wavelength, and the value of α_r which determines the magnitude of the absorption effect, for each relaxation frequency. The type of behavior illustrated in Fig. 28 appears to be characteristic of soft tissue and hemoglobin, although the specific example was chosen for illustrative purposes only. The unambiguous identification of the relaxation frequencies, their number and distribution require accurate experimental measurements

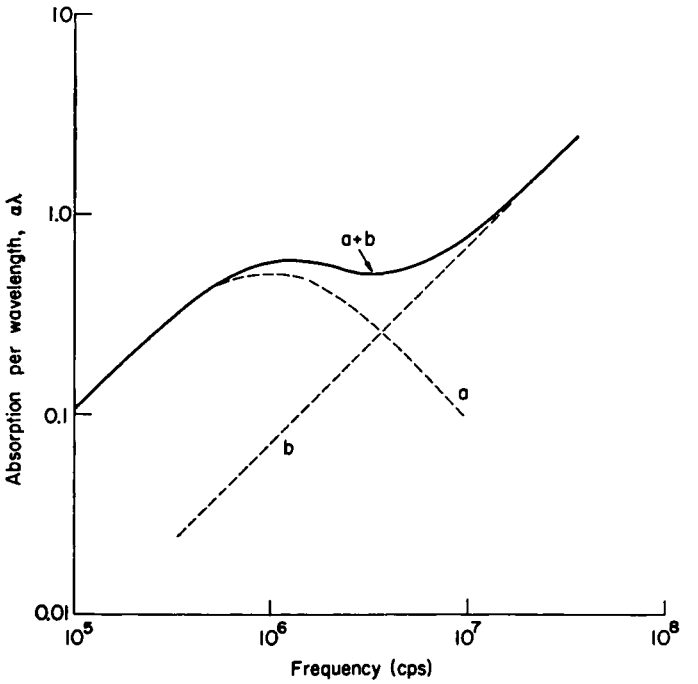

FIG. 28. Frequency dependence of $\alpha\lambda$ for a system with two relaxation frequencies (after Schwan).

over a much wider frequency range than that which has been covered thus far. It is not always possible to decide between the existence of a few discrete relaxation frequencies or a "continuous" distribution particularly when the maxima of the absorption per wavelength relation with frequency are not prominent. At present, it is preferable to assume that readily recognized maxima in the absorption per wavelength relation correspond to discrete relaxation frequencies rather than to "continuous" distributions.

(*3*) *Relative Motion.* Relative motion between structure elements and the imbedding liquid, produced by the acoustic field, results in absorption of energy from the field. This mechanism contributes a measurable fraction of the total absorption in suspensions of erythrocytes in saline (Carstensen and Schwan, 1959a). Whether such a mechanism is important on a molecular level has not yet been established.

The relative motion between suspended elements and suspending fluid, which results in viscous interaction, arises because of density differences between the elements and the fluid. An approximation analysis employing the concepts of frictional force constants and equivalent masses yields a relaxation-type expression for the absorption coefficient with the modifica-

tion that the "relaxation frequency" and the amplitude factor are frequency-dependent as shown by relation (75) below (W. J. Fry, 1952; Angerer *et al.*, 1951; Brandt *et al.*, 1937). The most general approach to this type of system (spherical particles) is that of Epstein (1941), who considers the problem of the absorption of sound in a medium containing spherical particles whose diameters are small compared to the acoustic wavelength. The absorption coefficient calculated from this treatment yields, to a first approximation, the same expression as that obtained from the approximation analysis which assumes that the structural elements are stiff in shear compared to the imbedding medium. The latter analysis indicates that the same form of expression applies in the case of nonspherical elements. This expression is

$$\alpha = \frac{C}{2v} \frac{(1 - \rho/\rho_e)^2}{\rho/\rho_e} \omega_0 \frac{(\omega/\omega_0)^2}{1 + (\omega/\omega_0)^2} \tag{75}$$

where $\omega_0 = R/M_e$, $\omega = 2\pi f$, v is the acoustic velocity, ρ and ρ_e are the densities of the imbedding medium and the structure elements, respectively, and C is the volume concentration of structure elements, i.e., the volume of fluid displaced by the elements per unit volume of suspension. The symbols R and M_e designate the frictional force constant and the effective mass of an element, respectively, and are given by the following relations for spherical particles (Lamb, 1945):

$$R = 6\pi a\eta[1 + (\rho/2\eta)^{1/2} a\omega^{1/2}] \tag{76}$$

$$M_e = M + m\left[\frac{1}{2} + \frac{9}{4(\rho/2\eta)^{1/2} a\omega^{1/2}}\right] \tag{77}$$

where η is the viscosity of the imbedding liquid, a is the radius and M is the mass of an element, and m is the mass of fluid displaced by the particle. The values for R and M_e for nonspherical elements can be estimated from (76) and (77) by inserting an average value for the radius if the element does not deviate greatly from a spherical shape. R and M_e are seen to be frequency-dependent, and consequently, the "relaxation frequency" $\omega_0/2\pi$ is frequency-dependent, and this is also true for the amplitude of the absorption coefficient given by (75).

The frequency dependence of the absorption coefficient due to relative motion as described by (75), (76), and (77) and that due to relaxation as described by (74) are compared in Fig. 29 where the absorption coefficient per wavelength is shown as a function of frequency. It is seen that, compared with a single relaxation process, a marked broadening of the absorption curve occurs when a relative motion mechanism is operative. Experimental results obtained on suspensions of beef erythrocytes in saline, after

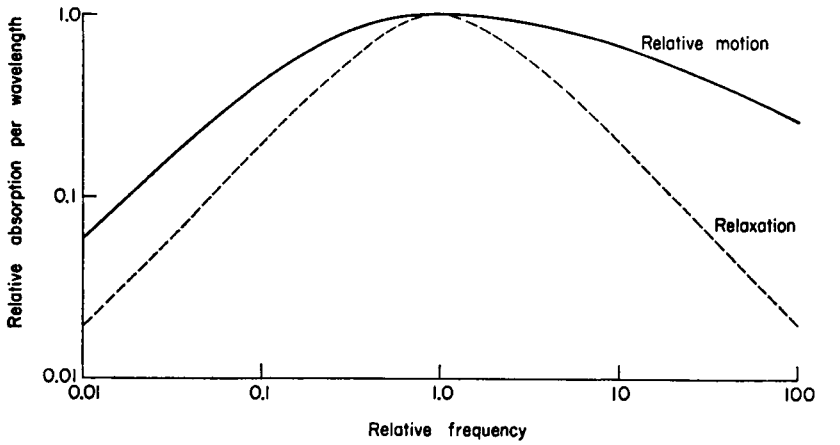

FIG. 29. Comparison of the frequency dependence of $\alpha\lambda$ due to relative motion and relaxation absorption (after Carstensen and Schwan, 1959a).

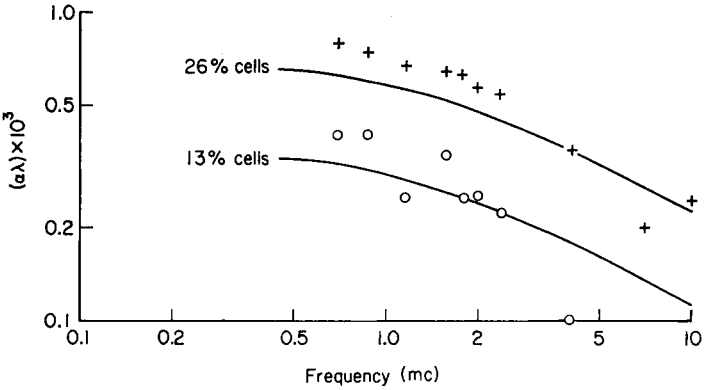

FIG. 30. Comparison of observed nonprotein absorption in beef erythrocytes in saline (points) with absorption computed for relative motion using $\rho_e = 1.084$ gm/cm^3, $\eta = 0.01$ poise, and $a = 2.3\mu$ (after Carstensen and Schwan, 1959a).

correction for absorption by the protein components, and values calculated from (75) are shown in Fig. 30 (Carstensen and Schwan, 1959a).

(*4*) *Bubble Effects.* The presence of gas bubbles in a liquid system exerts a marked influence on the propagation characteristics of ultrasound in the medium. Since some biological systems normally contain included gas bubbles (or bubbles may be introduced either inadvertently or by design of the investigator), it is important to consider quantitatively the effects of included gas bubbles on ultrasonic propagation (Dunn and W. J. Fry, 1961). When the bubble "diameter" is large, i.e., of the order of a wavelength or larger, its major effect is one of scattering the acoustic radiation. Since the

characteristic acoustic impedance of the medium (liquid or tissue) is much greater than that of the gas, most of the energy is reflected (see Section II, 2). When the bubble "diameter" is small compared with a wavelength, several physical processes become important in contributing to the absorption of acoustic energy and formulas for evaluating the magnitude of the effects produced by these processes will be given. [The expressions for the resonant frequency and the dissipation parameters are those given by Devin (1959)]. The time rate of dissipation of acoustic energy by a bubble is greatest when the resonant frequency of the bubble is equal to the frequency of the acoustic field. The diameter of a resonant bubble is small compared to the acoustic wavelength as can be seen from the following relation

$$f_0 = \left[\left(\frac{3\gamma P_0}{\rho}\right)\left(\frac{g}{\epsilon}\right)\right]^{1/2} \Big/ 2\pi R_0. \tag{78}$$

where

$$g = 1 + \frac{2\sigma}{P_0 R_0}\left(1 - \frac{1}{3h}\right) \tag{79}$$

$$\epsilon = 1 + \frac{3(\gamma - 1)}{2\Phi R_0}\left[1 + \frac{3(\gamma - 1)}{2\Phi R_0}\right] \tag{80}$$

$$\Phi = \left(\frac{\omega_0 \rho_g c_p}{2K}\right)^{1/2} \tag{81}$$

f_0 is the resonant frequency of the bubble, γ is the ratio of specific heat at constant pressure to that at constant volume ($\gamma = 1.4$ for O_2, N_2, air), P_0 is the static pressure, R_0 is the mean radius of the bubble, ρ is the density of the liquid, ρ_g is the density of the gas, σ is the surface tension, $h = \gamma/\epsilon$, c_p is the heat capacity of the gas at constant pressure, and K is the thermal conductivity coefficient of the gas. The quantity h lies between unity (isothermal case) and γ (adiabatic case); consequently g is always positive. Expression (74) is an implicit expression for f_0 which can be solved by a simple graphical procedure. The right-hand side of the equation is plotted as a function of f_0 and the left-hand side, on this same plot, is a straight line through the origin with a slope of unity. The intersection of these two curves occurs at the resonant frequency corresponding to the values chosen for the other parameters used in making the computation. For values of R_0 sufficiently large such that the second terms of g and ϵ are small compared with unity, (78) reduces to

$$f_0 = \left(\frac{3\gamma P_0}{\rho}\right)^{1/2} \Big/ 2\pi R_0 \tag{82}$$

This corresponds to the adiabatic state for the gas in the bubble. To illustrate the magnitudes of the quantities involved, it can be readily shown

that a resonant frequency of 1 mc for an air bubble in water corresponds to a bubble radius of approximately 3 μ.

The total dissipation parameter b is equal to the sum of the thermal, radiation, and viscous dissipation parameters, respectively, b_t, b_r, and b_v. The pressure absorption coefficient per unit path length α is related to the total dissipation parameter as follows:

$$\alpha = \frac{bnv}{4}\left\{\frac{\left(\frac{3\gamma P_0}{R_0^2}\right) + \omega^2\rho}{\left[\frac{1}{4\pi R_0}\left(\rho\omega^2 - \frac{3g\gamma P_0}{\epsilon R_0^2}\right)\right]^2 + b^2\omega^2}\right\} \tag{83}$$

where n designates the number of bubbles of diameter R_0 per unit volume and v is the acoustic velocity in the liquid. At the resonant frequency, (83) becomes

$$\alpha = \frac{nv}{4b\omega^2}\left(\frac{3\gamma P_0}{R_0^2} + \omega^2\rho\right) \tag{84}$$

Relations (83) and (84) apply to the case where all bubbles are of equal diameter. If this is not the case, a summation over all sizes is necessary. This can be accomplished by numerical integration of the right-hand side of (83) over the appropriate range of R_0.

Expressions for b_t, b_r, and b_v are required in order to evaluate (83) and (84). The complete expression for the thermal dissipation parameter is quite complex but approximate relations of simpler forms can be used to calculate it over most of the range of values of the parameters. When $2\Phi R_0 \leqslant 2$,

$$b_t \simeq B_t\left(\frac{\gamma - 1}{\gamma}\right)\frac{(2\Phi R_0)^2}{30} \tag{85}$$

and when $2\Phi R_0 \geqslant 5$,

$$b_t \simeq B_t\,\frac{1 - (1/\Phi R_0)}{1 + [2\Phi R_0/3(\gamma - 1)]} \tag{86}$$

where

$$B_t = \frac{3\gamma P_0 g}{4\pi R_0^3 \omega\epsilon} \tag{87}$$

The dependence of b_t on $2\Phi R_0$ is illustrated in Fig. 31 which shows b_t/B_t plotted as a function of $2\Phi R_0$ for $\gamma = 1.40$. The radiation dissipation parameter is given by

$$b_r = \frac{\rho\omega^2}{4\pi v} \tag{88}$$

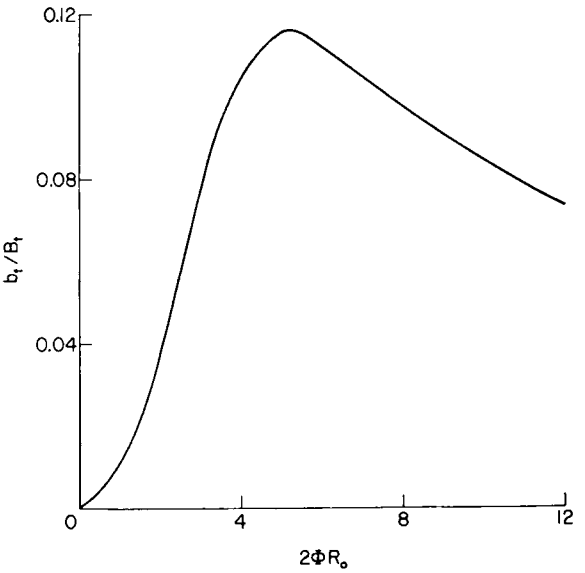

FIG. 31. Dimensionless thermal dissipation parameter versus dimensionless parameter $2\Phi R_0$ (after Devin).

and the viscous dissipation parameter by

$$b_v = \frac{\eta}{\pi R_0^3} \tag{89}$$

where η is the coefficient of viscosity of the liquid. The magnitudes of these dissipation parameters, for the individual processes and for the total dissipation parameter, are compared in Fig. 32 for resonant air bubbles in water as a function of frequency over the range from 1 to 1000 kc. The ordinates of the figure are the dissipation parameters multiplied by the quantity H, which is given by

$$H = \frac{4\pi R_0}{\omega_0 \rho} \tag{90}$$

It should be noted that, for both sufficiently large and sufficiently small values of the bubble radius, the resonant frequency is proportional to $1/R_0$. When this situation exists, the value of b_t at resonance is proportional to $1/R_0$ if R_0 is small and to $1/R_0^{5/2}$ if R_0 is large. The values of b_r and b_v are proportional to $1/R_0^2$ and $1/R_0$, respectively. The corresponding value of Hb_t is proportional to R_0 if R_0 is small and to $1/R_0^{1/2}$ if R_0 is large, Hb_r is constant, and Hb_v is proportional to R_0.

In deriving the expressions of this section, it has been assumed that the

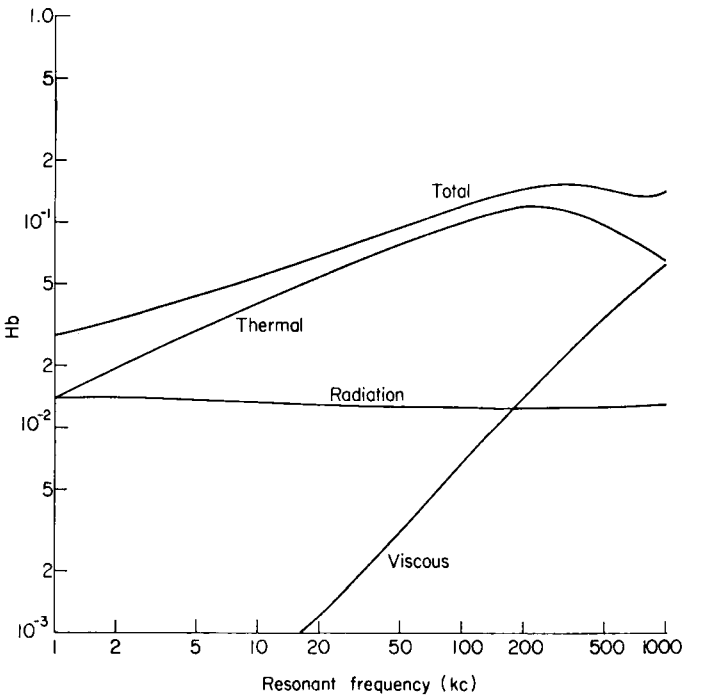

FIG. 32. Theoretical dimensionless thermal, radiation, viscous, and total dissipation parameters for resonant air bubbles in water (after Devin).

displacement amplitude of the bubble surface is sufficiently small that a linear theory adequately describes the phenomena.

6. Cavitation

The phenomena included under the term cavitation (defined below) will not be comprehensively treated in this chapter since the modifications of biological structures of interest here, produced by intense ultrasound, occur in the absence of cavitation and, in particular, require that cavitation be absent. As indicated in the introduction, the relatively gross disruptive effects produced in biological systems by cavitation were rather extensively studied in the early researches concerned with the application of ultrasound to the investigation of biological systems. It is important, however, to describe at least some of the phenomena which are generally included in the cavitation category and to present experimental results on the acoustic "threshold" conditions in order that experiments can be designed appropriately for its prevention. Accordingly, the results of the dependence of cavitation thresholds on various physical parameters which specify the state of the system are briefly summarized. A brief qualitative discussion

of some of the mechanisms which have been proposed to explain cavitation phenomena is given. Since theoretical work in this field has not progressed to the stage where unique and unifying descriptions of the mechanism(s) underlying the various aspects of cavitation can be given, no quantitative formulation of these theories is presented.

Cavitation phenomena are produced in a liquid medium subjected to an acoustic disturbance when the acoustic pressure during rarefaction reduces the hydrostatic pressure to some "threshold" value. This value of the acoustic pressure amplitude is a function of a number of physical parameters which describe the state of the medium (discussed below). The types of phenomena observed can be classified into two categories: (1) quiet degassing of a medium containing dissolved or entrained gas; and (2) catastrophic collapse (during the compression phase) of cavities accompanied by a broad band noise spectrum. The latter phenomena are initiated only if the medium experiences a tension stress during a portion of the rarefaction phase of the acoustic disturbance. In the following discussion the term cavitation refers to the second phenomena only, i.e., quiet degassing of the medium is excluded.

Theoretical estimates of the tensile strengths of liquids indicate values much greater than the tension stresses which are present when cavitation occurs (Blake, 1949a). Therefore, it is necessary to postulate that there exist sites at which the structure of the medium is weak. A number of mechanisms which embrace this concept have been proposed by various investigators. It should be noted first that the lifetime of a small free (undissolved) gas bubble in a liquid is quite short. For bubbles of about one micron diameter, the lifetime is of the order of several minutes. Therefore, such bubbles cannot be the source of weak spots or flaws in the medium at which cavitation phenomena are initiated. One mechanism which has been proposed to explain cavitation suggests that the flaws are small bubbles adherent to or included on hydrophobic surfaces (Blake, 1949b; Rosenberg, 1953; Willard, 1953). (It can be shown that small bubbles can remain stable indefinitely on hydrophobic particles which possess a concave surface.) The experimental evidence which supports this mechanism is that cavitation is more difficult to produce in liquid media which have been degassed or pressurized by subjection to a high hydrostatic pressure and that liquid media cavitate more readily after cavitation has once been produced. A second mechanism involves the suggestion that the gas nuclei are encapsulated in "organic" skins which form the surface layers of the bubbles and that these layers reduce the gas diffusion rate to such an extent that the bubble does not dissolve in the surrounding liquid. Here, the threshold of cavitation is a function of both the tearing strength of the skin and the bubble radius (Fox and Herzfeld, 1954). In a third mechanism proposed to

account for flaws or weak spots in the liquid, it is suggested that a homogeneous nucleation process occurs in which a gas, or germ nucleus, is formed by a small number of gas molecules. Such a nucleus would then constitute the site for growth of a cavity under the driving action of an ultrasonic field (Lindström, 1955).

Before discussing the various mechanisms which have been proposed to account for the growth and/or collapse of nuclei in the acoustic field, the experimental results which have been obtained in this field are summarized. Of particular interest are those results which bear upon the application of ultrasound to the study of biological systems. No single investigator has covered all aspects of cavitation effects in ultrasonic fields in a comprehensive fashion, i.e., variation with frequency, hydrostatic pressure, pulse length, dissolved gas content, etc. Most of the work has been done using water as the liquid medium although some information is available on other materials and mixtures of liquids. The method of preparation of the medium is important in determining the population distribution of nuclei or flaws and consequently the results on cavitation thresholds by different investigators and/or techniques do not always agree. The type of field used to produce the effects, i.e., traveling or standing waves, is another important feature which must be considered since this determines the length of time that a nucleus or flaw is subjected to the acoustic field at a specific level. Therefore, the experimental results included here to illustrate the principal features of cavitation phenomena are not necessarily quantitatively consistent with one another. However, they serve to illustrate the variations which occur as different physical parameters are varied.

The variation, with frequency, of the minimum acoustic pressure amplitude required for the production of cavitation (detected by the broad band noise spectrum produced) is shown in Fig. 33 for both degassed water and water saturated with air at room temperature (Esche, 1952). It is seen that the cavitation threshold at low frequencies (to about 10 kc) is approximately 2 atm or 1.3 w/cm^2 for degassed water under a hydrostatic pressure of one atmosphere. The threshold increases rapidly in the range from 100 kc to 1 mc where the threshold intensity is greater than 50 atm or 1000 w/cm^2.

Cavitation thresholds have been determined for some biological materials. Esche (1952) found that at a frequency of 500 kc, cavitation can be produced in fresh beef blood at minimum intensities in the "range" of 130–260 w/cm^2. No detailed discussion of the method of extracting and handling the blood is given in this report, hence it is difficult to decide whether nuclei were produced by the extraction procedure. It is interesting in this regard to recall the work of Harvey *et al.* (1944b) on the cavitation thresholds of blood and the precautions which were employed in extracting and handling

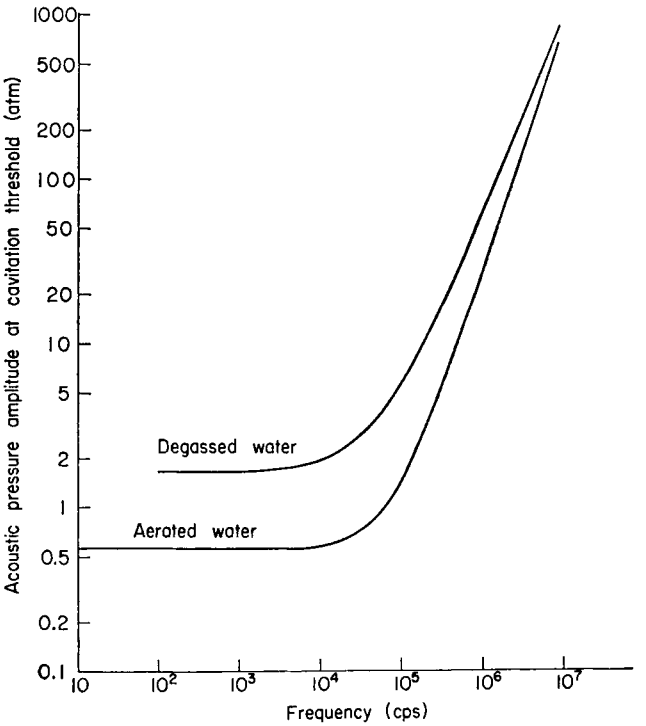

FIG. 33. Variation of the acoustic intensity cavitation threshold with frequency for both degassed and aerated water (after Esche).

this material in order to minimize the introduction of nuclei. Esche (1952) reports that no cavitation was produced in muscle (beef) at the highest intensity levels he employed (approximately 400 w/cm^2) at a frequency of 500 kc. Tissue of the central nervous system can be irradiated at pressure amplitudes of up to 50 atm at a frequency of 1 mc for periods of time up to two seconds without evidence of cavitation (Dunn, 1958; Barnard *et al.*, 1956).

The effect of hydrostatic pressure on the threshold value of the acoustic pressure amplitude required for the production of cavitation in water is illustrated in Fig. 34 for the temperature range from 10–50°C (Blake, 1949b). The data were obtained at a frequency of 60 kc in a standing wave type field (spherical resonator method). The pressure range covered in Fig. 34 is quite restricted, but no comprehensive investigation of the effect of hydrostatic pressure on the cavitation threshold over a much wider pressure range is available. It should be noted, however, that one method of preparing liquids is to subject them to a high hydrostatic pressure (as high as 1000 atm) in order to increase the ultrasonic cavitation threshold. Figure 35 shows the data of Fig. 34 replotted to illustrate the variation of the

acoustic cavitation threshold (pressure amplitude) as a function of temperature for various values of the hydrostatic pressure. It is seen that the pressure amplitude at cavitation threshold decreases as the temperature increases.

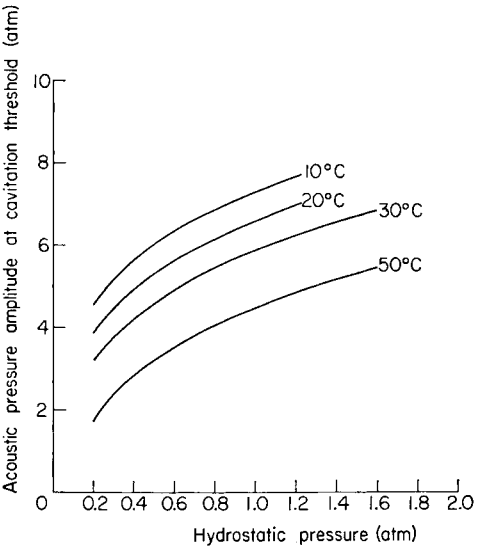

FIG. 34. Variation of the acoustic pressure cavitation threshold with hydrostatic pressure at 60 kc (after Blake).

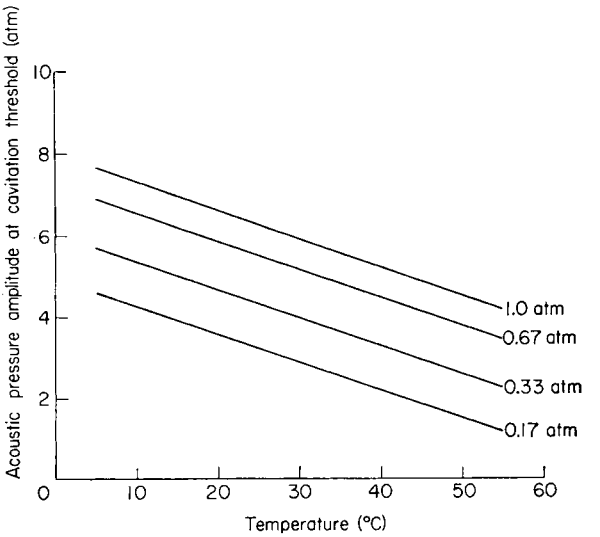

FIG. 35. Variation of the acoustic pressure cavitation threshold with temperature at 60 kc (after Blake).

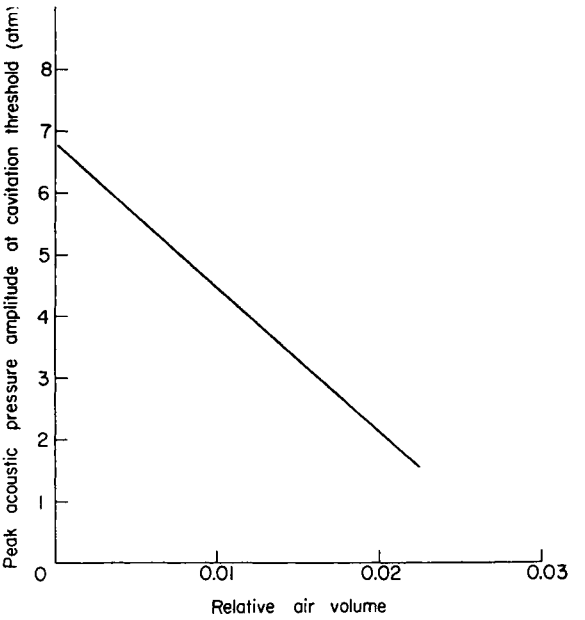

FIG. 36. Variation of the acoustic pressure cavitation threshold with dissolved air at 25 kc (after Strasberg).

The variation of the acoustic cavitation threshold (pressure amplitude) as a function of air content in water is illustrated in Fig. 36 (Strasberg, 1959). The data corresponds to 1 atm hydrostatic pressure and temperature in the range 20–24°C. It is seen that the pressure amplitude required for the initiation of cavitation decreases with increasing gas content. The data given in Fig. 36 were obtained at a frequency of 25 kc. The extrapolated value of the pressure amplitude at zero gas content agrees with that obtained from Fig. 35 for the appropriate temperature and hydrostatic pressure.

The minimum acoustic pressure amplitude for the production of cavitation increases as the pulse length of an acoustic disturbance is decreased (Hueter and Bolt, 1955). The particular range of pulse lengths over which this increase becomes marked is a function of the frequency. For example, this marked increase occurs for pulse lengths in the range of 300–500 msec at a frequency of about 400 kc for air saturated water. For degassed castor oil the sharp trend to higher threshold values occurs in the range of pulse lengths 30–40 msec at a frequency of 25 kc. The minimum acoustic intensity for cavitation also appears to be dependent upon the viscosity of the medium. High-viscosity liquids such as oils and solutions of high polymers impede the growth of bubbles and thereby possess relatively high cavitation thresholds (Hueter and Bolt, 1955).

Attempts to elucidate the mechanism(s) of the growth and/or collapse of gas bubbles or cavities in an acoustic field have included both the phenomena of quiet degassing and nonlinear collapse in both standing wave and traveling wave fields and at a variety of frequencies. High-speed photographic methods have been employed to observe the history of individual cavities and bubbles and acoustic methods have been used to detect accompanying phenomena. The mechanisms which have been proposed as underlying cavity and bubble growth and collapse include: (1) rectified diffusion (Blake, 1949b; Hueter and Bolt, 1955); (2) growth of gas-filled cavities to resonant dimensions during many cycles of the acoustic field and the production of periodic shock waves when resonance is reached (Willard, 1953); (3) explosive expansion and collapse of vapor-filled cavities over a single or relatively few cycles of the acoustic disturbance (Noltingk and Neppiras, 1950).

The process of rectified diffusion is presumed to occur in the following manner. In a liquid containing dissolved gas, diffusion occurs across the surface of a bubble. Bubble growth results as follows. During the positive pressure phase of the acoustic disturbance, gas diffuses into the liquid which is undersaturated with respect to the partial pressure of the gas in the bubble. During the negative phase of the cycle, gas diffuses from the liquid into the bubble which is then undersaturated with respect to the partial pressure of the gas dissolved in the liquid. Since the surface area of the bubble is larger during the negative half-cycle, there is a net ultrasonically induced diffusion of gas into the bubble. If the rate of net transfer of gas into the bubble exceeds the rate at which the gas of the bubble dissolves into the liquid as the result of the excess internal pressure caused by surface tension, the bubble grows. The acoustic pressure amplitude necessary for rectified diffusion to occur need not reduce the hydrostatic pressure of the liquid such that tension stress is produced. Thus rectified diffusion can result in "quiet degassing" of a liquid in which dissolved gas is present. Bubbles can grow to resonant size and vibrate with relatively large amplitude. The acoustic spectrum observed in this case, by measurements with an appropriate probe, exhibits the fundamental frequency and harmonics without a broad band noise spectrum.

The scheme in which it is proposed that growth occurs over many cycles to reach a catastrophic phase in acoustic fields in which the pressure amplitude is large enough to produce tension stresses is described briefly as follows. An initiation phase is characterized by the growth of volume oscillations of a gas-filled nucleus. This process continues for a relatively large number of cycles until the expanding cavity reaches resonant size for the frequency of the ultrasonic field. Once the resonant size is reached, the amplitude of oscillation increases markedly and nonlinear oscillations occur. Large amplitude expansion and violent collapse result in the production of

shock waves which exceed, by a large factor, the amplitude of the driving field. The periodically radiated shock waves are of sufficient amplitude to cause a multitude of microcavities in the neighborhood of the generating cavity. When the acoustic disturbance terminates, both the microcavities and the vibrating cavities collapse. In degassed liquids, no evidence of bubbles remains, however, in liquids containing dissolved gas, a gas bubble remains as a by-product.

The third theory describes the underlying mechanism of cavitation as an explosive expansion of a nucleus during one or possibly a few cycles of an acoustic disturbance. Such transient cavities occur when the hydrostatic pressure in the liquid is reduced during the rarefaction phase of the acoustic disturbance to such a value that the initial gas filled nucleus becomes unstable. The explosive expansion is followed by collapse of the cavity with the production of high peak pressures. The violence of the collapse increases with the ratio of the maximum cavity radius to the initial radius. Since this ratio decreases as the sound frequency increases, at constant acoustic pressure amplitude, the theory accounts for more pronounced cavitation effects at low frequencies. With a driving acoustic pressure amplitude of one atmosphere, it is possible to obtain shock waves of several hundred atmospheres pressure in the immediate neighborhood of the collapsing cavity (Moeller and Schach, 1941).

In concluding this brief qualitative description of cavitation phenomena it is desirable to note that various theories of the chemical actions associated with cavitation have been proposed. At least four different explanations have received attention by various investigators (Lindström, 1955). These explanations can be classified under the terms: (1) resonant bubble; (2) collapse; (3) discharge; and (4) mechanicochemical. According to the resonant bubble theory, the chemical effects are produced as thermal gas phase reactions (Fitzgerald *et al.*, 1956). The collapse theory proposes that the chemical effects are initiated by high pressures and temperatures produced at the time of collapse of the cavities (Weissler and Cooper, 1948). The discharge theory holds that ionization occurring in the atmosphere of the cavity is the cause of the chemical products produced (Lindström, 1955). In the mechanicochemical theory, it is assumed that the surface of the cavity is in a highly reactive state after rupture of the medium. It is presumed that chemical bonds are broken to produce ions and free radicals at the cavity surface. Subsequent reactions presumably result in the products observed (Marboe and Weyl, 1950).

7. Nonlinear Ultrasonic Fields

The previous parts of this section have been concerned with acoustic fields which can be quantitatively described in terms of a "linear" analysis

that is, it is assumed that the change in the density of the medium is directly proportional to the change in the pressure (i.e., it is assumed that the waves are of infinitesimal amplitude). For waves of finite amplitude, the linear analysis is not adequate to describe the acoustic field when there occurs appreciable deviation from the linear approximation to the relation between the incremental changes in density and pressure determined by the equation of state for the medium. The interest here is in the intermediate range between waves of infinitesimally small amplitude and strong shock waves. The incremental change in pressure may be written as the first two terms in a series expansion of density increments for a dissipationless medium, as

$$p = \rho_0 v^2 \left(\frac{\rho - \rho_0}{\rho_0}\right) + \frac{B}{2}\left(\frac{\rho - \rho_0}{\rho_0}\right)^2 \tag{91}$$

where ρ_0 is the undisturbed density, v is the velocity of propagation for the "linear" case (see Section II, 1), and the quantity B is a function of the pressure dependence of the adiabatic compressibility

$$\frac{B}{\rho_0 v^2} \simeq \left(\frac{\bar{K}_{ad} - K_{ad}}{\bar{K}_{ad}^2 P}\right) - 1 \tag{92}$$

where the quantity K_{ad} is the adiabatic compressibility ($\bar{K}_{ad}$ at zero pressure and K_{ad} at pressure P). The isothermal compressibility may be used in place of the adiabatic compressibility for estimating the magnitudes of some of the effects described here.

A number of distinct phenomena, not observed in low-amplitude acoustic fields, become apparent as the wave amplitude is increased. The more important phenomena are discussed here and quantitative relations are presented which are useful for obtaining values of the ultrasonic parameters of exposure and making computations associated with calibration procedures.

As an ultrasonic disturbance of finite amplitude propagates through a medium, energy is transferred from an initially monochromatic wave to its harmonics. Of particular interest here are the changes in the magnitudes of the harmonics compared to that of the fundamental as propagation proceeds. As a result of absorption in the medium, the waveform becomes "stabilized" at some distance from the source.

If structures possessing acoustic properties different from that of an imbedding medium are subjected to high level acoustic radiation, steady or unidirectional forces are exerted on them. The steady force resulting from radiation pressure is most important for the work discussed in this chapter and will be treated quantitatively. This force results when the acoustic energy density changes with position in the medium. This occurs at an

interface between two media of different acoustic properties and also results from absorption of acoustic energy in a homogeneous medium. Since radiation pressure methods are useful for the absolute calibration of ultrasonic probes in the megacycle frequency range, graphs and tables for this specific use are included.

The "average Stokes force" on a structure suspended in a high-intensity ultrasonic field arises from the temperature dependence of the viscosity of the medium. The viscosity is greater during a rarefaction (lower temperature) than during a compression (higher temperature) and, consequently, the time average of the product of the viscosity and particle velocity is not zero. The force exerted on a stationary sphere of radius a in a fluid medium having a viscosity η and moving with a velocity $\dot{\xi}$ is

$$F = 6\pi a\eta\dot{\xi} \tag{93}$$

which results in a unidirectional force exerted on the structure. In the case of a liquid, since the viscosity is decreased during compression and increased during rarefaction, the average force is oriented in a direction opposite to the direction of propagation of the acoustic field producing the fluid particle velocity (Hueter and Bolt, 1955; Westervelt, 1951). The Oseen steady force, which is independent of the temperature variations of the sound field, arises as the result of wave distortion and can be derived by extending (93) to include a term of second order in the velocity (Westervelt, 1951), i.e.,

$$F = 6\pi a\eta\dot{\xi}(1 + h\dot{\xi}) \tag{94}$$

If the ratio of the amplitude of the second harmonic to that of the fundamental is designated by s and the phase angle by ϕ such that

$$\dot{\xi} = \dot{\xi}_0[\sin \omega t + s \sin (2\omega t + \phi)] \tag{95}$$

and if h is approximated as $3\rho_0 a/8\eta$, the steady force exerted on the sphere is given approximately by

$$F \simeq -3a^2\rho_0 s\dot{\xi}_0^2 \sin \phi \tag{96}$$

It is seen from (96) that the direction of the force can be either toward or away from the source depending upon the magnitude of the phase angle ϕ. The average Stokes and Oseen forces will not be considered further in this chapter since, in liquids subjected to ultrasonic fields, other steady forces are of greater importance over the range of values of the field parameters of interest here.

Additional phenomena discussed in this section deal with the flow of a homogeneous fluid medium in which an acoustic disturbance is propagating. This results because absorption of sound in the medium causes a space gradient of the acoustic energy density and conservation of momentum

requires that the momentum disappearing from the field manifest itself as a steady force (and in most cases, in a resulting flow) of the medium. The magnitude of the flow velocity is a function of the absorption coefficient, viscosity, sound level, and boundary conditions. A phenomenon of importance with respect to suspensions results from the hydrodynamic flow pattern produced by an acoustic field in a region enclosing suspended structures. For example, the velocity of fluid flow between two nieghboring spheres (small compared to the wavelength), whose amplitude of cyclic movement is small compared to the fluid particle displacement, increases in the region of constriction between the particles. This results in a decreased hydrostatic pressure in the constriction which is manifest as a force of attraction between the particles.

It has not been demonstrated that any of the phenomena described above are of primary importance for the production of changes in biological systems by high-intensity ultrasonic fields. However, it is desirable that the investigator be familiar with the various ways by which ultrasound can give rise to steady forces in homogeneous and nonhomogeneous fluid media in order to be able to evaluate their possible role in the physical mechanisms of the action of ultrasound on tissue and other biological structures. In addition, an understanding of these "nonlinear" effects is extremely important for designing appropriate measurement methods to determine precise values of the parameters of the ultrasonic fields used in irradiation procedures.

a. Energy Transfer to Harmonics

An acoustic wave of finite amplitude, initially monochromatic, becomes distorted as it propagates; i.e., harmonics are generated, and energy is transferred from the fundamental to the harmonics (Zarembo and Krassilnikov, 1959). As the original monochromatic form of the wave takes on a spectral character, the waveform becomes stabilized at that distance from the source where the time rate of energy input to the harmonics equals the time rate of energy dissipated through absorption. The region of stabilization of the second harmonic, for example, is defined as the region in which the ratio of the second harmonic to that of the fundamental is maximum. Near the source, which radiates monochromatic waves, the absorption coefficient is nearly that for waves of infinitesimal amplitude; in the stabilization region, it is maximal; and at great distances, where the wave returns to the sinusoidal form, the absorption coefficient again approaches that for waves of small amplitude. Consequently, in contrast to the absorption of infinitesimal waves, the absorption of finite amplitude waves has a nonexponential character.

The amount of energy transferred to the harmonics per unit path length

is a function of the nonlinearity of the equation of state of the medium at the hydrostatic pressure and the pressure amplitude of the acoustic disturbance. If relation (91) is assumed, and the amount of distortion is small, then the ratios of the amplitudes of the second and third harmonics to that of the fundamental are given approximately as (Fox and Wallace, 1954; Krassilnikov *et al.*, 1957; Zankel and Hiedemann, 1959),

$$P_2/P_1 = \Gamma f x P_1 \tag{97}$$

$$P_3/P_1 = 3\Gamma^2 f^2 x^2 P_1^2 \tag{98}$$

where

$$\Gamma = \frac{\pi(B/\rho_0 v^2 + 2)}{2\rho_0 v^3} \tag{99}$$

In these expressions B is given by (92), f is the frequency, x is the distance propagated from the source, ρ_0 is the undisturbed density of the medium, v its acoustic velocity, and P_1, P_2, and P_3 are the pressure amplitudes of the fundamental, second, and third harmonics, respectively. These expressions are not applicable to the calculation of the pressure amplitude ratios at distances at which absorption has accounted for an appreciable reduction of the intensity. That is, they do not yield the appropriate ratios of the harmonics at distances at which the waveform becomes relatively stabilized since absorption is important in the stabilizing mechanism. However, they can be used to obtain the space rates of decrease of intensity of the fundamental and increase of the second and third harmonics due to transfer alone.

For the purpose of presenting relations from which estimates of the space decrement of the fundamental and the ratio of the intensity of the second harmonic to the fundamental can be made, only the rate of energy transfer to the second harmonic is considered. In the analysis from which the following formulas are obtained, the space gradient of the intensity of the fundamental is considered as the result of absorption and energy transfer to the second harmonic. These two processes are quantitatively characterized as

$$\frac{dI_1}{dx} = -2\alpha I_1 \tag{100}$$

for absorption and

$$\frac{dI_1}{dx} = -\beta I_1^2 \tag{101}$$

if $x \geqslant x_0 = (1/\beta I_{10})$, for energy transfer to the second harmonic where

$$\beta = \Gamma f \sqrt{2\rho v/I_{10}} \tag{102}$$

In these expressions I_{10} is the intensity of the fundamental at $x = 0$, I_1 is the intensity of the fundamental as a function of x (the distance traveled by the acoustic disturbance), and f is the frequency of the fundamental. In an analogous fashion, the amplitude of the second harmonic is zero at $x = 0$ and is considered to result from the transfer of energy from the fundamental and dissipation of energy by absorption. Transfer of energy from the second harmonic is neglected. The following approximate expression is obtained for the intensity I_1 of the fundamental

$$\frac{I_1}{I_{10}} \simeq \frac{(2\alpha/\beta I_{10})e^{-2\alpha x}}{[1 + (2\alpha/\beta I_{10})] - e^{-2\alpha x}} \tag{103}$$

Although this formula is strictly applicable only when $x \geqslant (1/\beta I_{10})$, I_1 reduces to I_{10} when $x = 0$. Also, it reduces to the form characteristic of the propagation of infinitesimal amplitude disturbances when the transfer of energy to the harmonics is negligible ($\beta I_{10} \to 0$).

It is useful to have available an expression for the ratio of the intensity I_{1a} of the fundamental if absorption alone were present and that obtaining when both absorption and transfer of energy to the harmonics are present simultaneously. This is

$$\frac{I_{1a}}{I_1} = 1 + (1 - e^{-2\alpha x})\frac{\beta I_{10}}{2\alpha} \tag{104}$$

and this ratio is always greater than unity. The intensity I_2 of the second harmonic can be expressed approximately as

$$I_2 = 4\beta(\alpha/\beta)^2 e^{-2\alpha_2 x} \int_0^x \frac{e^{2\alpha_2 z}\, dz}{\{1 - [1 + (2\alpha/\beta I_{10})]e^{2\alpha z}\}^2} \tag{105}$$

where α_2 is the pressure absorption coefficient per unit path length for the second harmonic. For many materials, the absorption coefficient per unit path length is approximately proportional to the square of the frequency; however, for soft tissue, it is nearly proportional to the first power of the frequency (see Section II, 5). These two forms of the frequency dependence of the second harmonic amplitude absorption coefficient per unit path length in terms of that of the fundamental yield $\alpha_2 = 2\alpha$ for linear dependence and $\alpha_2 = 4\alpha$ for quadratic dependence. These expressions inserted into (105) yield relations which can be integrated in terms of elementary functions. For the linear dependence,

$$I_2 = \frac{2(\alpha/\beta)e^{-4\alpha x}}{[1 + (2\alpha/\beta I_{10})]^2}\left\{\log_e\left[\frac{[1 + (2\alpha/\beta I_{10})] - e^{-2\alpha x}}{2\alpha/\beta I_{10}}\right] - \frac{1}{[1 + (2\alpha/\beta I_{10})] - e^{-2\alpha x}} - \frac{1}{2\alpha/\beta I_{10}}\right\} \tag{106}$$

TABLE XI

NUMERICAL EXAMPLES OF NONLINEAR ACOUSTIC FIELD QUANTITIES

Medium	f (cps)	α (cm^{-1})	$B/\rho v^2$	ρv (gm/cm² sec)	Γf (sec^2/gm)	I_{10} (w/cm²)	β (w/cm)$^{-1}$	x_0 (cm)	$I_1(x_0)$ (w/cm²)	$I_{1a}(x_0)$ (w/cm²)	$(I_{1a}/I_1)x_0$
Multiply figures in table by	10^6	1	1	10^5	10^{-9}	1	10^{-3}	1	1	1	1
Water	1	2×10^{-4}	10	1.5	5.6	10	3.1	32	4.7	5.2	1.1
	1	2×10^{-4}	10	1.5	5.6	1000	0.31	3.2	1000	1000	1
	10	2×10^{-2}	10	1.5	56	10	31	3.2	5.9	6.5	1.1
Brain tissue	1	0.1	10	1.5	5.6	10	3.1	32	0.015	0.017	1.15
(linear dependence)	1	0.1	10	1.5	5.6	1000	0.31	3.2	304	770	2.5

The integrated form for the quadratic dependence is somewhat more complex and is not tabulated here.

Some specific numerical results are tabulated in Table XI in order to illustrate the formulas of this subsection.

b. STEADY FORCES AT INTERFACES AND ON IMBEDDED STRUCTURES

(*1*) *Radiation Pressure at Interfaces.* Radiation pressure can exert steady forces on interfaces between media having different values of acoustic velocity and/or density and within absorbing media. The force of radiation pressure at a plane interface, whose minimum thickness is large compared with a wavelength of the radiation, is dependent upon the relative amounts of incident energy reflected and transmitted or absorbed and is quantitatively equal to the difference in the energy densities in the two media. The energy density, or total energy per unit volume, of a plane wave is given by

$$E_0 = I/v \tag{107}$$

where I is the acoustic intensity and v is the acoustic velocity. The radiation force per unit area F_r/A can be expressed as

$$F_r/A = DE_0 = D(I/v) \tag{108}$$

where D is given in Table XII for a variety of physical configurations (Hueter and Bolt, 1955). It is possible to compute the total acoustic power or average intensity of a sound beam using relations (107) and (108) by measuring the force exerted by an ultrasonic beam on a reflector or absorber of large size. In order to accomplish this, it is essential, if a reflector is used,

TABLE XII

THE CONSTANT D OF EQ. (108) FOR VARIOUS PHYSICAL CONFIGURATIONS

Physical Configuration	D
Perfect absorber, normal incidence, $r_{2/1} = 1$	1
Perfect reflector, normal incidence, $r_{2/1} = 0$ or $r_{2/1} = \infty$	2
Perfect reflector, incident at angle Θ to sound beam, $r_{2/1} = 0$ or $r_{2/1} = \infty$	$2 \cos^2 \theta$
Nonreflecting interface, normal incidence, $r_{2/1} = 1$, $v_1 \neq v_2$ For $v_1 < v_2$, force in direction of propagation For $v_1 > v_2$, force opposite to direction of propagation	$1 - v_1/v_2$
Partially reflecting interface, normal incidence, $r_{2/1} \neq 1$	$2\left[\frac{(r_{2/1} - 1)^2 + 2r_{2/1}(1 - v_1/v_2)}{(r_{2/1} + 1)^2}\right]$
Note: $r_{2/1} = \rho_2 v_2/\rho_1 v_1$	

that none of the energy reflected at the interface be allowed to return to the source to modify its acoustic output. This condition can be realized by using a deflecting reflector and absorbing the reflected energy (Hueter and Bolt, 1955). It should be noted that in some cases the direction of the radiation force is opposite the direction of propagation, for example, at the nonreflecting interface between two media of equal characteristic impedances where the acoustic velocity of medium 1 is greater than that of medium 2.

(*2*) *Radiation Perssure on Spheres.* The radiation force exerted on a "soft" sphere (i.e., one such that the pressure amplitude is zero over its surface) suspended in a traveling wave ultrasonic field is a function of the ratio of the diameter of the sphere to the wavelength of the sound. For a "rigid" sphere, i.e., one whose surface does not deform, the radiation force is dependent, in addition, upon the relative densities of the sphere and the imbedding medium. Both types of spheres are useful in the calibration of ultrasonic fields. In order to obtain precise values for the acoustic field variables at a specific location in a beam, it is desirable to employ a method of radiation pressure measurement in which the volume of the region is small enough so that the variation in the values of the variables is small. The radiation force measured with spheres of small size permits accurate determinations of acoustic field parameters at specific sites in the field. Radiation pressure techniques utilizing large reflectors or absorbers permit

the determination of total radiated power, but do not readily lend themselves to the determination of "point" values since a precise field distribution pattern over the surface of the reflector or absorber must be available in order to compute "point" values from average values. Sound field calibration measurements determined by radiation pressure on a small sphere agree with those obtained from thermocouple probe measurements (see Section II, 5, *b*) within the accuracy of the available values for the parameters entering the formulas. The quantitative specification of the ultrasonic exposure parameters (see Section III, 2) for the irradiation of biological systems requires higher absolute accuracy (specification of the pressure amplitude within 1% is desirable) than can be currently realized using the thermocouple probe method. However, the availability of more accurate values for the absorption coefficient of the imbedding liquid used in the thermocouple probe would permit this latter method to replace the radiation pressure method.

The radiation pressure method utilizes a small stainless steel sphere (from ½ to 1 wavelength in diameter) suspended by a bifilar arrangement in the sound field (Fox and Griffing, 1949). The radiation force F_r deflects the sphere and the magnitude of this deflection Δ_r (measured by a cathetometer) permits accurate evaluation of the force exerted by the radiation field. For small angular deflections of the suspension from the vertical,

$$F_r = \frac{\Delta_r(m_s - m)g}{L} \tag{109}$$

where L is the length of the suspension, m_s is the mass of the sphere, m is the mass of the displaced liquid, and g is the gravitational constant. Figure 37 schematically illustrates the experimental arrangement. In practice, the sound level is varied, for example, by changing the voltage across the transducer, and the deflection of the sphere is plotted as a function of the square of the driving voltage since the latter is proportional to the intensity and consequently directly proportional to the energy density.

In order to compute the energy density in the field from the calculated force, it is convenient to present the results of computations in the form of graphs and tables. The "rigid" sphere case is considered first. The radiation force is expressed in terms of the energy density and radius of the sphere as

$$F_r = [f(ka, \rho_s/\rho_0) + d(ka, \rho_s/\rho_0)]\pi a^2 E_0 \tag{110}$$

where $k = 2\pi/\lambda$ is the wave number, a is the radius of the sphere, ρ_s is the density of the sphere, and ρ_0 is the undisturbed density of the liquid medium. The first expression in the bracket of (106) is plotted in Fig. 38 as a function of ka for various values of the ratio of the density of the sphere to that of the imbedding medium (Maidanik, 1957). In order to permit accurate

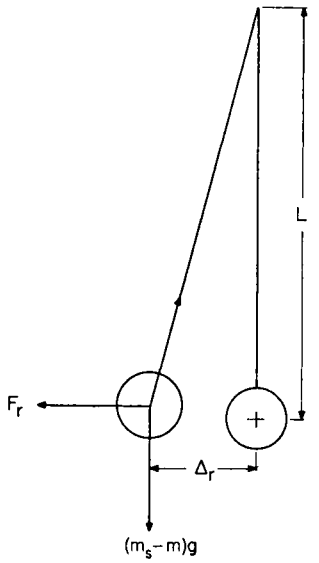

FIG. 37. Schematic illustration of experimental arrangement for determining acoustic radiation force on a sphere.

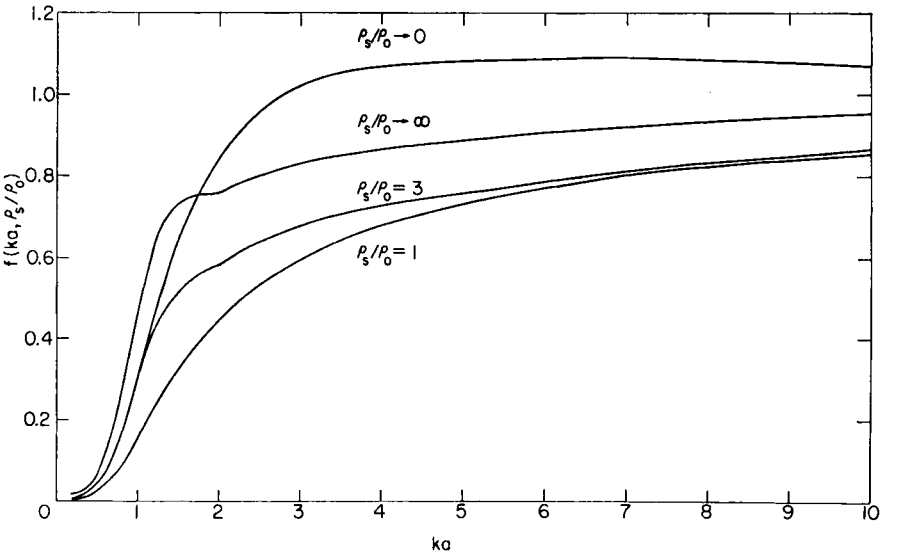

FIG. 38. The function $f(ka,\rho_s/\rho_0)$ for "rigid" spheres versus ka for several values of ρ_s/ρ_0 (after Maidanik).

TABLE XIII

TABULATION OF THE FUNCTION $f(ka, \rho_s/\rho_0)$ FOR RIGID SPHERES (AFTER MAIDANIK)

ka	$f(ka, \rho_s/\rho_0)$			
	$\rho_s/\rho_0 \to 0$	$\rho_s/\rho_0 = 1$	$\rho_s/\rho_0 = 3$	$\rho_s/\rho_0 \to \infty$
0.2	0.001	0.001	0.001	0.002
0.4	0.024	0.011	0.019	0.032
0.6	0.072	0.039	0.071	0.126
0.8	0.177	0.098	0.172	0.282
1.0	0.311	0.157	0.294	0.474
1.2	0.453	0.229	0.417	0.638
1.4	0.582	0.290	0.492	0.723
1.6	0.691	0.355	0.535	0.746
1.8	0.791	0.405	0.563	0.755
2.0	0.846	0.449	0.581	0.760
2.4	0.938	0.518	0.628	0.793
2.8	0.998	0.571	0.670	0.818
3.2	1.033	0.615	0.691	0.844
3.6	1.059	0.650	0.710	0.855
4.0	1.063	0.678	0.730	0.867
6.0	1.086	0.768	0.778	0.913
10.0	1.061	0.849	0.860	0.949

determinations of the force, Table XIII lists the function $f(ka,\rho_s/\rho_0)$ for various values of ka and ρ_s/ρ_0. The second expression in the bracket of (106), $d(ka,\rho_s/\rho_0)$, is shown in Fig. 39 and tabulated in Table XIV (Maidanik and Westervelt, 1957). For the "soft" sphere case, the radiation force can be expressed as

$$F_r = f(ka)\pi a^2 E_0 \tag{111}$$

The function $f(ka)$ is shown in Fig. 40 and tabulated in Table XV (Maidanik, 1957). Measurements with "soft" spheres have not been extensively employed except in a preliminary fashion for the absolute calibration of ultrasonic fields. The use of "soft" spheres has the advantage that the force exerted on the sphere in the sound field is a monotonic function of ka and thus a higher degree of absolute accuracy may be attained in this case.

Since the analysis of nonlinear phenomena in acoustic fields has not reached the stage where highly accurate expressions for specific effects are available, it is essential that calibration measurements be reported in terms of the specific procedure employed. This should include sufficient detail to permit other investigators to make calculations for the purpose of correlating their experimental data.

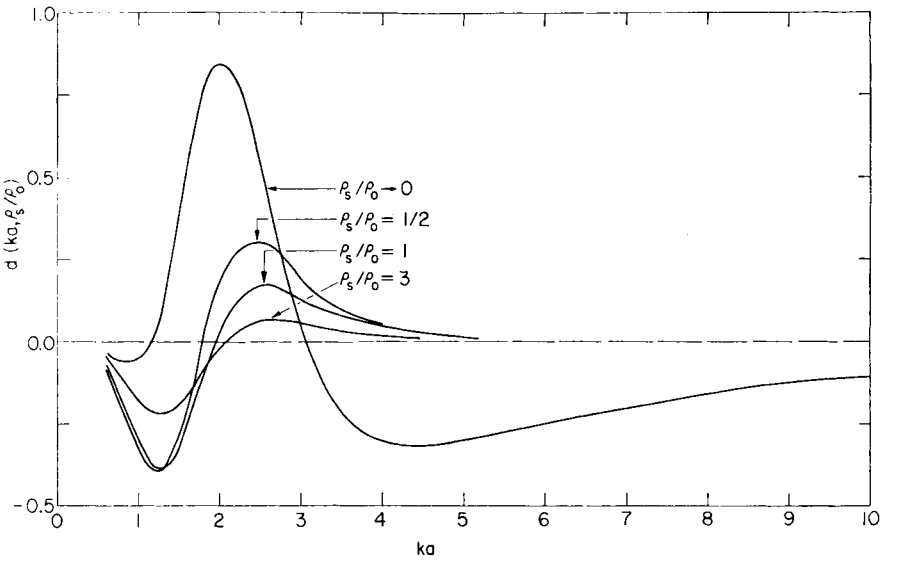

FIG. 39. The function $d(ka,\rho_s/\rho_0)$ for "rigid" spheres versus ka for several values of ρ_s/ρ_0 (after Maidanik and Westervelt).

TABLE XIV

TABULATION OF THE FUNCTION $d(ka, \rho_s/\rho_0)$ FOR RIGID SPHERES (AFTER MAIDANIK AND WESTERVELT)

ka	$d(ka, \rho_s/\rho_0)$			
	$\rho_s/\rho_0 \to 0$	$\rho_s/\rho_0 = \frac{1}{2}$	$\rho_s/\rho_0 = 1$	$\rho_s/\rho_0 = 3$
0.6	−0.0314	−0.0857	−0.0756	−0.0419
0.8	−0.0664	−0.2048	−0.1850	−0.1062
1.0	−0.0549	−0.3278	−0.3067	−0.1807
1.2	+0.0220	−0.3974	−0.3864	−0.2313
1.4	+0.2326	−0.3498	−0.3687	−0.2269
1.6	+0.5241	−0.1858	−0.2524	−0.1694
1.8	+0.7612	+0.0095	−0.1019	−0.0926
2.0	+0.8634	+0.1748	+0.0361	−0.0217
2.4	+0.6311	+0.2964	+0.1658	+0.0543
2.8	+0.2112	+0.2377	+0.1575	+0.0619
3.2	−0.0846	+0.1510	+0.1124	+0.0476
3.6	−0.2352	+0.0909	+0.0758	+0.0337
4.0	−0.2955	+0.0549	+0.0511	+0.0236
5.2	−0.2879	+0.0136	+0.0178	+0.0088
6.0	−0.2466	+0.0061	+0.0099	+0.0050
8.4	−0.1474	+0.0009	+0.0025	+0.0013
10.0	−0.1089	+0.0003	+0.0012	+0.0007

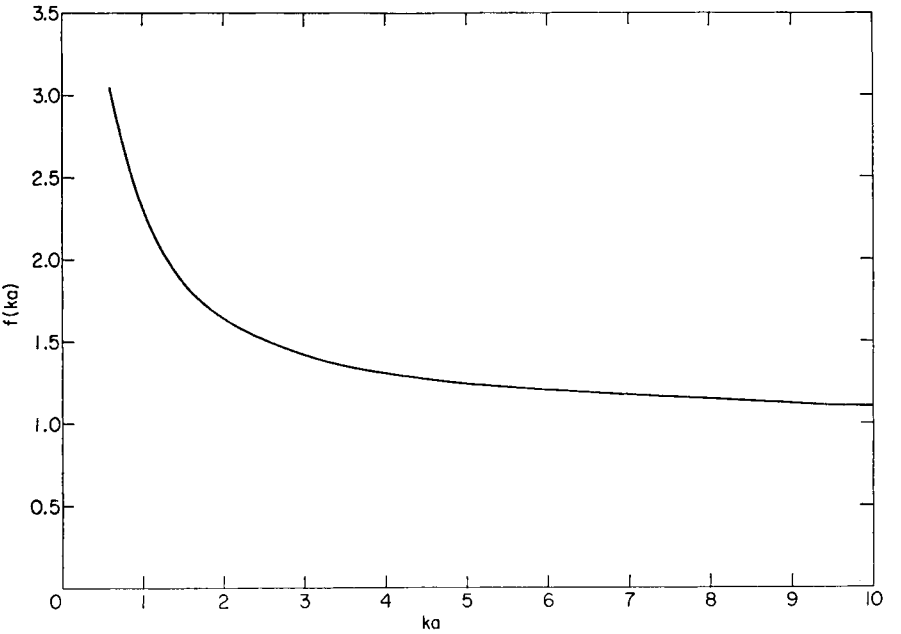

FIG. 40. The function $f(ka)$ for "soft" spheres versus ka (after Maidanik).

TABLE XV

TABULATION OF THE FUNCTION $f(ka)$ FOR SOFT SPHERES (AFTER MAIDANIK)

ka	$f(ka)$
0.6	3.049
0.8	2.616
1.0	2.309
1.2	2.093
1.4	1.934
1.6	1.814
1.8	1.724
2.0	1.646
2.4	1.531
2.8	1.451
3.2	1.389
3.6	1.339
4.0	1.298
6.0	1.194
10.0	1.096

c. STREAMING

In the case of an absorbing medium the space gradient of the radiation pressure P_r is related to the absorption coefficient as follows

$$dP_r/dx = -2\alpha E_0 \tag{112}$$

where E_0 is the energy density. This pressure gradient, in general, produces streaming in the medium.

It is desirable to present an expression for roughly estimating streaming speeds from a knowledge of the values of the pressure absorption coefficient per unit path length, the beam diameter, the shear viscosity coefficient, and the sound level (Nyborg, 1953; Liebermann, 1949; Eckart, 1948). Although there is a well-founded basic theory, from which in specific cases acoustic streaming can be calculated, the computations to obtain flow velocity relations involve approximations to realize tractability. Calculations by different investigators indicate that the computed values are in the range of the experimentally measured values. The following formula for obtaining at least an order-of-magnitude estimate of the streaming speed is useful when the magnitude of the absorption coefficient is such that $2\alpha L \leqslant 3$, where α is the pressure absorption coefficient per unit path length and L is the "length" of the beam. For a focused beam, L can be taken as several times the length of the axial diameter D_a of the focal region. For the unfocused beam case, it appears reasonable to take L equal to at least ten times the beam diameter. This latter criterion should not be considered particularly reliable in view of the present meager stage of *quantitative* knowledge of this phenomenon. If the streaming speed is designated by v_f then (Nyborg, 1953)

$$v_f \simeq \alpha\rho a^2 U^2/2\eta \tag{113}$$

where U is the acoustic particle velocity amplitude (axial value for a focused beam and average value for an unfocused beam), a is the beam radius (in the focused beam case $2a$ can be taken equal to twice the transverse diameter, D_t) and α, ρ, and η are the pressure absorption coefficient per unit path length, the density, and the shear viscosity coefficient of the medium, respectively. As a specific example consider a 1 mc focused beam in water at room temperature. If $a = 0.2$ cm, $\rho = 1.0$ gm/cm^3, $\alpha = 2 \times 10^{-4}$cm^{-1}, $\eta = 0.01$ poise, and $U = 300$ cm/sec, then $v_f = 36$ cm/sec.

d. INTERACTING PARTICLES

The hydrodynamic flow pattern produced by an acoustic field in a region containing closely neighboring suspended particles results in a Bernoulli attraction (Hueter and Bolt, 1955). This situation obtains if the amplitude of the periodic displacement of the particles is only a small fraction of the

amplitude of the periodic displacement of the fluid. It is assumed here that laminar flow obtains. This is insured in the case of a liquid if the Reynolds number [Re = $(2av_f\rho/\eta)$] is less than 1000. In this expression v_f is the flow velocity in the constriction between the particles, a is the particle radius, ρ is the density of the imbedding liquid, and η is the shear viscosity coefficient. The force of attraction between the particles can be expressed in terms of the acoustic intensity and a factor which depends upon the geometry of the flow pattern. For two spherical particles of radii a_1 and a_2 spaced a distance d between centers in a medium of acoustic velocity v, the force of attraction is

$$F = \frac{3\pi a_1^3 a_2^3}{d^4} \frac{I}{v} \tag{114}$$

If the particles are free to move, the speed of coalescence is determined by the viscous forces acting upon them in addition to the Bernoulli attraction. If the particles are elastically fastened to other structures, a stretching of these elastic bonds occurs.

III. Applications of Ultrasonic Fields to the Study and Modification of Biological Systems

The specific examples discussed in this section on the uses of ultrasonic fields to examine and modify biological structures are chosen to illustrate the range of possible applications. A comprehensive review of all important current work is not intended. Rather, it is hoped that the specific investigations reviewed here will indicate both current and potential uses of precisely controlled ultrasound. The most informative method of treating these examples would entail detailed presentation of specific designs. This would serve to illustrate the use of the formulas of Section II to specific cases. Although this would be desirable, it is not possible in a review of this length.

It is convenient for the purpose of this review to classify current research and medical applications utilizing ultrasound into two major categories: (1) those employing acoustic field conditions such that the biological system is relatively unmodified either permanently or temporarily by the acoustic energy (designated here as *passive* uses); and (2) those employing acoustic field conditions which modify permanently or temporarily the structure and/or mechanisms of operation of the biological systems subjected to the acoustic fields (designated here as *active* uses).

This review of some current applications includes brief descriptions of results obtained, techniques of irradiation and preparation, and important features of the instrumentation. The importance of each specific example to fundamental biological investigations or to medicine is indicated together with the types of results which can be obtained. The description of instru-

mentation includes the principles of operation and indicates the limitations of the specific method. The details of electronic circuitry are not included since this constitutes an extensive field and is not directly involved in the design of experiments or interpretation of results, except insofar as electronic circuits are employed to provide power or detect electrical changes from acoustic probes. This does not mean to imply that there are no major problems involved in satisfying electronic requirements for the instrumentation. On the contrary, realization of a complete system requires that considerable effort be placed on the design of the electronic components and, in some cases, a development program may be necessary in order to obtain the desired component. In the following discussions of specific examples, the major specifications which must be satisfied by the electronics are indicated. It should be noted that, in general, the designing of ultrasonic instruments and electronic equipment usually involves individuals of different professional disciplines.

1. Passive Uses

Acoustic field conditions which do not disrupt or appreciably modify biological systems can be used to study and examine such systems from the submicroscopic level of structure to the macroscopic anatomy of gross tissue. These studies depend upon the ultrasonic absorption and/or reflection and refraction characteristics of the system. The study of structures at the submicroscopic and microscopic level can be illustrated by recent investigations leading to the determination of ultrasonic absorption coefficients of protein solutions and suspensions of biologically significant structures. It appears that the microscopic structural level can be visualized by ultrasonic methods and that structures may be made apparent which are not possible by other microscopic methods. The macrostructure of soft tissue is discussed from the viewpoint of the visualization of gross anatomical structures.

a. Ultrasonic Absorption in Protein Solutions and Suspensions

The most precise and comprehensive investigations reported in the literature on the absorption of ultrasound in cellular suspensions and solutions of proteins are those of Carstensen and Schwan (1959a, b). Acoustic velocity and absorption measurements of red cells in suspension, hemoglobin solutions, plasma and extracts from liver were determined as a function of the temperature, hydrogen ion concentration, and concentration of the structures or molecular species in the medium over the frequency range from 0.5 to 10 mc. Measurements of this type yield knowledge of structure, that is, form and degree of association of macromolecular species in solution. Information on the rates of energy exchange or configuration arrangement

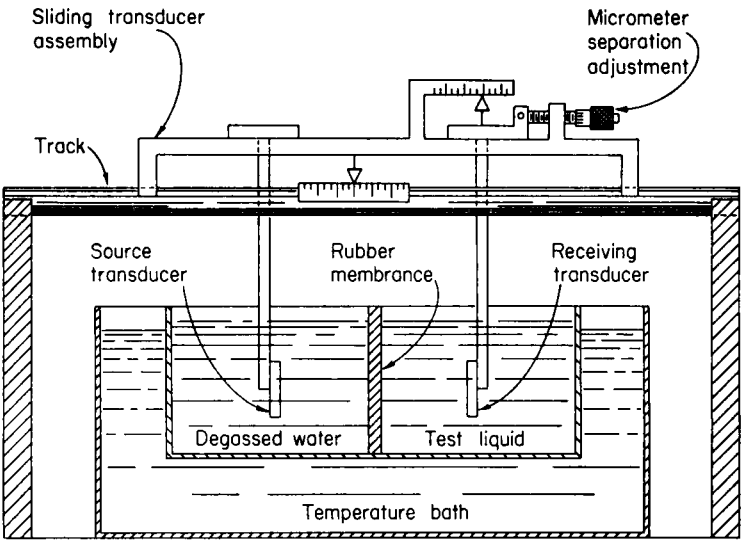

FIG. 41. Schematic diagram of mechanical instrumentation for determination of acoustic velocity and absorption (after Piersol *et al.*).

can be obtained by determining the relaxation spectrum of such suspensions and solutions. Research in this area has not yet progressed to the stage where this has been accomplished. It appears that measurements over a much wider frequency range are required before such results are forthcoming.

Another important feature of such studies is the attempt to elucidate the mechanism of acoustic absorption of ultrasound in tissue by measuring the absorption of the tissue components in solution. The elucidation of the absorption mechanism in tissue and the determination of the absorption coefficients of specific molecular structures (for example, proteins) will aid the studies of molecular distributions on a microscopic level of structure (see Section III, 1, *b*).

The type of ultrasonic instrumentation employed in this work is illustrated in Fig. 41 (Piersol *et al.*, 1952). The method employed makes possible the realization of absorption coefficient measurements and velocity differences to a better degree of accuracy than has been attained by other methods. The basic principle employed is one of a comparison of the acoustic properties of the medium of interest with those of water. In the arrangement shown in Fig. 41, the sound tank is divided into two compartments by a diaphragm. One compartment contains water, the other contains the solution under investigation. The ultrasonic transducers are mounted on a precision sliding mechanism. The source transducer is placed in the chamber containing water and the receiver is placed in the chamber containing

the medium of interest. For high stability, X-cut quartz plates are used for both source and receiver (see Section II, 3). Moving the mechanism along the axis of the sound tank makes possible the substitution of any desired path length of the solution (or suspension) for equal acoustic path lengths of water. The attenuation of acoustic energy as a function of the position of the sliding assembly, measured by a micrometer, is used to compute the absorption coefficient. The over-all error in the determination of the pressure absorption coefficient is estimated to be between 0.002 and 0.005 cm^{-1}. The arrangement indicated in the figure minimizes the problems associated with varying the separation distance (distance in terms of wavelengths) between the source and receiver transducers. This type of equipment also can be used for making measurements of acoustic velocity. This is accomplished by comparing the phase of the output of the ultrasonic receiver with a direct signal from the electronic generator while the transducer separation is changed by micrometric control.

It is clear that the temperature of the materials in the sound tank must be accurately controlled, particularly if small changes in velocity between the medium and the comparison liquid are to be accurately measured. This follows from the fact that, since the velocity is temperature-dependent, the wavelength separation between source and receiver changes with the temperature. The effect of reflections from the walls of the confining chamber is eliminated by employing a pulse technique. The direct transmitted signal from the source to the receiver can be separated from reflected signals by utilizing oscilloscope display. A block diagram of the electronic equipment is illustrated in Fig. 42 (Schwan and Carstensen, 1952). The electronic pulse generating equipment, which supplies power to the source transducer, must have a stable output level since small changes in the absorption coefficient must be measured when high accuracy is to be obtained. In the

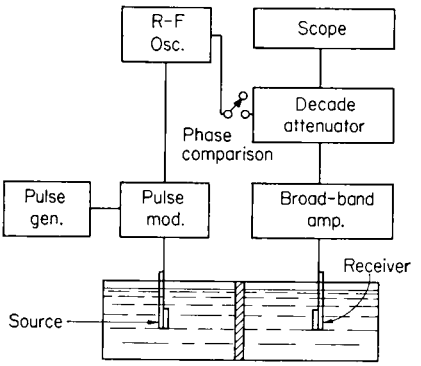

FIG. 42. Block diagram of electronic instrumentation for determination of acoustic velocity and absorption (after Schwan and Carstensen).

receiver circuit, a precision attenuator is employed in conjunction with a stable amplifier and an oscilloscope. Difficulties caused by the nonlinear response of the oscilloscope can be avoided by adjusting the attenuator until a constant deflection for the direct transmitted signal appears on the screen. The linearity of the amplifier is, however, a limiting factor in determining the attainable accuracy.

A thermocouple probe of the type discussed in Section II, 5 can also be employed as a receiver. However, the minimum measurable sound intensity, for a single junction probe, is of the order of 10^{-2} w/cm^2 for a pressure absorbtion coefficient of the order of 0.1 cm^{-1}, as compared with intensity values in the range from 1 μw/cm^2 to 1 mw/cm^2 if a piezoelectric plate receiver is employed. The same system can be used for measuring the absorption coefficient of solid tissue. This is accomplished by filling the sound tank with physiological saline and placing tissue samples of different thicknesses in the acoustic path (Hueter, 1948). Such a measurement yields an average value of the absorption coefficient of the bulk tissue. In order to obtain values of the absorption coefficient on a smaller scale (semimicroscale), the thermocouple method can be employed (W. J. Fry and R. B. Fry, 1953; W. J. Fry and Dunn, 1956; Dunn, 1958). In this case, the thermocouple junction is inserted into the tissue at the site at which the ultrasonic absorption coefficient is to be determined. It is necessary in this case to know the sound intensity at the thermocouple junction and the heat capacity per unit volume of the tissue. The absorption coefficient is computed from expression (63).

b. Ultrasonic Absorption Microscopy

Since different proteins appear to be characterized by different values for the ultrasonic absorption coefficient (Carstensen and Schwan, 1959b), it is possible to develop an ultrasonic absorption "microscope" to examine microstructure of biological systems. Since the different components of cells would not, in general, exhibit the same differential absorption for ultrasonic and electromagnetic energy, because the mechanisms of absorption are completely different, it is reasonable to expect to "see" structure ultrasonically which is not seen by microscopes using visible light or energy in other regions of the electromagnetic spectrum, and vice versa. Some work has been accomplished on the design of such an instrument (Dunn and W. J. Fry, 1959).

The principle of operation of the ultrasonic absorption microscope is illustrated in Fig. 43. High-frequency sound waves are generated in a "coupling" medium by a piezoelectric transducer (an X-cut quartz plate operating at an odd harmonic frequency). The coupling liquid fills the irradiation chamber and serves to conduct the sound to and from the specimen which is interposed between the source and a small thermoelectric

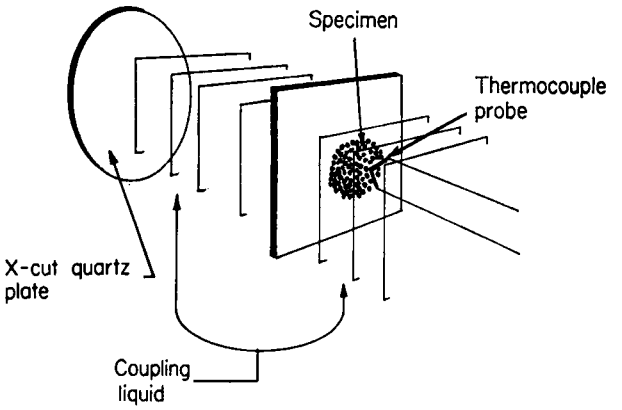

FIG. 43. Schematic representation of ultrasonic absorption microscope.

probe. The piezoelectric crystal is excited electrically by voltage pulses of rectangular temporal envelope. The small thermocouple probe detects the acoustic energy level of the sound which passes through the portion of the specimen in its immediate neighborhood and the variation in the transmitted energy level, as a function of position of the probe relative to the specimen, constitutes an acoustic image of the ultrasonically detected structure. In practice, it is more expedient to move the specimen normal to the axis of sound propagation rather than to move the probe. This is a result of the fact that it is extremely difficult to realize a perfectly uniform field and if the probe were to be moved, it would detect not only the structure in the specimen, but also that of the field and these individual variations may not be distinguishable. Ultimately, an instrument of this type could incorporate a two-dimensional array of probes so that the complete acoustic image could be obtained with a single pulse of sound.

The resolving power of the ultrasonic absorption microscope is determined by the size and properties of the materials from which the thermocouple is constructed, the intensity and duration of the acoustic pulse, and the proximity of the thermocouple junction to the specimen. An approximate analysis of the resolving power is summarized here. In order to accomplish this, the basic formulas derived by W. J. Fry and R. B. Fry (1954a) are employed.

Let μ designate the acoustic intensity absorption coefficient per unit path length of the specimen. The structure of the specimen exhibits a variation in the value of μ from one position to another. Consider a site at which the value of μ is a maximum. The resolution of the instrument is calculated by determining the minimum diameter of a cylindrical element of the specimen (with μ maximum in the center) which can be detected. Let

$$\mu = \mu_0 + \Delta u \tag{115}$$

where μ_0 is the average value of μ. Let

$$\Delta\mu = \Delta\mu_m f(a) \tag{116}$$

where a is the radial distance from the position of maximum absorption μ_m and $f(0) = 1$. Let

$$f(a) = 1 - Ba^2 \tag{117}$$

which is a parabolic fit to the μ distribution function. If $\Delta\mu$ drops to 0.7 of $\Delta\mu_m$ in a distance $a = \Delta a$, then

$$0.7 = 1 - B(\Delta a)^2$$

and

$$B = 0.3/(\Delta a)^2 \tag{118}$$

From formula (41) of the above reference, the ratio of the heat conducted away from the element, H_{ct}, to that generated above the average, H_{at}, both in the interval t, can be written as

$$\frac{H_{ct}}{H_{at}} = \frac{Kt}{\rho c_p}\left(\frac{f''(a)}{f(a)}\right)_{a=0} \tag{119}$$

where K is the coefficient of thermal conductivity, ρc_p is the heat capacity per unit volume, and t is the time duration of irradiation. Expressions (117), (118), and (119) thus yield

$$\frac{H_{ct}}{H_{at}} = \frac{Kt}{\rho c_p}\frac{0.6}{(\Delta a)^2} \tag{120}$$

If values for the physical constants are chosen to be equal to that for water, i.e., $\rho c_p = 4.2$ joules/cm^3/°C and $K = 0.0054$ w/cm/°C, which are sufficiently close to the characteristics of tissue for the purposes of this analysis, and if the ratio H_{ct}/H_{at} is chosen to be ½ and the time interval equal to 10^{-6} sec, then $\Delta a \simeq 4 \times 10^{-5}$ cm.

The incremental temperature rise is now computed. Integration of formula (1) of the above reference yields

$$\Delta T = \frac{\Delta\mu_m It}{\rho c_p} \tag{121}$$

where I is the sound intensity. It is assumed that the absorption coefficient retains the linear dependence on frequency at the high frequencies of interest here, which has been observed in the low megacycle region such that

$$\mu = \mu_{f_1}\left(\frac{f}{f_1}\right) \tag{122}$$

If a deviation from (122) occurs, it is probable that at any given frequency, the value of μ is greater than that given by formula (122). If $\Delta\mu_m$ is written as

$$\Delta\mu_m = e\mu \tag{123}$$

where e is a measure of the fluctuation of the absorption coefficient from the average value, then

$$\Delta\mu_m = e\mu_{f_1}\left(\frac{f}{f_1}\right) \tag{124}$$

and

$$\Delta T = e\mu_{f_1}\left(\frac{f}{f_1}\right)\frac{It}{\rho c_p} \tag{125}$$

From experiment, $\mu_{f_1} \simeq 0.2\ \text{cm}^{-1}$ at $f_1 = 1$ mc/sec. If it is desired to detect a structure whose absorption coefficient differs by 5% from the average, i.e., $e = 0.05$, and if it is assumed that $f = 1000$ mc/sec, t is 1 μsec and $I = 1000\ \text{w/cm}^2$, then $\Delta T \simeq 2.4 \times 10^{-3}$°C. It should be noted that a specimen with the absorption coefficient value used here and as thick as 10 μ would absorb only 20% of the acoustic energy from the beam. If the thermoelectric power of the probe is 50 μv/°C, then the above temperature change corresponds to a thermal emf of 0.12 μv. This signal strength is sufficiently high to be separated from noise, particularly if the specimen is exposed, for example, to 100 pulses of the radiation.

Heat conduction in the thermocouple leads limits the resolution. The maximum "diameter" of the leads consistent with the resolution calculated above is now determined. The fractional decrease in the temperature at the site of the junction caused by heat conduction in the leads is given by formula (112) of the above reference at the point $a = 0$ as

$$\frac{\delta T}{\Delta T_m} = -\frac{3a_0^2}{2}\left(\frac{K_w}{K}\right)\left(\frac{f''(a)}{f(a)}\right)_{a=0} \tag{126}$$

where δT is the difference between the temperature of the absorbing structure and that of the thermocouple junction resulting only from heat conduction away from the junction by the wires, ΔT_m is the temperature rise in the absorbing structure in the absence of the thermocouple junction, a_0 is the radius of the wire, and K_w is the coefficient of thermal conductivity of the wire. Using the numerical values previously given, letting $\delta T/\Delta T_m = 0.5$, and choosing the value of K_w approximately that of iron, (126) yields

$$a_0 = 0.12\Delta a \tag{127}$$

Choosing $\Delta a = 4 \times 10^{-5}$ cm gives $a_0 \simeq 0.5 \times 10^{-5}$ cm and the maximum diameter of the leads is thus 0.1 μ.

If the length of the small diameter portion of the thermocouple leads is designated by L, then the electrical resistance R of the thermocouple is (using the value for the resistivity of iron)

$$R \simeq \frac{L}{\pi a_0^2} \times 10^{-5} \tag{128}$$

and if $L = 100\ a_0$, then $R = 64$ ohms.

Summarizing, a structure with an acoustic absorption coefficient 5% different from the average, can be detected if it has a "radius" of 0.4 μ. To realize this the ultrasonic frequency is 1000 mc, the ultrasonic intensity is 1000 w/cm^2, the ultrasonic pulse duration is 1 μsec, the thermocouple lead "diameter" is 0.1 μ, the thermal emf produced is 0.1 μv, the resistance of the thermocouple is in the range of 50 to 100 Ω, and the repetition rate of exposure, although not critical, should probably lie somewhere in the range from 10^3 to 10^4 pps. If the absorption coefficient of the structure differs from the average by more than 5%, then a smaller structure can be detected.

A limitation on the detection of structural variations is imposed by the stability of the electronic apparatus and by the temperature stability of the system. The output pulses from the driver need not be restricted to a rectangular envelope form, or any particular form, but the shape must be accurately reproducible. In addition, the amplitude must be stable in order that the variation in the acoustic field level detected by the probe, as the specimen is moved, be the result of variations in the absorption coefficient at various sites in the structure and not the result of amplitude variations in the field. The absolute sound level need not be known nor is it necessary that the sound level be accurately reproducible from one period of operation to another. The gain of the electronic receiver must be stable for the same reasons given above. If a multiple array of probes is employed and individual amplifiers are not practical for each probe, a stable switching circuit must be employed to operate at microvolt levels.

It should be noted that an ultrasonic microscope employing lens or reflector focusing would not be practical at the frequencies necesasry to obtain high resolution since the acoustic absorption coefficients per unit path length in the media are too high for the path lengths which must be employed.

c. Ultrasonic Visualization of Macrostructure of Soft Tissue

With appropriately designed instrumentation, ultrasound can be used to visualize directly soft tissue structure. Resolution in the submillimeter range is obtainable for structures of the dimensions of those of the eye. Tissue of greater thickness or at greater depths below the body surface (leg structure, neck, etc.) can be visualized at somewhat reduced resolution. Nearly all

soft tissue components possess essentially the same x-ray densities and therefore cannot be visualized directly by x-ray methods. By contrast, since tissue structure is not acoustically homogeneous, a small fraction of the incident ultrasound is reflected at the interface between tissue components as a result of their slightly different acoustical properties. The acoustic intensities required for such work are far below the levels at which changes are induced in tissue. Ultrasound employed in this fashion produces no cumulative or delayed effects. Foreign bodies and pathological structures possessing the same x-ray density as soft tissue can be visualized and the geometric position can be determined accurately by acoustic means (Ludwig and Struthers, 1949; Baum and Greenwood, 1958). Ultrasound can be employed to investigate both the static and dynamic characteristics of soft tissue structures. For example, it is possible to observe displacement of blood vessels and characteristics of heart motion (Howry, 1957; Edler and Hertz, 1954). The early work in this field was accomplished by Howry (1955, 1957) and by Wild and Reid (1952a, 1957) and their collaborators. More recently, ultrasonic tissue visualization methods have been applied to ophthalmology (Baum and Greenwood, 1958) and cardiology (Satomura, 1957; Edler and Gustafson, 1957; Effert *et al.*, 1957). Early cancer diagnosis by ultrasonic methods has occupied the attention of several investigators (Wild and Reid, 1952b; Kikuchi *et al.*, 1957; Howry *et al.*, 1954).

By using a narrow or small diameter beam of ultrasound and short pulse lengths, it is possible to resolve structure in both azimuth and range (along the beam axis) and thus to reconstruct a three-dimensional "picture" of tissue structure. Transmission methods of detecting soft tissue structure do not have the extent of applicability of reflection methods. Transmission methods can be used to obtain a two-dimensional projection of structures; however, this is not nearly as enlightening as a three-dimensional view. In addition, this method lacks contrast, when, for example, absorption in a structure to be detected constitutes only a small fraction of the total absorption along the transmission path (Ballantine *et al.*, 1954). A number of major design problems arise when one attempts to realize an ultrasonic soft tissue structure visualization system which is capable of reconstructing, in a three-dimensional fashion, structures of soft tissue without the introduction of distortion or artifact. In order to realize the required resolution, it is necessary to operate at frequencies of 1 mc and above. At these frequencies the absorption per unit path length is relatively high (see Table II) so that structures reflecting the same percentage of incident acoustic energy from different depths might return, to the receiving transducer, ultrasonic energy differing in intensity by as much as a factor of 10^5. It is necessary, therefore, to incorporate gain compensation into the system to correct for loss by absorption. Since the sound level along the axis of the beam is not

constant (for example, if a focused beam is used to attain a small cross-section, the sound level decreases as one moves away from the center of the focal region along the beam axis), it is necessary to include an equalizer arrangement which corrects for variations in level along the "working length" of the beam. Further, it is apparent from direct measurements on tissue that the orientation of the reflecting surface is important in determining the direction of the incident acoustic energy which is returned to the receiving transducer. For example, an angular shift from normal incidence of 10° can reduce the amplitude of the received signal by a factor of approximately 10^2. Therefore, it is necessary to view the structure of interest from a number of different directions. A multiple or compound scanning technique improves the picture detail, eliminates shadows, and suppresses artifacts. In a compound scanning system the transducer is moved along a curvilinear path (usually rectilinear) while it is simultaneously rotated in a cyclic fashion about an axis in the face of the vibrating element. The compound scanning method at least partially eliminates shadows by viewing the structure from a large number of different directions. Resolution is improved since it is possible to adjust the presentation system (in which the ultrasonic information is used to construct a visual image) so that only echoes which plot at the same site, on the presentation screen, for different scans appear visually. Artifacts produced by multiple reflections shift position on the presentation screen when such a compound scan is employed, and therefore do not result in a superposition and reinforcement of patterns.

The type of results which have been obtained are illustrated in Figs. 44 and 45. Figure 44 shows an ultrasonogram of a highly myopic aphakic eye which has both a retinal and choroidal detachment (Baum). This diagnosis could only be demonstrated by ultrasonic means since it is not possible to "see" behind the retina with any other ophthalmic instruments. Figure 45 shows serial ultrasonograms of a human leg at mid-calf (Howry). It is apparent that the ultrasonic visualization methods are clinically useful at the present time to furnish diagnostic information which cannot be obtained by other methods.

A block diagram of the equipment required for such a system is shown in Fig. 46; it is seen that fairly extensive electronic instrumentation is required (Baum and Greenwood, 1958). The transducer is driven by a pulsed rf supply and the received signal is amplified and processed by an appropriate display system. In order to obtain a short transmitted pulse, the first excitation pulse is followed by a second one of opposite phase and proper amplitude to stop all oscillation except the first cycle (Howry, 1955), thereby producing essentially a single cycle of oscillation.

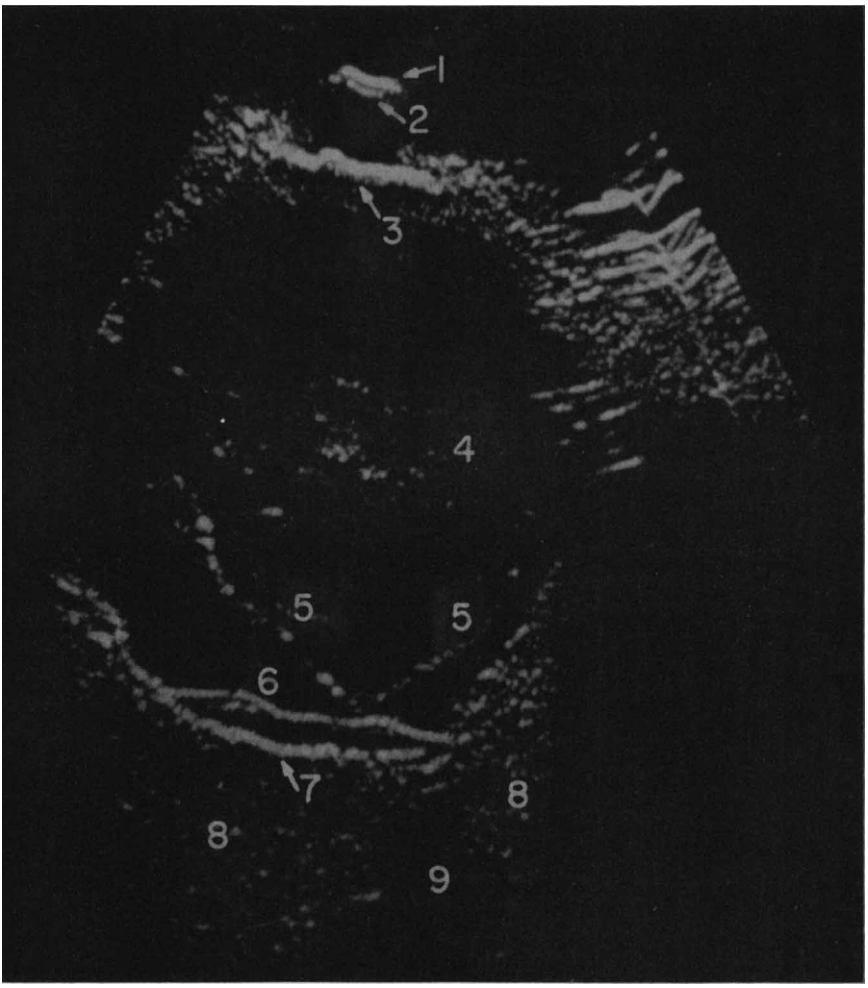

FIG. 44. An ultrasonogram of a highly myopic aphakic eye with both a retinal and choroidal detachment (after Baum). (1) Anterior surface of the cornea; (2) posterior surface of the cornea; (3) iris; (4) vitreous opacities; (5) detached retina; (6) detached choroid; (7) posterior sclera; (8) orbital fat; (9) passage of the optic nerve through the orbital fat.

d. OTHER PASSIVE USES

Other passive uses of ultrasound in the study of biological systems are also of current interest and receiving attention. It is not the purpose of this chapter to list all present investigations. However, it is of interest to note that ultrasonic instruments have been developed for the measurement of

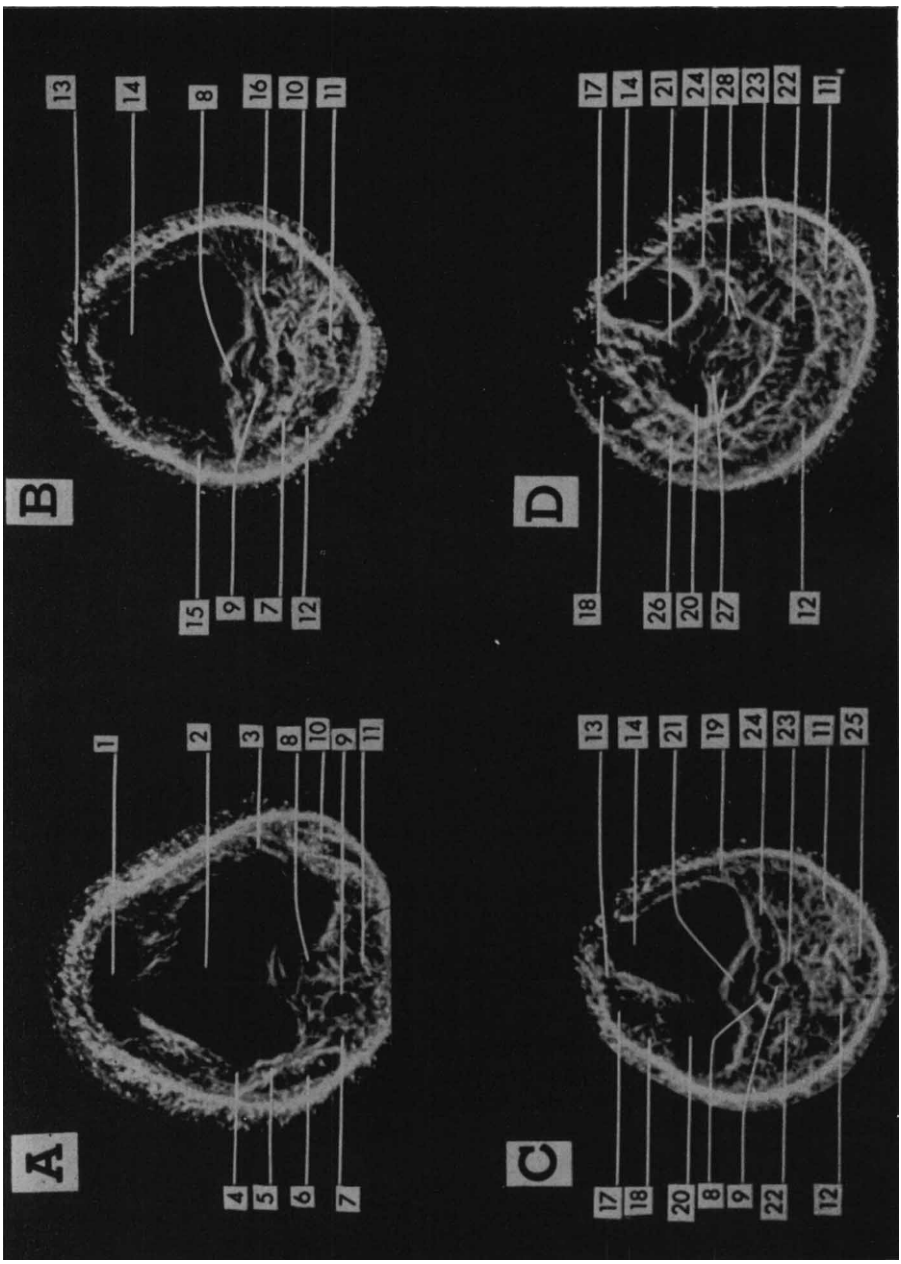
A
1
2
3
8
10
9
11
4
5
6
7
B
13
14
8
16
10
11
15
9
7
12
C
13
14
21
19
24
23
11
25
17
18
20
8
9
22
12
D
17
14
21
24
28
23
22
11
18
26
20
27
12

FIG. 45.

blood flow through major vessels. The present status of this work is described in the publication of a recent symposium (Herrick and Anderson, 1959; Farrall, 1959; Franklin *et al.*, 1959).

2. Active Uses of Ultrasonic Fields to Affect Biological Structure and Function

High level ultrasound can be employed to produce either permanent or temporary changes in tissue. In this section the terms *ultrasonic parameters of exposure* and *conditions of exposure* are used. The former term includes the specification of values of appropriate acoustic field variables (intensity, particle velocity amplitude, pressure amplitude, etc.), time duration and sequence of exposure(s), and the shape of the acoustic envelope(s). The latter term includes a description of the physicochemical state of the preparation (temperature, hydrostatic pressure, level of anesthesia, etc.). When both terms collectively are implied, the terminology *ultrasonic irradiation event* is used. By appropriate choice of the ultrasonic irradiation event, it is possible to produce selective permanent disruption of tissue components or to produce temporary interruption of function. A considerable effort has been expended in the investigation of the ultrasonic parameters of exposure which result in changes of specific tissue components of the central nervous system. Consequently, it is convenient to outline very briefly the results of this work and to include a description of the instrumentation and a discussion of the techniques employed in such investigations. The study and modification of tissue components other than those of the central nervous system can be initiated by using modifications of the methods and techniques already developed. The types of changes which can be produced in the nervous system, by appropriate ultrasonic irradiation events, provide new methods of approach to the study and function of this system in experimental animals and also furnish a new and versatile tool for studying and modifying neurological disorders in the human.

By moving the focus of an acoustic beam from site to site in the brain tissue, it is possible to produce changes in predetermined regions of desired sizes, shapes, and orientations in deep structures without producing con-

FIG. 45. A serial ultrasonogram of the left leg (after Howry). (A) Section through mid-patella; (B) section 6.33 cm below (A); (C) section 1.27 cm below B; (D) section 10.16 cm below C (mid-calf). (1) Patella; (2) femur; (3) medial epicondyle; (4) lateral epicondyle; (5) gastrocnemius tendon (lateral head); (6) biceps femoris M.; (7) plantaris M.; (8) popliteal artery; (9) popliteal vein; (10) sartorius M.; (11) gastrocnemius M. (medial head); (12) gastrocnemius M. (lateral head); (13) patellar ligament; (14) tibia; (15) biceps femoris M. tendon; (16) semitendinous M. tendon; (17) tibialis anterior M.; (18) extensores longi digitorium et hallucis; (19) sartorius gracilis et semitendinous tendons; (20) fibula; (21) tibialis posterior M.; (22) soleus M.; (23) plantaris M. tendon; (24) popliteus M.; (25) small saphenous vein; (26) peroneus longus et brevis; (27) peroneal artery et vein; (28) posterior tibal artery et vein.

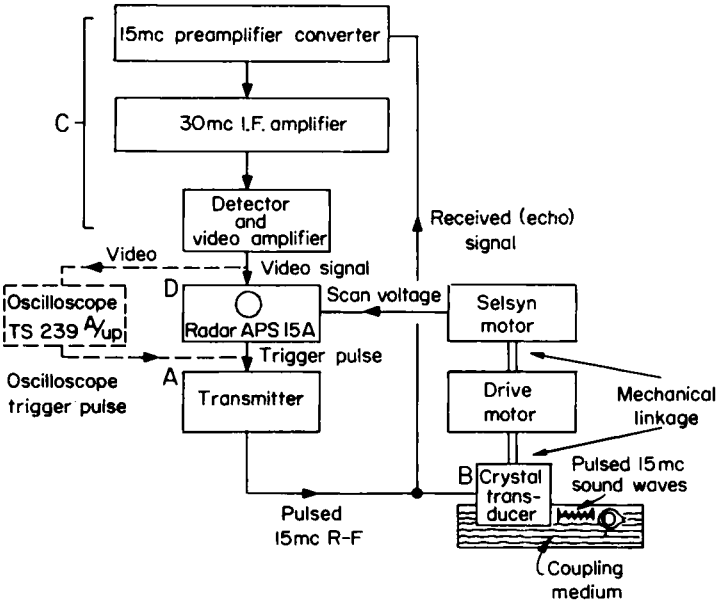

FIG. 46. Block diagram of major components of ultrasonic ophthalmic instrument (after Baum and Greenwood).

comitant changes in intervening tissue. The selectivity which ultrasound displays among the tissue components of the central nervous system is extremely useful in investigations of the complex anatomical structure. Post-mortem microscopic examination of sound-irradiated tissue shows that within the brain, blood vessels are the most resistant element and that it is possible to destroy selectively the fiber tracts of white matter without damaging gray matter irradiated with equal ultrasonic parameters of exposure. A detailed review of this work has been prepared by W. J. Fry (1958) and should be consulted for details and technical literature. The brief review given here is concerned with the important aspects of techniques and instrumentation which illustrate the application of the design principles discussed in Section II.

A great deal of experimental work has been carried out on animals to investigate the types of tissue changes which can be produced for different ultrasonic irradiation events. This work shows that accurate reproducibility of lesions, as regards position, size, and degree of selectivity, can be accomplished only with precision control of the ultrasonic parameters of exposure and properly designed instrumentation for placing the focus accurately at the desired sites in the brain. In experimental animal work, the bone, which is removed to admit the sound to the brain is either replaced or a plastic substitute is used immediately after irradiation. That is, the

irradiation itself is carried out with the skin flap open. In the case of the human, the ultrasonic irradiation procedures may be performed by first removing a bone flap, allowing the skin incision to heal, and then carrying out the irradiation at some subsequent time. The conscious patient is irradiated through the intact skin and is thus unstressed, thereby making it possible to modify subtly complex behavior and the signs and symptoms of neurological disorders. With the patient prepared in this fashion (i.e., an acoustic window of appropriate aperture provided by the absence of bone), the time course of changes can be followed and modified by irradiation procedures spaced at any desired time intervals from days to years. Neurological disorders which were previously intractable can now be successfully treated by ultrasonic methods (W. J. Fry *et al.*, 1958; Meyers *et al.*, 1960).

The employment of the ultrasonic focusing methods allows the investigator to modify deep tissue structures without the limitations of methods requiring the insertion of instruments such as tubes, electrodes, and cannulae. Penetrating instruments can be inserted at most a few times to reach sites in a deep structure. The focus of the ultrasonic beam, however, is unrestricted in this sense and, in fact, can be placed at hundreds of different positions in a single patient during one irradiation procedure, if desired. The only method which can be compared to ultrasound in this regard is high-energy ionizing particles or ionizing radiation (Tobias *et al.*, 1954; Larsson *et al.*, 1958). These latter methods suffer from the disadvantages that changes are produced in all tissue structures in the path of the beams; i.e., there is no selectivity, and the effects are cumulative. In addition, no evidence has been forthcoming to show that reversible changes can be produced by ionizing radiation. Because reversible or temporary changes can be produced by ultrasound, this technique may ultimately supplant the need to employ x-ray methods to identify landmarks from which the positions of brain structures are computed. Roentgenography, in conjunction with the use of contrast media, does not permit the location of many specific brain structures to be determined, but makes manifest the positions of particular structures which can be used as landmarks. Measurements made using these landmarks as references, together with the aid of available brain atlases (Spiegel and Wycis, 1952; Schaltenbrand and Bailey, 1959) permit one to locate desired structures. Since all brains are not identical and the scaling from one to another involves difficulties, a method which permits identification of selected sites by first producing temporary effects in these structures (or in neighboring ones) and observing the results before producing irreversible changes, is much to be preferred.

The foci used for the work on the central nervous system are much too small for treating large tissue masses, e.g., advanced neoplasms, and in such

cases a completely different type of focusing system is required. Superficial tumors have been successfully treated with unfocused ultrasound (Burov, 1956; Burov and Andreewskaya, 1956). The beam used in this work had a radiating area of 50 cm^2 and an acoustic intensity of 500 w/cm^2. The successful treatment of deep tumors must await the development of intense ultrasonic beams of large focal regions.

In deep-lying structures having complex shape and large size, changes are produced without disruption of intervening tissue, by moving the focal region of the ultrasonic beam over an array of positions. The wavelength of the sound in the propagation medium and the aperture angle of the focusing system are the important factors determining the "minimum volume" of tissue which can be affected by a single exposure [see relations (47) and (48)]. This "minimum volume" limits the degree of complexity of shape of larger volumes which can be affected without producing concomitant changes in bounding tissue. Since the minimum realizable dimensions of the focal region decrease as the frequency increases, it is desirable, for the production of changes in brain, to operate at frequencies where the wavelength is of the order of a millimeter or less. For example, at a frequency of 1 mc, where the wavelength of sound in brain tissue is approximately 1.5 mm (see Table II) at 37°C, it is possible to produce lesions of a few cubic millimeters in volume. Most of the work on experimental animals and humans has been accomplished using this frequency. At a frequency of 4 mc, it is possible to restrict the volume of tissue affected to a few hundredths of a cubic millimeter. This choise of frequency is especially useful in the study of the brains of experimental animals, such as the cat, where brain structures are relatively small compared with the human.

An upper limit on frequency is imposed by the thickness of tissue which must be penetrated in order to reach a desired site. The ultrasonic absorption coefficient per unit path length is directly proportional to the frequency (Section II, 5, *c*) and the intensity absorption coefficient per unit path length for mammalian brain is approximately 0.2 cm^{-1} at 1 mc and 38°C.

One type of extensively used focusing irradiator is the multibeam instrument illustrated in Fig. 47. This irradiator generates four individually focused beams of ultrasound. The sound is produced by circular X-cut quartz plates vibrating in the fundamental thickness mode (see Section II, 3, *a*). Plastics have been extensively employed as the lens materials of these irradiators (polystyrene, Lucite). Castor oil is a suitable coupling liquid between the crystal plate and the lens. The electroded face of the crystal adjacent to the lens is maintained at the electrical potential (ground) of the stainless steel housing. The irradiator housings are provided with tilt adjustments, to permit the individual beams to be brought into coincidence at a common focal region, and, with phase adjustments, to permit maximiz-

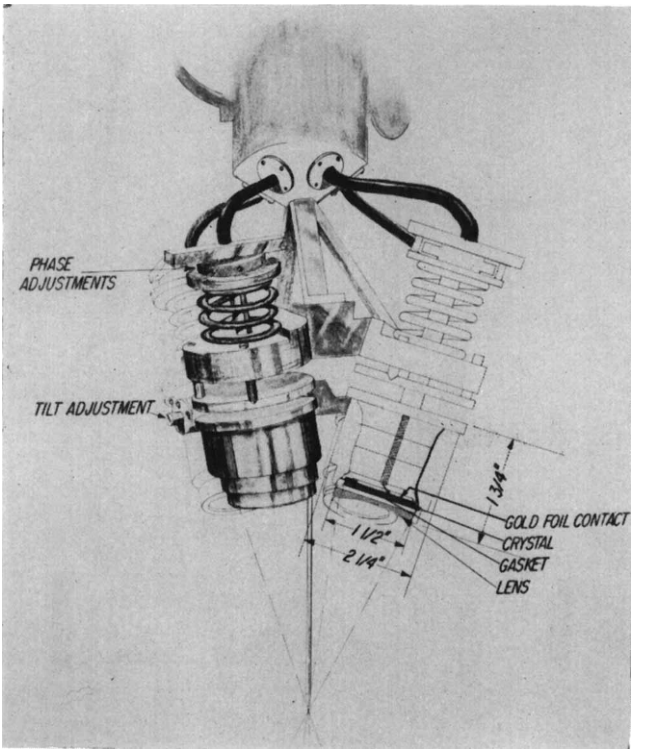

FIG. 47. Schematic diagram of multibeam focusing irradiator.

ing the sound level (pressure amplitude or particle velocity amplitude) in the region of intersection. The tip of the retractable pointer, illustrated in the figure, is adjusted so that, when in the lowered position, it coincides with the midpoint of the focal region. This permits the common focus to be placed at prescribed positions relative to landmarks on the stereotaxic instrument. The reflector-type focusing irradiator is illustrated in Fig. 48. The sound, produced by an X-cut quartz plate vibrating in the fundamental thickness mode, is reflected uniformly at right angles to the axis of the irradiator by a cone with a 90° apex angle. The sound is again reflected by a parabolic surface which serves to focus the energy. The parabolic reflector-type irradiator has the advantage over the multibeam type in that its side lobes are much lower in amplitude. This point is illustrated in Fig. 49 in which the beam patterns transverse to the axes of propagation are shown. The reflector-type irradiator also has the advantage of not requiring lenses. Plastics which have been used almost exclusively for the fabrication of lenses, have relatively high acoustic absorption with the result that more

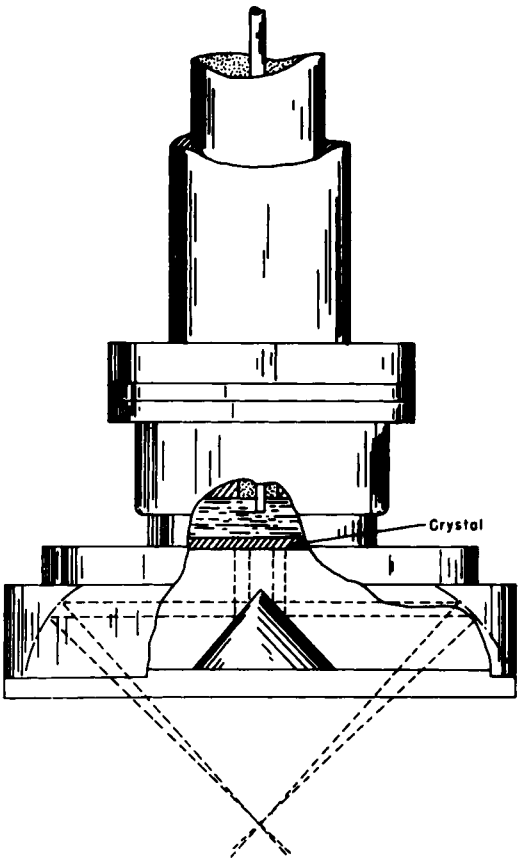

FIG. 48. Schematic diagram of reflector focusing irradiator.

heat is produced in the lens. If the period of irradiation and sound level are too great, such heating can produce disturbances of the beam position and the shape of the focal region or in extreme cases fracture of the lens. The lens-type irradiator has the advantages over the reflector type instrument in that it produces a much greater acoustic power output for the same effective diameter and also yields smaller dimensions for the axial focal diameter. It appears to be possible to surmount the disadvantages of the lens-type focusing irradiator by employing metal lenses capable of continuous operation at high sound levels and developing a large single lens instrument to have greatly reduced side lobes.

The ultrasonic energy is conducted from the irradiator to the tissue (e.g., brain) via degassed physiological saline. This liquid differs by approximately 2% (see Table II) in its characteristic acoustic impedance from that of brain tissue. Consequently, the amount of acoustic energy reflected

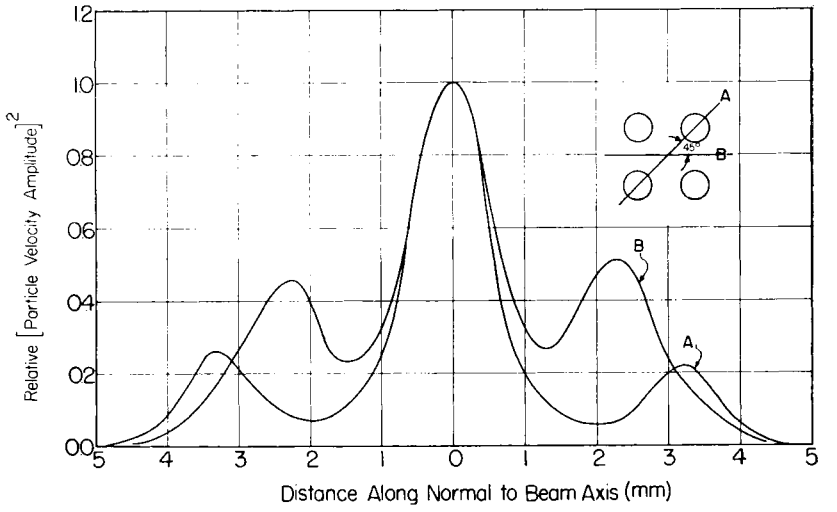

(a)

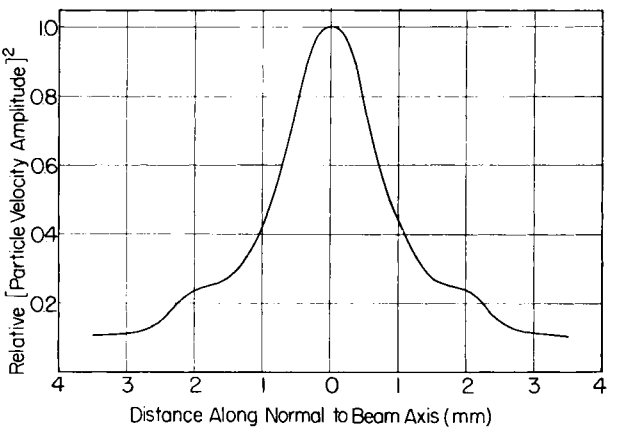

(b)

FIG. 49a. Transverse beam patterns of multibeam focusing irradiator through center of focal region (directions of highest and lowest side lobes illustrated).

FIG. 49b. Transverse beam pattern of reflector irradiator through center of focal region.

at the brain-saline interface is negligible for this application. The refraction of the sound at the brain-saline interface can be computed from values of the acoustic velocities in the two media (see Table II). Calculations show that, for angles of incidence as large as 45°, and at depths as great as 10 to 12 cm, the shift of the focal spot from its position in saline, can be as large as 0.7 mm. The calculated value agrees with measured values obtained by

inserting brains into the path of the converging beam and observing the lateral shift of the focal spot. Measurements also show that focal regions of practically identical size and shape are produced when the sound passes through the entire thickness of the brain (cat), as when the sound field is entirely confined to saline (F. J. Fry and W. J. Fry, 1959). The multiple interfaces within the brain reflect only a very small fraction of the incident acoustic energy and, therefore, scattering does not interfere with the production of the desired results of the type described here. The change in acoustic impedance at the interface of the ventricles and brain tissue is probably of the same order as that between brain tissue and saline and therefore the percentage of reflected energy should represent the maximum percentage of energy reflected at any interface along the transmission path. The saline transmitting liquid must be degassed to eliminate cavitation nuclei which produce cavities or bubbles when subjected to the stresses of the intense sound field (see Section II,6). These bubbles cannot be tolerated since they interfere with the transmission of sound by scattering and absorbing acoustic energy. Freshly boiled saline is a suitable medium for transmitting ultrasound (up to an intensity of 8 kw/cm^2) at 1 atm hydrostatic pressure, temperatures in the range from 0°C to 40°C, and at a frequency of 1 mc.

Bone, present in the path of the converging sound beams, must be surgically removed since it has a high ultrasonic absorption coefficient (Goldman and Hueter, 1956) implying a high rate of heat production during transmission of intense ultrasound thereby producing damage to underlying brain tissue by conduction. In addition, the acoustic velocity and impedance of bone differ so greatly from those of brain tissue (Theismann and Pfander, 1949; Goldman and Hueter, 1956) that the nonuniform thickness and variable radii of curvature characteristic of the skull would cause both undesirable modification of the beam shape and difficulties in precise positioning. The transmitting liquid is supported by a hopper which includes either a tourniquet for making a water-tight connection to the skin of the experimental animal or an inflatable rubber cuff for insuring a water-tight seal to the skin of a human patient. The temperature of the saline bath must be maintained accurately at a specified value which is usually that at which the body temperature of the animal is held. This is essential since the relation between the acoustic output of the transducer and the voltage applied to it is dependent upon the operating temperature of the transducer. The ultrasonic parameters of exposure required to produce a given change in tissue are also a function of temperature of the tissue.

A head holder, illustrated in Fig. 50, is employed to rigidly support the skull of the experimental animal and the hopper. For cats and monkeys, an instrument utilizing ear bars, infraorbital, and oral clamps is employed and the animal must be anesthetized. The midpoint of the ear bars provides a

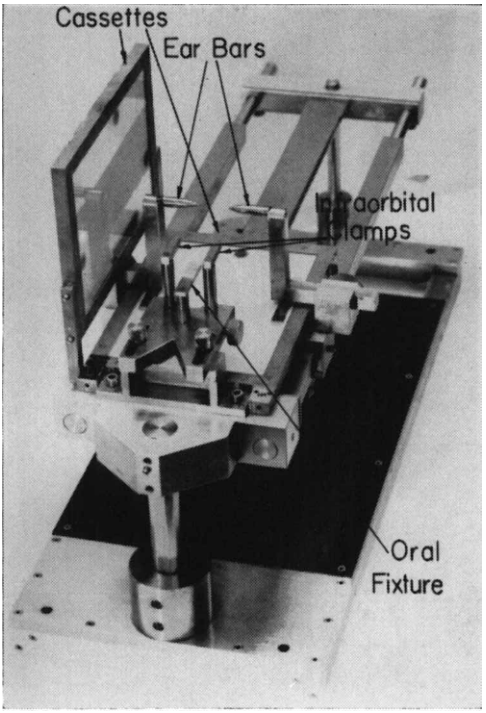

FIG. 50. Animal stereotaxic machine (cats and monkeys).

convenient reference position from which measurements can be made. Atlases, constructed for the experimental animals which utilize the same reference system (Jasper and Ajmone-Marson, 1954; Olszewski, 1952), are employed to determine the positions of desired brain structures. The use of both lateral and vertical roentgenograms of the skull, reduces by a factor of 4 to 5 the uncertainty in the position of deep structures. X-ray cassettes (shown in Fig. 50) for enclosing the film are rigidly mounted on the head holder and the x-ray tube and holder are held in fixed, reproducible positions relative to one another. A lateral roentgenogram, showing the the internal bony landmarks of the cat (subject cat) in which changes are to be made, is compared with those of a set of reference cats, the positions of whose brain structures are known. The midline of the base of the brain case (assumed to correspond to the midline of the deep brain) of the subject cat is obtained directly from a vertical roentgengram. This method yields the increased accuracy indicated above. After the roentgenograms are taken, the soft tissues are incised and a skull cap of appropriate shape and size is removed at the desired position. The dura mater is not opened unless the

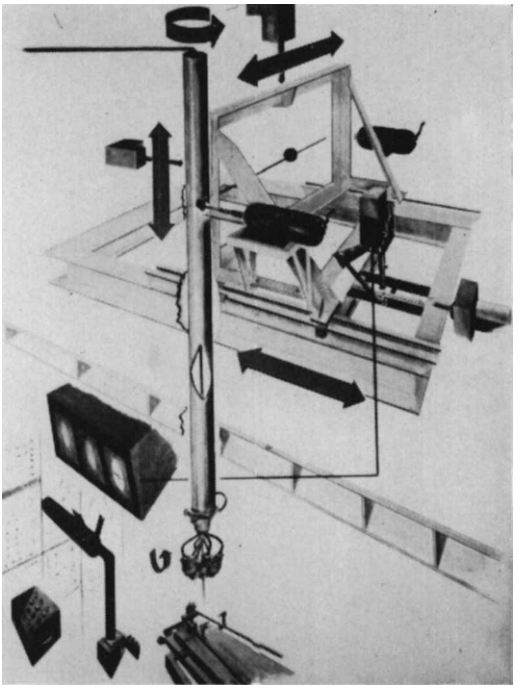

FIG. 51. Schematic diagram of an ultrasonic irradiation facility.

cortical configuration is to be examined. After the hopper is engaged in water-tight connection with the skin, it is filled with the sterile saline solution and the irradiator is moved into position such as to place the focal region at the site to be irradiated.

Although a number of different designs for the carriage unit which supports the irradiator are feasible, it is especially convenient to use the type illustrated schematically in Fig. 51 (F. J. Fry, 1958). The diagram shows the instrumentation in a double-deck arrangement. The upper room houses the motor-driven coordinate poistioning system which supports and moves the irradiator. This positioning system allows movements along three rectangular coordinates plus two rotational motions. The lower room contains the apparatus for supporting the animal, the calibrating system for determining dosage, equipment for controlling the positioning system, and instrumentation for recording spontaneous activity and evoked potentials and stimulating various end receptors or nerve tissue directly. Positioning the irradiator is facilitated by employing closed-circuit television systems by which scales on the coordinate positioning system located in the upper room are observed in the lower room. Speed controls allow the focus of the

transducer to be moved through the tissue with ease and precision. Figures 52 and 53 show the equipment in these two rooms.

The following is a brief discussion of the auxiliary electronic instruments required in the production of modifications of biological systems. The frequency at which the piezoelectric crystals are excited can be controlled by a signal generator powered from a voltage regulated supply. At an operating frequency of 1 mc, control of the frequency within ± 100 cps is adequate. A crystal calibrator is used to set the frequency of the signal generator. The duration of the exposure period is controlled by a digital timer with a unit time interval of 1 msec. A temperature-controlled electronic tuning fork provides the time base reference. The uncertainty in the duration of the exposure period is $\pm \frac{1}{4}$ msec. The envelope of the acoustic pulse must be accurately reproducible since the basic physical mechanism is not presently known and, therefore, it is not possible to compute the effects of different shaped envelopes in determining the dosage conditions. A rectangular envelope is most convenient for use at present. In order to obtain the necessary degree of accuracy in the control of the ultrasonic parameters of exposure, it is essential that the electronic driver be designed with an appropriate feedback loop to stabilize the output. Present methods require that the calibration procedure be accomplished at one range of sound levels and that irradiation take place at a higher range. Accordingly, it is very important to be able to scale accurately the driving voltage applied to the transducers and to be able to reproduce this voltage precisely. Presently available vacuum tube voltmeters do not approach the required accuracy to accomplish the necessary control (for example, an accuracy of $\pm 3\%$ can, with the number of steps involved in going from calibration to irradiation, introduce an uncertainty of 20%). This difficulty can be solved by employing a comparator method[7] in which an accurate voltage divider supplies a radio-frequency voltage to a siutably designed rectifier circuit whose output is compared with a precision dc power supply. Such a method permits the driving level to be set with an accuracy of $\pm 0.5\%$, which is essential in obtaining quantitative reproduction of selective lesions in the brain.

If electrical activity of the brain is to be recorded, either during the ultrasonic exposure period or in the intervals between exposure periods, it is convenient to incorporate electrode clamps in the hopper. In order to record either spontaneous activity or evoked electrical potentials during ultrasonic exposure, and at the beginning and end of an exposure period, it is essential that the electrodes be constructed so that electrical artifacts are not produced either by direct action of the intense sound on the insulation of the electrode leads or by the flow of the coupling liquid in the in-

[7] Unpublished work of this laboratory, still in process of development.

FIG. 52.

tense sound field (see Section II, 7, *c*). Satisfactory electrodes for a number of studies can be fabricated from 0.010 in. diameter Nichrome wire covered with a thin layer of Formvar insulation. On the basis of results obtained in the investigations of temporarily induced changes in evoked cortical potentials during irradiation of thalamic structures by ultrasound, it appears that the quantitative reproduction of these reversible changes requires that the level of anesthesia be controlled accurately. Such control can be obtained by employing an automatic injector which delivers a controlled amount of anesthetic at short time intervals (2 min apart). Changes in the electrocorticogram can be used as a guide in automatic setting of the level of anesthesia.

The head of the human patient is supported in a different fashion from that of the experimental animal. The ear and eye bars are not used to support the head but are employed only for orientation with respect to the head holder axes (see Fig. 54). Four stainless steel rods, mounted individually on universal supports, are brought into position to support the skull after the head is properly oriented in the holder with respect to the ear bars and infraorbital fixtures. The tips of these sterilized rods are rounded to fit into previously prepared indentations of equal radius in the skull. The rod tips can be moved into place after the skin over the indentations has been opened. Micrometers mounted on each individual support permit accurate reproduction of the rod tip position from one time to another. This is necessary since the patient may have to be placed in the holder a number of times. Instead of employing internal bone landmarks as in the case of the experimental animal (cat), for the human, internal brain landmarks are used as references for positioning the focus of the ultrasonic beams. X-ray cassettes are provided on the head holder, and a radio opaque material is introduced into the ventricular system to provide the necessary contrast. From appropriate measurements made on the roentgenograms, it is possible to locate the positions of the brain landmarks in space and, with the use of atlases (Spiegel and Wycis, 1952; Schaltenbrand and Bailey, 1959), to compute the positions of the specific brain structures in each patient. The development of the technique of employing the reversible effects induced by ultrasound will ultimately eliminate the present

FIG. 52. Photograph of the irradiation room (lower portion of Fig. 51) showing the animal stereotaxic machine containing a monkey skull. The open-bottom hopper, shown in position over the skull, engages the opened skin of the animal and contains the acoustic transmitting liquid (sterile degassed saline). For irradiation, the four beam irradiator is lowered into the saline. The calibration tank, shown to the right of the stereotaxic machine, rides on a track which positions it under the irradiator. This tank supports an acoustic probe and saline bath in which the irradiator is partially submerged for determination of acoustic field characteristics and irradiator calibration purposes.

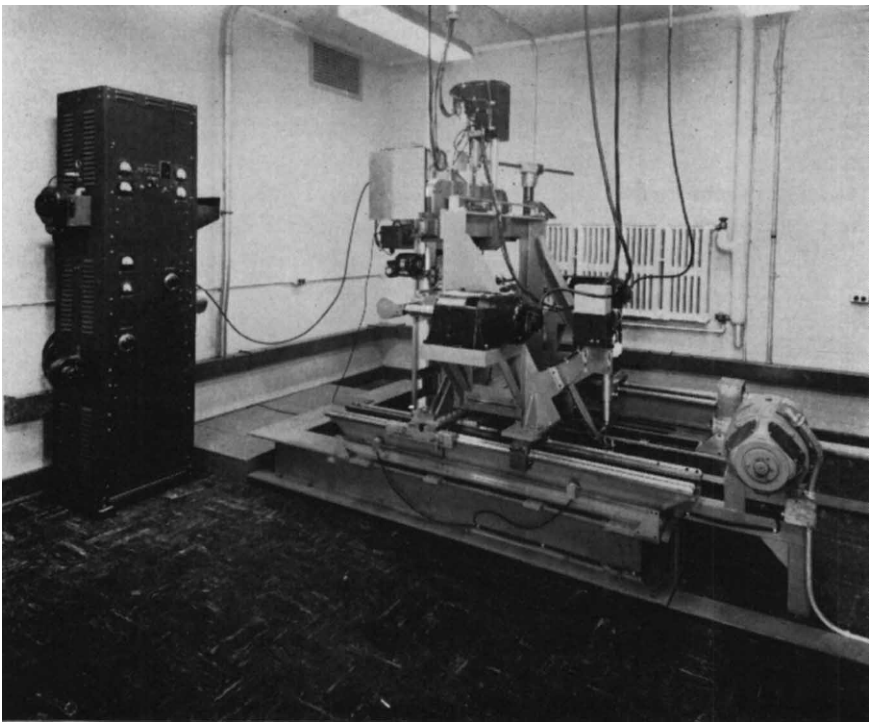

FIG. 53. Photograph of room which houses the coordinate positioning system (upper portion of Fig. 51).

complete dependence on reference landmarks. An awake and alert patient can be supported without discomfort in a head holder of the type illustrated in Fig. 54. This makes it possible to carry on a continuous interview and examination of the individual and observe subtle changes in behavior and subjective sensation during an irradiation procedure. Virtually any number of irradiation procedures can thus be carried out and the patient need not be subjected to repetitive surgery. The machine arrangement currently in use for the human work is illustrated in Fig. 55. A block diagram of the over-all electronic system and auxiliary equipment for neurophysiological studies on experimental animals and for human ultrasonic neurosurgery is illustrated in Fig. 56.

IV. Appendix: Thermocouple Probe Design and Construction and Auxiliary Instrumentation

In the megacycle (and above) frequency range, the thermocouple probe method for the determination of acoustic field distributions and calibration

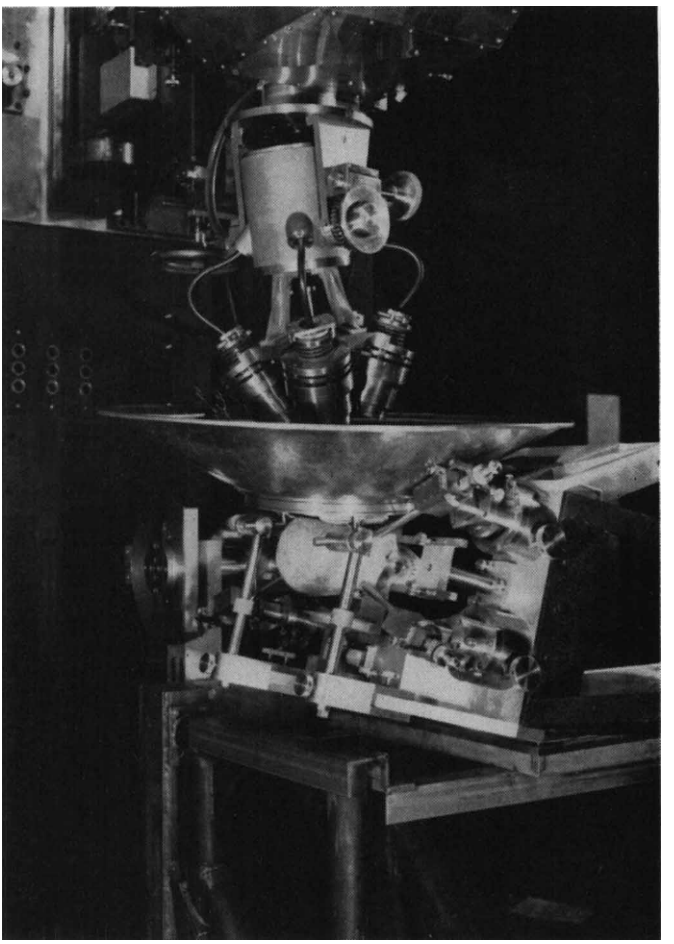

FIG. 54. A view of the four beam ultrasonic focusing irradiator, the hopper which supports the transmitting liquid and the stereotaxic machine (with skull in position for irradiating through the side). The stainless steel rods, which fit into indentations in the skull bone, are supported by adjustable posts provided with micrometers for accurate repositioning of the rod tips.

of irradiators has been extremely useful in studies of the type described in Section III, 2. The theory underlying the operation of thermocouple probes is treated briefly in Section II, 5, *b*. In this appendix, the construction of such probes is described and the technique used in the determination of the probe response is outlined.

The construction of the thermocouple probe for use in both focused and narrow beam unfocused fields is illustrated in Fig. 57. The housing for the

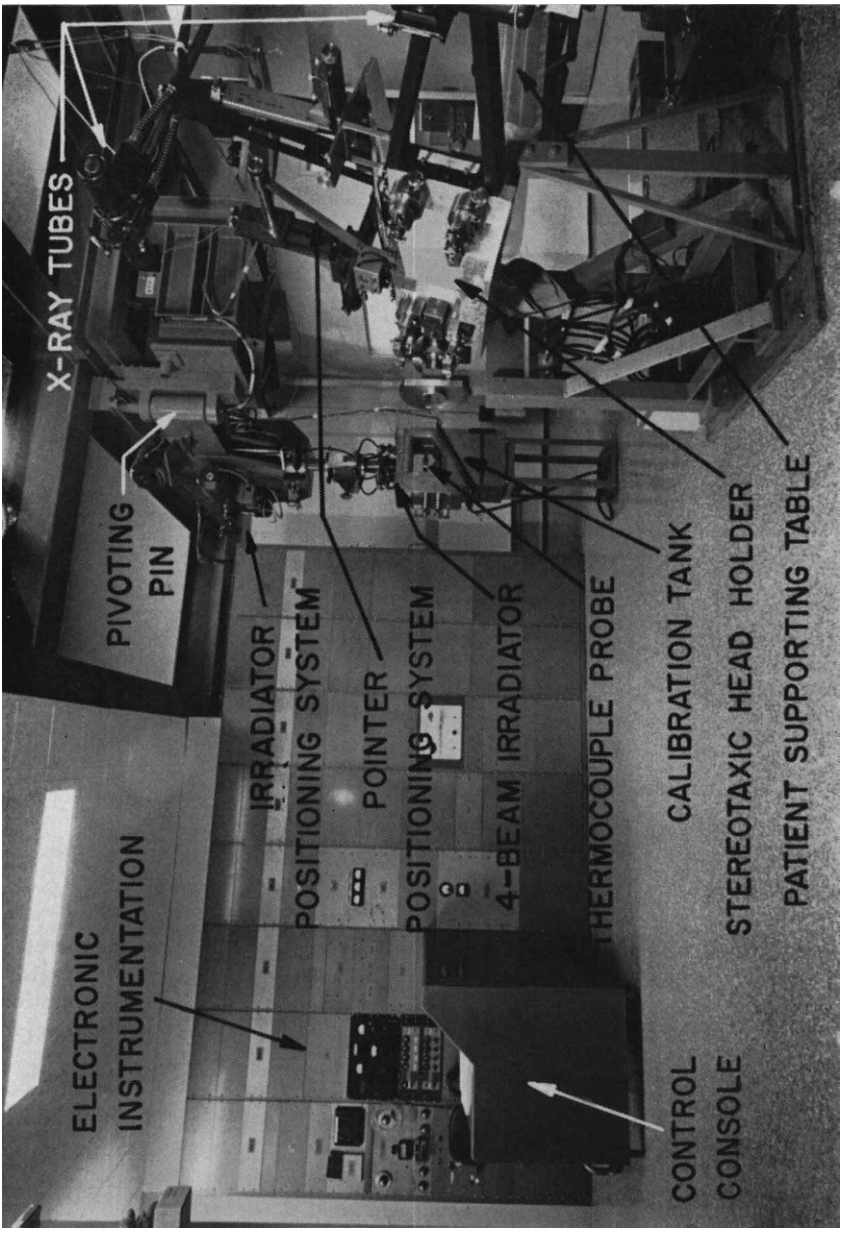
X-RAY TUBES
PIVOTING PIN
IRRADIATOR POSITIONING SYSTEM
POINTER POSITIONING SYSTEM
4-BEAM IRRADIATOR
THERMOCOUPLE PROBE
CALIBRATION TANK
STEREOTAXIC HEAD HOLDER
PATIENT SUPPORTING TABLE
ELECTRONIC INSTRUMENTATION
CONTROL CONSOLE

FIG. 55.

probe is in the shape of a thick disc, the inner diameter of which must be greater than the cross-sectional dimensions of the sound beam in order not to interfere with the field. The supporting rings are provided with glass-to-metal lead-throughs (Kovar seals) so that the thermocouple can be mounted along a diameter of the housing. For operation in the low megacycle frequency range, the thermocouple is assembled from 0.003 in. diameter wire (e.g., copper and constantan), which, by etching in acid, is tapered to 0.0005 in. diameter in the neighborhood of the junction. Thin windows (0.003 in. polyetyhlene sheet) separate the absorbing medium (castor oil or DC-710 silicone oil) from the external medium (physiological salt solutions). The thermocouple wires are soldered or welded together at the junction. Since the fine tapered wires and the junction may be subjected to considerable shock in ordinary laboratory treatment, it is desirable to incorporate a small spring in the thermocouple leads lying within the housing. This can be accomplished by coiling the constantan wire. Since both castor oil and DC-710 silicone oil closely match physiological saline solution as regards acoustic impedance (difference of 10% for castor oil and 3% for the DC-710 silicone oil, both at 30°C (Del Grosso and Smura, 1953), and since these materials have relatively high acoustic intensity absorption coefficients per unit path length (approximately 0.1 cm^{-1} at 1 mc and 30°C), they are a reasonable choice for imbedding media. It is extremely desirable, from the viewpoint of determining the geometric position of the focal spot of an irradiator relative to a given reference, to construct the probe so that the small thermocouple junction can be visualized. It is desirable, therefore, that the imbedding medium and the window be optically transparent. A photograph of a completed probe is shown in Fig. 58.

The two methods illustrated schematically in Fig. 59 (a and b) have been used to display and record the voltage output of the thermocouple. Figure 59a shows the probe connected directly to a magnetic oscillograph. The deflection of the oscillograph light beam is recorded photographically. Figure 59b shows the probe connected to a low noise amplifier which is in turn coupled to an oscilloscope. The deflection of the oscilloscope beam can be observed visually and also recorded photographically, if desired. The amplifier-oscilloscope method is especially convenient in the determination of field configurations. By observing the responses produced by 0.1 sec pulses, it is possible to determine quickly details of a relatively complex field. For the purpose of absolute determinations of sound levels, the oscilloscope and

FIG. 55. Configuration of irradiation room for ultrasonic human neurosurgery illustrating stereotaxic machine and associated x-ray apparatus, ultrasonic irradiator and positioning system, calibration equipment, and placement of electronic instrumentation.

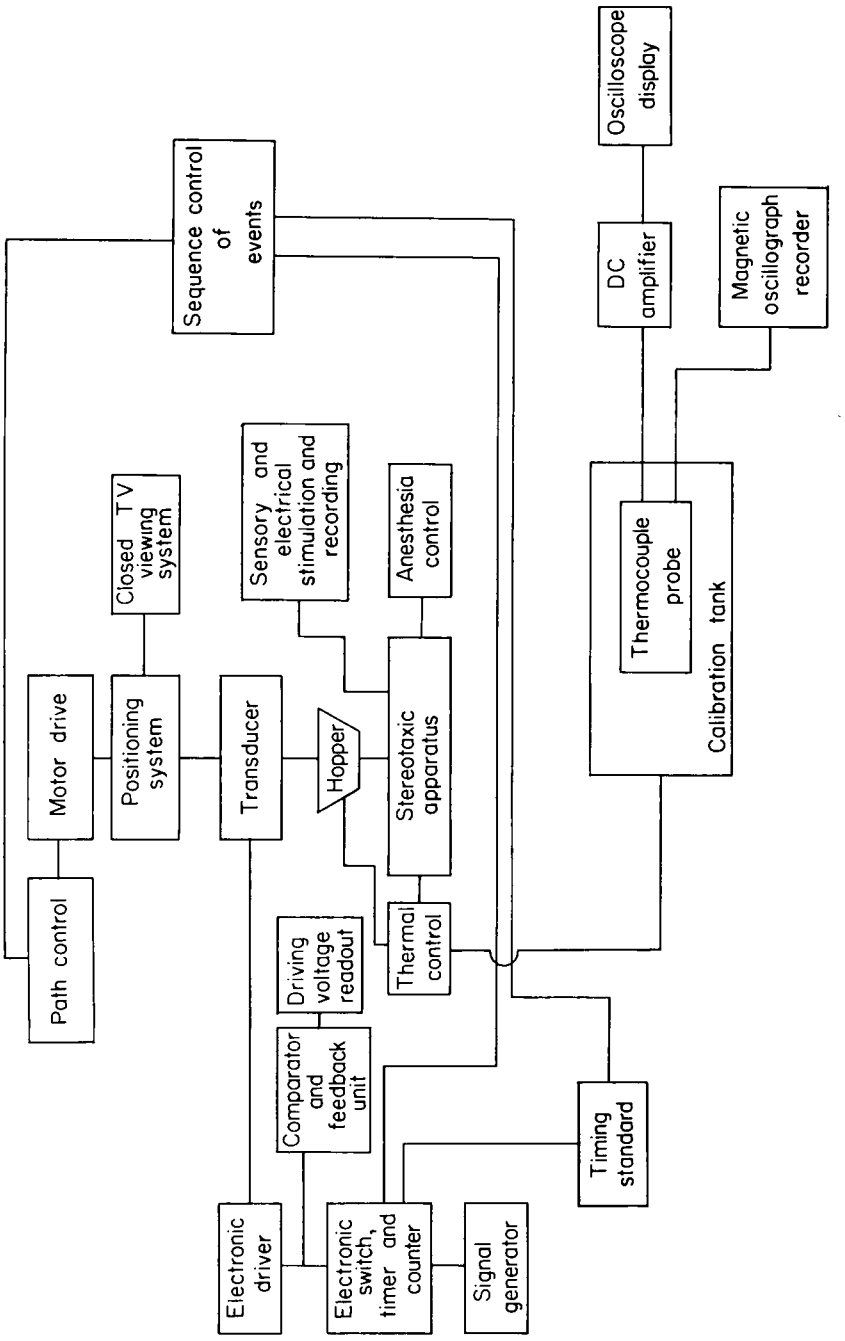
Sequence control of events
Oscilloscope display
DC amplifier
Magnetic oscillograph recorder
Sensory and electrical stimulation and recording
Anesthesia control
Closed TV viewing system
Motor drive
Positioning system
Transducer
Hopper
Stereotaxic apparatus
Thermocouple probe
Calibration tank
Path control
Driving voltage readout
Thermal control
Comparator and feedback unit
Timing standard
Electronic driver
Electronic switch, timer and counter
Signal generator

FIG. 56.

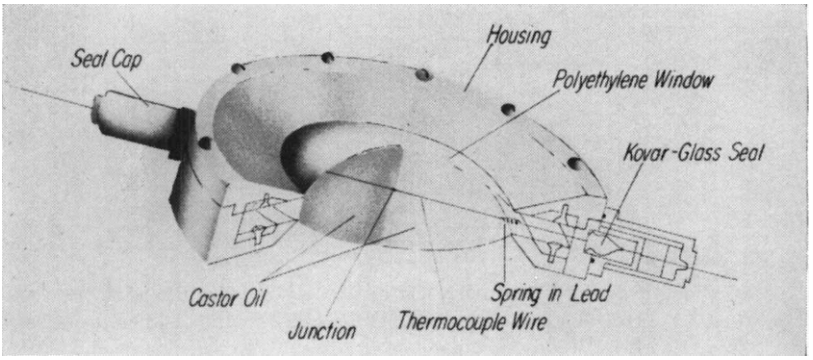

FIG. 57. Schematic diagram of thermocouple probe.

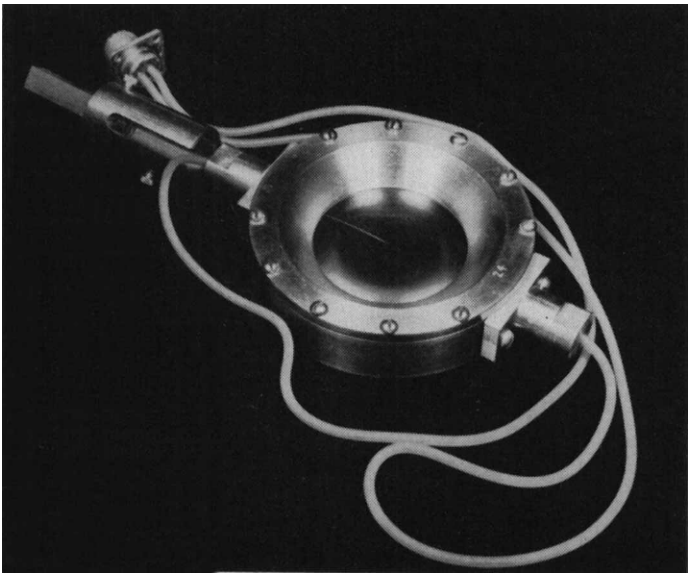

FIG. 58. Photograph of thermocouple probe.

a camera, or the magnetic oscillograph with its associated camera unit, can be used for recording the responses to one second pulses.

As indicated in Section II, the thermocouple probe can be used to determine absolute sound levels in accordance with relation (67) if the absorption coefficient of the imbedding material is known with sufficient accuracy.

FIG. 56. Block diagram of instrumentation for ultrasonic irradiation of the central nervous system including position sequence equipment and electronic controls, calibration of transducers, and stimulation and recording.

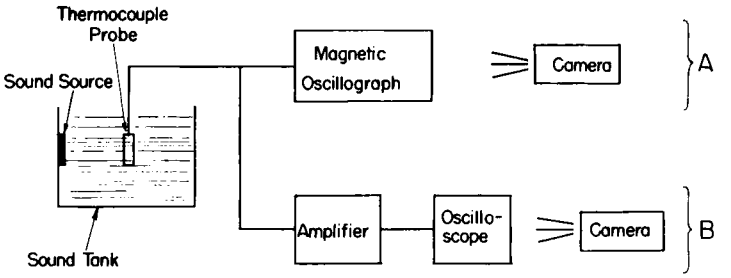

FIG. 59. Block diagram illustrating the display system for use with the thermocouple probes for determination of acoustic field configurations and recording equipment employed with these probes during calibration of acoustic fields.

If such is not the case, the radiation pressure method (Fox and Griffing, 1949; W. J. Fry and R. B. Fry, 1954b) can be used for calibrating the probe. Such a procedure is conveniently performed in a plane traveling wave field. The radiation pressure detector is a small stainless steel sphere ($\frac{1}{16}$ in. diameter is suitable for measurements at a frequency of 1 mc) suspended at a specific position in the medium. The unidirectional force resulting from radiation pressure (see Section II, 7, *b*) deflects the sphere from the initial equilibrium position. The sphere is then returned to this position (with the sound field present in the medium) by moving the positioning system which supports the bifilar suspension of the sphere. When the sound field is cut off, the sphere deflects from this position and the amount of this deflection, measured by a cathetometer, is used to compute the sound level (intensity, pressure amplitude, etc.).

A detailed discussion of the operation of the probe, the interpretation of information obtained using it, and discussion of the calibration procedures can be obtained by reference to a number of papers which have appeared in the technical literature (W. J. Fry and R. B. Fry, 1954a, b; Dunn and W. J. Fry, 1957; Hueter, 1957).

List of Symbols

a	Radius of element	B	See relation (92)
a_0	Radius of wire	B	Constant
a_1, a_2	Radii of spherical particles	B_t	See relation (87)
A	Particle acceleration amplitude	c_p	Heat capacity per gram at constant pressure
A	Area		
b	Total dissipation parameter, $b = b_t + b_r + b_v$	c_v	Heat capacity per gram at constant volume
b_r	Radiation dissipation parameter	C	See Fig. 6
b_t	Thermal dissipation parameter	C	Volume concentration of structure element
b_v	Viscous dissipation parameter		

C_c	Cable capacitance
C_L	Shunt capacitance of electrical load
C_0	Static capacitance of piezoelectric element
C_r	Reflection coefficient
C_t	Transmission coefficient
d	Piezoelectric constant
d	Spacing distance between centers of spheres
D	See relation (108)
D	Particle displacement amplitude
D	Lens diameter
D_a	Axial diameter of focal region
D_e	Diameter of piezoelectric element
D_t	Transverse diameter of focal region
e	Base of natural logarithms
e	Piezoelectric constant
e	Measure of the fluctuation of the absorption coefficient from the average value
E	Voltage
E_{in}	Probe voltage with specimen in field
E_{out}	Probe voltage with specimen out of field
E_0	Energy density
$\mathcal{E}$	Electric field intensity
f	Frequency
f_0	Resonant frequency of the bubble
f_r	Frequency of resonance
f_r	Relaxation frequency
f_l	Frequency in the low megacycle region
$f_{1/2}$	Frequency at which sensitivity drops to one-half that of frequency f_r
F	Force
F	Focal length
F_A	Shearing force per unit area
F_r	Radiation force
g	Surface tension factor, see relation (75)
g	Gravitational constant
G_c	Gain factor
G_l	Gain of lens
$\bar{G}_p$	Gain of plate system greater than unity
$\underline{G}_p$	Gain of plate system less than unity
G_r	Gain of reflector system
G_s	Gain of composite focusing system
h	See Section II, 7
h	γ/ϵ, see relation (79)
H	Working distance of lens system
H	See relation (90)
H_{at}	Heat generated in the element in time t
H_{ct}	Heat conducted away from the element in time t
I	Acoustic intensity
I_{av}	Average acoustic intensity
I_p	Peak acoustic intensity
I_r	Acoustic intensity at radius r
I_1	Acoustic intensity of the fundamental
I_2	Acoustic intensity of the second harmonic
I_{10}	Acoustic intensity of the fundamental at $x = 0$
I_{1a}	Acoustic intensity of the fundamental for absorption only
j	$\sqrt{-1}$
J_1	Bessel function of the first kind
k	Wave number, $2\pi/\lambda$
k_a	Dimensionless lens constant
k_t	Dimensionless lens constant
K	Relative dielectric constant
K	Coefficient of thermal conductivity
K_{ad}	Adiabatic compressibility
$\bar{K}_{ad}$	Adiabatic compressibility at zero pressure
K_T	Isothermal compressibility
K_w	Coefficient of thermal conductivity of the wire
L	"Length" of sound beam
L	Thickness, length
L_c	Thickness of piezoelectric element
L_p	Thickness of plate
L_s	Thickness of spacing element
m	An integer
m	Slope
m	Mass of displaced fluid
m_s	Mass of sphere
M	Mass of element
M_e	See relation (77)
n	An integer
n	Index of refraction

n	Normal to surface
n	Number of bubbles per unit volume
N	Number of maxima in near field
p	Pressure
P	Pressure amplitude
P_p	Peak pressure amplitude
P_0	Undisturbed pressure, static pressure
P_+	Pressure amplitude of incident wave
P_-	Pressure amplitude of reflected wave
P_1	Pressure amplitude of the fundamental
P_2	Pressure amplitude of the second harmonic
P_3	Pressure amplitude of the third harmonic
P_r	Radiation pressure
q	A variable which undergoes change due to the presence of an acoustic disturbance in the medium
Q	Amplitude of q
Q	Quality factor, $\omega L/R$, $f_r/\Delta f$
r	Resistivity
$r_{n/m}$	$\rho_n v_n/\rho_m v_m$
R	Resistance
R	Radius
R	See relation (76)
R	See Fig. 6
R_C	Shunt resistance of piezoelectric element
R_L	Shunt resistance of load
R_0	Mean bubble radius
Re	Reynolds number
s	Condensation
s	Ratio of amplitude of second harmonic to that of fundamental
S	Condensation amplitude
S	Standing wave ratio
t	Time
T	Temperature
T_b	Breaking stress of piezoelectric material
U	Particle velocity amplitude
v	Free field sound velocity
v_c	Velocity of sound in piezoelectric element
v_f	Flow velocity
v_0	Acoustic velocity at low frequencies
v_p	Velocity of sound in plate
v_r	Velocity of sound at the relaxation frequency
v_s	Velocity of sound in spacing element
V	Volume
x	Space variable
x_d	Lens depth
x_0	Position of zeroth order maximum
x_0	See relation (101)
x_s	Stabilization distance
y	Space variable
z	Variable of integration
Z_e	Electrical input impedance
α	Acoustic amplitude absorption coefficient per unit path length
α_r	Absorption coefficient at the relaxation frequency
α_2	Acoustic amplitude absorption coefficient per unit path length of the second harmonic
β	Coefficient of thermal expansion
β	See relation (60)
β	See relation (102)
γ	Ratio of specific heats
γ_c	See Fig. 4
Γ	See relation (99)
δT	See relation (126)
δx	See Fig. 15b
Δ	Increment of variable
Δ_r	Deflection of sphere by acoustic radiation force
ΔT_m	See relation (126)
ϵ	See relation (80)
ϵ_0	Permititivity of free space
ζ	Lateral shift of beam axis
η	Efficiency factor
η	Coefficient of shear viscosity
θ_1	Angle of incidence
θ_2	Angle of reflection
λ	Wavelength
λ_p	Wavelength of sound in plate material
λ_r	Wavelength of sound at the relaxation frequency
μ	Acoustic intensity absorption coefficient per unit path length
μ_m	Maximum value of μ

μ_0	Average value of μ	σ	Surface tension at bubble surface
μ_{f_1}	Value of μ at frequency f_1	τ	Period of oscillation, $1/f$
ξ	Particle displacement	ϕ	Angular coordinate deviation from the axis of the radiating element
$\dot{\xi}$	Particle velocity		
$\ddot{\xi}$	Particle acceleration		
ρ	Density	ϕ	Phase angle
ρ	Density of imbedding material	ϕ_1	Half-width of main beam
ρ_e	Density of structure element	Φ	See relation (81)
ρ_g	Density of gas	ψ	Half-aperture angle
ρ_0	Density of undisturbed medium	ω	Angular frequency, $2\pi f$
ρ_p	Density of plate material	ω_0	$2\pi f_0$
ρ_s	Density of spacing material	ω_0	R/M_e
ρ_s	Density of sphere	ω_r	$2\pi f_r$
σ	See relation (17)	ω_r	See relation (69)

References

Ackerman, E., and Holak, W. (1954). *Rev. Sci. Instr.* **25,** 857.

Angerer, O. A., Barth, G., and Güttner, W. (1951). *Strahlentherapie* **84,** 601.

Ballantine, H. T., Hueter, T. F., and Bolt, R. H. (1954). *J. Acoust. Soc. Am.* **26,** 581.

Barnard, J. W., Fry, W. J., Fry, F. J., and Brennan, J. F. (1956). *A.M.A. Arch. Neurol. Psychiat.* **75,** 15.

Baum, G., and Greenwood, I. (1958). *A.M.A. Arch. Ophthalmol.* **60,** 263.

Blake, F. G. (1949a). Acoust. Research Lab., Harvard University, Tech. Memo No. 9.

Blake, F. G. (1949b). Acoust. Research Lab., Harvard University, Tech. Memo No. 12.

Brandt, O., Freund, H., and Hiedemann, E. (1937). *Z. Physik* **104,** 511.

Brunschwig, F. S., and Fry, W. J. (1959). Ann. Rept. Natl. Science Foundation, Grant No. 2427.

Burov, A. K. (1956). *Doklady Akad. Nauk S.S.S.R.* **106,** 239.

Burov, A. K., and Andreewskaya, G. D. (1956). *Doklady Akad. Nauk S.S.S.R.* **106,** 445.

Carstensen, E. L., and Schwan, H. P. (1959a). *J. Acoust. Soc. Am.* **31,** 185.

Carstensen, E. L., and Schwan, H. P. (1959b). *J. Acoust. Soc. Am.* **31,** 305.

Carstensen, E. L., Li, K., and Schwan, H. P. (1953). *J. Acoust. Soc. Am.* **25,** 286.

Davids, N., Thurston, E. G., and Mueser, R. E. (1952). *J. Acoust. Soc. Am.* **24,** 50.

Del Grosso, V. A., and Smura, E. J. (1953). Naval Research Lab. Rept. NRL-4191.

Devin, C. (1959). *J. Acoust. Soc. Am.* **31,** 1654.

Dunn, F. (1956). Ph.D. Thesis, University of Illinois, Urbana, Illinois.

Dunn, F. (1958). *Am. J. Phys. Med.* **37,** 148.

Dunn, F. (1958). Unpublished data.

Dunn, F. (1960). *J. Acoust. Soc. Am.* **32,** 1503.

Dunn, F., and Fry, W. J. (1957). *IRE Trans. on Ultrasonic Eng.* **UE-5,** 59.

Dunn, F., and Fry, W. J. (1959). *J. Acoust. Soc. Am.* **31,** 632.

Dunn, F., and Fry, W. J. (1961). *Phys. in Med. and Biol.* **5,** 401.

Eckart, C. (1948). *Phys. Rev.* **73,** 68.

Edler, I., and Gustafson, A. (1957). *Acta. Med. Scand.* **156,** 85.

Edler, I., and Hertz, C. H. (1954). *Kgl. Fysiograf. Sällskap. Lund., Förh.* **24,** 1.

Effert, S., Erkens, H., and Grosse-Brockhoff, F. (1957). *Ger. Med. Mon.* **2,** 325.

Epstein, P. S. (1941). *In* "Theodor von Karman Anniversary Volume." California Inst. Technol., Pasadena.

Esche, R. (1952). *Akust. Beih.* **4,** 208.
Farrall, W. R. (1959). *IRE Trans. on Med. Electronics* **ME-6,** 198.
Fitzgerald, M. E., Griffing, V., and Sullivan, J. (1956). *J. Chem. Phys.* **25,** 926.
Fox, F. E., and Griffing, V. (1949). *J. Acoust. Soc. Am.* **21,** 352.
Fox, F. E., and Herzfeld, K. F. (1954). *J. Acoust. Soc. Am.* **26,** 984.
Fox, F. E., and Wallace, W. E. (1954). *J. Acoust. Soc. Am.* **26,** 994.
Franklin, D. L., Baker, D. W., Ellis, R. M., and Rushmer, R. F. (1959). *IRE Trans. on Med. Electronics* **ME-6,** 204.
Fry, F. J. (1958). *Am. J. Phys. Med.* **37,** 152.
Fry, F. J., and Fry, W. J. (1959). Unpublished data.
Fry, W. J. (1952). *J. Acoust. Soc. Am.* **24,** 412.
Fry, W. J. (1956). *Neurology* **6,** 693.
Fry, W. J. (1958). *Advances in Biol. and Med. Phys.* **6,** 281.
Fry, W. J., and Brunschwig, F. S. (1958). Ann. Rept. Natl. Science Foundation, Grant No. 2427.
Fry, W. J., and Dunn, F. (1956). *J. Acoust. Soc. Am.* **28,** 129.
Fry, W. J., and Dunn, F. (1961). *J. Acoust. Soc. Am.* to be published.
Fry, W. J., and Fry, R. B. (1953). *J. Acoust. Soc. Am.* **25,** 6.
Fry, W. J., and Fry, R. B. (1954a). *J. Acoust. Soc. Am.* **26,** 294.
Fry, W. J., and Fry, R. B. (1954b). *J. Acoust. Soc. Am.* **26,** 311.
Fry, W. J., Taylor, J. M., and Henvis, B. W. (1948). "Design of Crystal Vibrating Systems." Dover Publns., New York.
Fry, W. J., Meyers, R., Fry, F. J., Schultz, D. F., Dreyer, L. L., and Noyes, R. F. (1958). *Trans. Am. Neurol. Assoc.* p. 16.
Goldman, D. E., and Hueter, T. F. (1956). *J. Acoust. Soc. Am.* **28,** 35.
Gould, R. K., and Nyborg, W. L. (1960). *J. Acoust. Soc. Am.* **32,** 775.
Grabar, P. (1953). *Advances in Biol. and Med. Phys.* **3,** 191.
Harvey, E. N., Barnes, D. K., McElroy, W. D., Whiteley, A. H., Pease, D. C., and Cooper, K. W. (1944a). *J. Cellular Comp. Physiol.* **24,** 1.
Harvey, E. N., Whiteley, A. H., McElroy, W. D., Pease, D. C., and Barnes, D. K. (1944b). *J. Cellular Comp. Physiol.* **24,** 23.
Herrick, J. F., and Anderson, J. A. (1959). *IRE Trans. on Med. Electronics* **ME-6,** 195.
Herzfeld, K. F., and Litovitz, T. A. (1959). "Absorption and Dispersion of Ultrasonic Waves." Academic Press, New York.
Howry, D. H. (1955). *IRE Convention Record* Part 9, 75.
Howry, D. H. (1957). *In* "Ultrasound in Biology and Medicine" (E. Kelly, ed.), p. 49. Am. Inst. Biol. Sci., Washington, D.C.
Howry, D. H., Stott, D. A., and Bliss, W. R. (1954). *Cancer* **7,** 354.
Hueter, T. F. (1948). *Naturwissenschaften* **35,** 285.
Hueter, T. F. (1951). *J. Acoust. Soc. Am.* **23,** 590.
Hueter, T. F. (1957). *J. Acoust. Soc. Am.* **29,** 735.
Hueter, T. F., and Bolt, R. H. (1955). "Sonics." Wiley, New York.
Jasper, H. H., and Ajmone-Marson, C. (1954). "A Stereotaxic Atlas of the Diencephalon of the Cat." Natl. Research Council of Canada, Ottawa.
Kikuchi, Y., Uchida, R., Tanaka, K., and Wagai, T. (1957). *J. Acoust. Soc. Am.* **29,** 824.
Kinsler, L. E., and Frey, A. R. (1950). "Fundamentals of Acoustics." Wiley, New York.
Krassilnikov, V. A., Shklovskaya-Kordy, V. V., and Zarembo, L. K. (1957). *J. Acoust. Soc. Am.* **29,** 642.

Lamb, H. (1945). "Hydrodynamics," 6th ed. Dover, New York.
Larsson, B., Leksell, L., Rexed, B., Sourander, P., Mair, W., and Andersson, B. (1958). *Nature* **182,** 1222.
Lehmann, J. F., and Krusen, F. H. (1958). *Am. J. Phys. Med.* **37,** 173.
Liebermann, L. N. (1949). *Phys. Rev.* **75,** 1415.
Lindström, O. (1955). *J. Acoust. Soc. Am.* **27,** 654.
Ludwig, G. D., and Struthers, F. W. (1949). Naval Med. Research Inst., Natl. Naval Med. Center, Project NM-004-001, Rept. No. 4.
McLachlan, N. W. (1955). "Bessel Functions for Engineers." Oxford Univ. Press, London and New York.
Maidanik, G. (1957). *J. Acoust. Soc. Am.* **29,** 738.
Maidanik, G., and Westervelt, P. J. (1957). *J. Acoust. Soc. Am.* **29,** 936.
Marboe, E. C., and Weyl, W. A. (1950). *J. Appl. Phys.* **21,** 937.
Markham, J. J., Beyer, R. T., and Lindsay, R. B. (1951). *Revs. Modern Phys.* **23,** 353.
Mason, W. P. (1948). "Electromechanical Transducers and Wave Filters." Van Nostrand, New York.
Mason, W. P. (1950). "Piezoelectric Crystals and Their Application to Ultrasonics." Van Nostrand, New York.
Meyers, R., Fry, F. J., Fry, W. J., Eggleton, R. C., and Schultz, D. F. (1960). *Neurology* **10,** 271.
Mikhailov, I. G. (1958). *Soviet Phys.—Acoust.* **3,** 187.
Mintzer, D., and Tanenbaum, B. S. (1960). *J. Acoust. Soc. Am.* **32,** 67.
Moeller, H. G., and Schach, A. (1941). *Akust. Z.* **6,** 165.
Morse, P. M. (1948). "Vibration and Sound." McGraw-Hill, New York.
Noltingk, B. E., and Neppiras, E. A. (1950). *Proc. Phys. Soc. (London)* **B63,** 369.
Nyborg, W. L. (1953). *J. Acoust. Soc. Am.* **25,** 68.
Olszewski, J. (1952). "The Thalamus of the Macaca Mulatta." Karger, Basel.
Piersol, G. M., Schwan, H. P., Pennell, R. B., and Carstensen, E. L. (1952). *Arch. Phys. Med.* **33,** 327.
Pinkerton, J. M. M. (1949). *Proc. Phys. Soc. (London)* **B62,** 129.
Rosenberg, M. D. (1953). Acoust. Research Lab., Harvard University, Tech. Memo No. 26.
Satomura, S. (1957). *J. Acoust. Soc. Am.* **29,** 1181.
Schaltenbrand, G., and Bailey, P. (1959). "Introduction to Stereotaxis with an Atlas of the Human Brain." Thieme, Stuttgart.
Schwan, H. (1956). Wright Air Development Center, Project No. 54-670-2, Air Force Contract No. 33(616)-2494, Tech. Rept. No. 2.
Schwan, H. P., and Carstensen, E. L. (1952). *Electronics* **25,** 216.
Schwan, H. P., and Carstensen, E. L. (1956). Wright Air Development Center, Tech. Rept. WADC-56-389.
Spiegel, E. A., and Wycis, H. T. (1952). "Stereoencephalatomy." Grune & Stratton, New York.
Strasberg, M. (1959). *J. Acoust. Soc. Am.* **31,** 163.
Theismann, H., and Pfander, F. (1949). *Strahlentherapie* **80,** 981.
Tobias, C. A., Van Dyke, D. C., Simpson, M. E., Anger, H. O., Huff, R. L., and Koneff, A. A. (1954). *Am. J. Roentgenol., Radium Therap. Nuclear Med.* **72,** 1.
von Gierke, H. E., Oestreicher, H. L., Franke, E. K., Parrack, H. O., and von Wittern, W. W. (1952). *J. Appl. Physiol.* **4,** 886.
Weissler, A., and Cooper, H. W. (1948). *Mfg. Chemist* **19,** 505.
Westervelt, P. J. (1951). *J. Acoust. Soc. Am.* **23,** 312.
Wild, J. J., and Reid, J. M. (1952a). *Science* **115,** 226.

Wild, J. J., and Reid, J. M. (1952b). *Am. J. Pathol.* **28,** 839.
Wild, J. J., and Reid, J. M. (1957). *In* "Ultrasound in Biology and Medicine" (E. Kelly, ed.), p. 30. Am. Inst. Biol. Sci., Washington, D.C.
Willard, G. W. (1953). *J. Acoust. Soc. Am.* **25,** 669.
Zankel, K. L., and Hiedemann, E. A. (1959). *J. Acoust. Soc. Am.* **31,** 44.
Zarembo, L. K., and Krassilnikov, V. A. (1959). *Uspekhi Fiz. Nauk* **68,** 687 [*Soviet Phys. - Uspekhi* **2,** 580].